NATIONAL ADVISORY COMMITTEE FOR AERONAUTICS

TECHNICAL NOTE 4013

LOW-SPEED EXPERIMENTAL INVESTIGATION OF THE MAGNUS EFFECT ON VARIOUS SECTIONS OF A BODY OF REVOLUTION WITH AND WITHOUT A PROPELLER

By M. J. Queijo and Herman S. Fletcher

Langley Aeronautical Laboratory
Langley Field, Va.

Washington
August 1957

1Q

NATIONAL ADVISORY COMMITTEE FOR AERONAUTICS

TECHNICAL NOTE 4013

LOW-SPEED EXPERIMENTAL INVESTIGATION OF THE MAGNUS EFFECT ON VARIOUS SECTIONS OF A BODY OF REVOLUTION WITH AND WITHOUT A PROPELLER

By M. J. Queijo and Herman S. Fletcher

SUMMARY

An experimental investigation has been made at low speed to determine the Magnus effect on various sections of a body of revolution of which several sections could be rotated either as individual units or in combinations. The investigation included the measurement of the Magnus effect on the body alone and also on the body with a three-blade propeller. The tests were made over an angle-of-sideslip range from -5° to 30°, and at rotational speeds from 0 to 8,000 rpm with the propeller off and from 0 to 5,000 rpm with the propeller on.

The results of the investigation showed that with the propeller off, rotation of sections in the expanding portion of the body (that is, at the nose of the body) produced no appreciable Magnus force on these sections. However, rotation of these sections did produce an appreciable Magnus force on the part of the body downstream of the maximum diameter. These results are believed to be associated with the position and strength of the vortices shed from the body. With the propeller off, the center of pressure of the Magnus force on the body was about 70 percent of the body length behind the nose and moved forward with increase in rotational speed. With a propeller on the body of revolution, a large Magnus force was developed on sections of the body behind the propeller. The Magnus force on sections ahead of the propeller was small and independent of whether these sections were rotating.

INTRODUCTION

A rotating body placed in an airstream experiences a force component, due to rotation, which is normal to the plane defined by the axis of rotation and the direction of the relative wind. This force (generally referred to as the Magnus effect) can have an important effect on the motion of a body which is rotating as a unit or which has some external component rotating and, hence, has been the subject of many experimental and theoretical investigations. (See refs. 1 to 4, for example.)

Since many present-day missiles are spin-stabilized, the Magnus effect has become of great interest in regard to the stability of such missiles. (See refs. 5 and 6, for example.) In experimental investigations of the Magnus effect, the entire missile generally is spun at various speeds and the resultant force and moment due to rotation are measured. This procedure yields the net Magnus force, but yields no information on the buildup of the force along the body. In theoretical investigations, the approach generally has been to consider only circular cylinders; hence, nose-shape effects were neglected.

The purpose of the present investigation is to determine the Magnus force on five sections of a body of revolution of which the first four sections can be spun either as individual units or in combinations. Measurements of the Magnus force and the resulting moment are made for various sections of the body; hence, it is possible to determine which sections of a rotating body are effective in producing a Magnus force on themselves and on stationary sections of the body. The apparatus used in the investigation also makes it convenient to determine whether the Magnus force on a section ahead of the propeller depends on whether the section is rotating or stationary.

SYMBOLS

The data presented herein are referred to the body system of axes shown in figure 1. All forces and moments were measured about the moment center located on the fuselage center line at a distance of 31.5 inches from the fuselage nose. The symbols and coefficients used are defined as follows:

A	maximum cross-sectional area of body, sq ft
C_L	lift coefficient, $\frac{\text{Lift}}{\frac{1}{2}\rho V^2 A}$
$C_{L,o}$	lift coefficient with stationary sections
C_m	pitching-moment coefficient, $\frac{\text{Pitching moment}}{\frac{1}{2}\rho V^2 l A}$
$C_{m,o}$	pitching-moment coefficient with stationary sections
C_Q	torque coefficient, $\frac{\text{Torque}}{\frac{1}{2}\rho V^2 l A}$

C_T	thrust coefficient, $\frac{\text{Thrust}}{\frac{1}{2}\rho V^2 A}$
l	body length, 3.75 ft
r	body radius, ft unless otherwise specified
V	free-stream velocity, ft/sec
x	axial distance along body axis, measured from body nose, ft
$\bar{x}$	axial distance to center of pressure of Magnus force, ft
β	angle of sideslip, deg
ρ	air density, slugs/cu ft

MODEL AND APPARATUS

The model used in this investigation was a body of revolution 45 inches long and was made primarily of magnesium. The model was made in five sections (see fig. 2), of which the first four could be rotated individually or in the various combinations listed in table I. The sections were rotated in a clockwise direction when viewed from downstream. The model and sting support were designed so that the aerodynamic forces could be measured on the entire body or on the sections indicated in table I.

A 27-horsepower water-cooled electric motor was used to spin the sections. The sections were geared to the motor by means of a hollow shaft. Through the hollow shaft passed a stationary shaft which was used to hold nonrotating sections upstream of the rotating sections. The rotational speed of the drive motor was measured by means of a Stroboconn unit.

The motor and model sections on which forces and moments were to be measured were rigidly fastened to a sting-type support which, in turn, was attached to a six-component balance system. Sections on which forces were not to be measured were fastened to the sting fairing and became part of the fairing.

The propeller used in part of the investigation was formed by mounting three duralumin blades in equally spaced holes in one of the rotating sections. (See fig. 3.) The blades were fastened at the center

of the section. All the holes in the model were plugged before testing except those in which the propeller blades were mounted. In tests involving several rotating sections and the propeller, the propeller was always on the section farthest from the nose of the model. The diameter of the propeller was 22.89 inches.

TESTS

Tests of this investigation were made in the 6- by 6-foot test section of the Langley stability tunnel at zero angle of attack and for angles of sideslip from -5° to 30°. Tests without the propeller were made at a dynamic pressure of 24.9 pounds per square foot, which corresponds to a Mach number of 0.14 and a Reynolds number of 3.86×10^6 based on the body length. Rotational speeds of the sections were varied from 0 to 8,000 rpm for the propeller-off configurations.

Tests with the propeller on were made at a dynamic pressure of 8 pounds per square foot, which corresponds to a Mach number of 0.07 and a Reynolds number of 1.99×10^6. Propeller rotational speeds varied from 0 to 5,000 rpm. The propeller blade angle was 26°, measured at a station 75 percent of the blade radius from the axis of rotation.

RESULTS AND DISCUSSION

Presentation of Data

In order to determine the Magnus force and resulting moment on the model, tests were made with the angle of sideslip varied and with the angle of attack set at 0°. The Magnus force and resulting moment appeared in the form of changes in lift and pitching-moment coefficients due to rotational speed. The basic tunnel data, from which this information can be obtained, are given in figures 4 to 14 for the propeller-off configurations and in figures 15 to 25 for the propeller-on configurations. The data for any specific configuration can be located by referring to table I.

The data are presented in the following manner: Each figure contains data for the variation of C_m and C_L with rotation of one specific section or combination of sections of the model. The data are further separated with respect to the sections on which the lift and pitching-moment coefficients were measured. For example, figure 4 presents data obtained with section 1 rotating, and the data are separated as follows:

Figure 4(a), C_m and C_L measured on section 1

Figure 4(b), C_m and C_L measured on sections 1, 2, 3, and 4

Figure 4(c), C_m and C_L measured on sections 1, 2, 3, 4, and 5

Inasmuch as the data of all figures show essentially the same trends, the force and moment characteristics are discussed in a general manner.

Propeller Off

Force characteristics.- The Magnus force on rotating sections and sections upstream of rotating sections was small for all configurations tested. Even with sections 1, 2, 3, and 4 rotating (29 percent of the model length), the Magnus force measured on sections 1, 2, 3, and 4 was very small (fig. 7(a)). However, the data showed that, with any section rotating, the Magnus force on the entire model became fairly large at high angles of sideslip. Therefore, it appears that even though sections upstream of section 5 could produce no appreciable Magnus force on themselves, they could cause a Magnus force on section 5 (which is downstream of the maximum diameter).

The foregoing results can be explained qualitatively on the basis of an analysis presented in reference 7. Consider the crossflow on a section of a cylinder at an angle of attack. (See fig. 26.) There is present in the boundary layer some vorticity due to the boundary-layer velocity gradient. For a circular cylinder the net vorticity is zero because the vorticity is equal and opposite on the two sides of the plane including the cylinder center line and the cross wind (fig. 26(a)). If the flow separates from the cylinder, there are two shed vortices of equal strength but of opposite sign (fig. 26(b)) and, hence, the system as a whole remains with no net vorticity. If the cylinder is rotated, the shed vortices become displaced as indicated in figure 26(c). The points of separation and, thus, the velocities and strengths of the two vortices are no longer equal. It is assumed that the separation point located in the region where the peripheral velocity is in the direction of the free-stream velocity moves downstream, but the other separation point does not move, as has been indicated experimentally. The separation point which did not move is in a region of higher velocity than the displaced separation point and, hence, is the source of the stronger shed vortex. Since the vorticity of the entire system must still be zero, a retained vortex of strength equal to the difference in strengths of the two shed vortices remains with the fuselage. This retained vortex is the origin of the Magnus force. If there were no flow separation and hence no shed vortices, it would be expected that there would be no Magnus force associated with rotation. Since the Magnus force is dependent on boundary layer and separation characteristics,

both of which are strongly influenced by Reynolds number, then the Magnus force should be dependent, to some extent, on Reynolds number. This fact has been observed experimentally on infinite cylinders and is discussed in references 4 and 7.

It is possible to use the foregoing concepts to rationalize the results of the present investigation. On a moderately blunt fuselage, flow separation does not occur at the nose but some distance back because of the favorable pressure gradient at the nose. Therefore, over some sections of the nose there should be no Magnus force if the fuselage is rotating. Rotation of the nose, however, causes the flow to rotate and hence displaces the shed vortices which are trailing over the rear part of the fuselage, and the result is a Magnus force. On this basis, it would be expected that for a sharp-nose fuselage, on which separation occurs very close to the nose and at low angles of attack (ref. 8), sections near the nose would yield a Magnus force due to rotation of the nose.

The results of the present investigation showed that the magnitude of the Magnus force on the entire model generally varied approximately linearly with the rotational speed of any rotating section for angles of sideslip up to about 15°. At higher angles of sideslip, the Magnus force increased linearly with rotational speed only at the lower rotational speeds. The total force on the model at a given angle of sideslip and rotational speed was greater when section 1 was rotating than when any other individual section was rotating, particularly at low rotational speeds. (Compare figs. 4(c) and 8(c), for example). Rotating any combination of sections yielded greater Magnus effect on the entire body than rotating any individual section - not because of the force on the sections themselves but probably because of the increased displacement of the shed vortices over the rear part of the body.

Moment characteristics.- The measured pitching-moment data are presented about an axis located at 70 percent of the body length from the nose. This location for the moment center was chosen so as to make the center of mass of the model and support fall approximately on the center of the balance system and hence minimize variations of static moments with angle of sideslip. The pitching-moment data are primarily of interest in determining the location of the center of pressure of the Magnus force. The location of the center of pressure of the Magnus force can be found from the equation $\frac{\bar{x}}{l} = -\frac{C_m - C_{m,o}}{C_L - C_{L,o}} + 0.70$. The results showed that the center of pressure of the Magnus force on the whole body generally was slightly behind the $\bar{x}/l = 0.70$ position at low rotational speeds and moved forward as the rotational speed was increased. This fact is illustrated in figure 14 for the body with section 2 rotating. Results are given only for angles of sideslip from 15° to 30°; at lower angles of sideslip, the Magnus force and moment are too small to permit accurate determination of $\bar{x}/l$.

Propeller On

The propeller thrust and torque characteristics for a blade angle of 26° are given in figure 15 for $\beta = 0^{\circ}$. The torque characteristics can be used to determine the actual direction of rotation of the air flow over the part of the body behind the propeller and, hence, to indicate the direction of the Magnus force which might be expected for various angles of sideslip. A positive torque coefficient indicates clockwise rotation of the air over the body when viewed from downstream and should yield a negative value of C_L for positive values of β.

Force characteristics.- The force characteristics of the model with the propeller on did not show as smooth a variation with rotational speed as that obtained with propellers off. The data showed that any section behind the propeller was capable of producing a Magnus force which became appreciable at high angles of sideslip and high rotational speeds. This effect (previously investigated in ref. 9) was due to the circulation induced by the propeller.

Any Magnus force on sections ahead of the propeller was obscured by the rather erratic variation of C_L with propeller rotational speed.

Moment characteristics.- The moment characteristics of the model with propeller on showed a smoother variation with propeller rotational speed than did the force data. The results indicated rather large moments at high angles of sideslip and high rotation speeds on sections behind the propeller.

The moment measured only on sections ahead of and including the propeller consisted of the moment due to direct propeller force and the moment due to any Magnus force. Since the total moment was essentially independent of the number of sections ahead of the propeller and of whether these sections were rotating, the Magnus force on sections ahead of the propeller was very small.

It should be noted that in actual application the circulatory flow behind a propeller is reduced by a wing or any protuberances from the fuselage; hence, the Magnus force and resulting moment would tend to be smaller than indicated in the present investigation.

CONCLUSIONS

An experimental investigation has been made at low speed to determine the Magnus effect on various sections of a body of revolution of which several sections could be rotated either as individual units or in combinations. The investigation included the measurement of the

Magnus effect on the body alone and also on the body with a three-blade propeller. The tests were made over an angle-of-sideslip range from -5° to 30°, and at rotational speeds from 0 to 8,000 rpm with the propeller off and from 0 to 5,000 rpm with the propeller on. The results of the investigation led to the following conclusions:

1. With the propeller off, rotation of sections in the expanding portion of the fuselage (that is, at the nose of the body) produced no appreciable Magnus force on these sections. However, rotation of these sections did produce an appreciable Magnus force on the part of the body downstream of the maximum diameter. These results are believed to be associated with the position and strength of the vortices shed from the body.

2. With the propeller off, the center of pressure of the Magnus force on the body was about 70 percent of the body length behind the nose and moved forward with increase in rotational speed.

3. With a propeller on the body of revolution, a large Magnus force was developed on sections of the body behind the propeller. The Magnus force on sections ahead of the propeller was small and independent of whether these sections were rotating.

Langley Aeronautical Laboratory,
National Advisory Committee for Aeronautics,
Langley Field, Va., June 10, 1957.

REFERENCES

1. Lafay, M. A.: Sur l'Inversion du Phénomène de Magnus. Comptes Rendus, t. 151, Nov. 14, 1910.

2. Betz, A.: The "Magnus Effect," the Principle of the Flettner Rotor. NACA TM 310, 1925.

3. Reid, Elliot G.: Tests of Rotating Cylinders. NACA TN 209, 1924.

4. Kelly, Howard R., and Van Aken, Ray W.: The Magnus Effect at High Reynolds Numbers. Jour. Aero. Sci. (Readers' Forum), vol. 23, no. 11, Nov. 1956, pp. 1053-1054.

5. Martin, John C.: On Magnus Effects Caused by the Boundary Layer Displacement Thickness on Bodies of Revolution at Small Angles of Attack. Rep. No. 870 (Revised), Ballistic Res. Labs., Aberdeen Proving Ground, June 1955.

6. Kelly, Howard R.: An Analytical Method for Predicting the Magnus Forces and Moments on Spinning Projectiles. TM-1634, U. S. Naval Ord. Test Station (Inyokern, Calif.), Aug. 12, 1954.

7. Buford, William E.: Magnus Effect in the Case of Rotating Cylinders and Shell. Memo. Rep. No. 821, Ballistic Res. Labs., Aberdeen Proving Ground, July 1954.

8. Gowen, Forrest E., and Perkins, Edward W.: A Study of the Effects of Body Shape on the Vortex Wakes of Inclined Bodies at a Mach Number of 2. NACA RM A53I17, 1953.

9. Ribner, Herbert S., and MacLachlan, Robert: Effect of Slipstream Rotation in Producing Asymmetric Forces on a Fuselage. NACA TN 1210, 1947.

TABLE I.- INDEX TO DATA FIGURES

Sections rotating	Sections in which force and moment were measured	Figure
Propeller off		
1	1	4(a)
	1, 2, 3, and 4	4(b)
	1, 2, 3, 4, and 5	4(c)
1 and 2	1 and 2	5(a)
	1, 2, 3, and 4	5(b)
	1, 2, 3, 4, and 5	5(c)
1, 2, and 3	1, 2, and 3	6(a)
	1, 2, 3, and 4	6(b)
	1, 2, 3, 4, and 5	6(c)
1, 2, 3, and 4	1, 2, 3, and 4	7(a)
	1, 2, 3, 4, and 5	7(b)
2	1 and 2	8(a)
	1, 2, 3, and 4	8(b)
	1, 2, 3, 4, and 5	8(c)
2 and 3	1, 2, and 3	9(a)
	1, 2, 3, and 4	9(b)
	1, 2, 3, 4, and 5	9(c)
2, 3, and 4	1, 2, 3, and 4	10(a)
	1, 2, 3, 4, and 5	10(b)
3	1, 2, and 3	11(a)
	1, 2, 3, and 4	11(b)
	1, 2, 3, 4, and 5	11(c)
3 and 4	1, 2, 3, and 4	12(a)
	1, 2, 3, 4, and 5	12(b)
4	1, 2, 3, and 4	13(a)
	1, 2, 3, 4, and 5	13(b)
Propeller on[a]		
1	1	16(a)
	1, 2, 3, and 4	16(b)
	1, 2, 3, 4, and 5	16(c)
1 and 2	1 and 2	17(a)
	1, 2, 3, and 4	17(b)
	1, 2, 3, 4, and 5	17(c)
1, 2, and 3	1, 2, and 3	18(a)
	1, 2, 3, and 4	18(b)
	1, 2, 3, 4, and 5	18(c)
1, 2, 3, and 4	1, 2, 3, and 4	19(a)
	1, 2, 3, 4, and 5	19(b)
2	1, 2, 3, and 4	20(a)
	1, 2, 3, 4, and 5	20(b)
2 and 3	1, 2, and 3	21(a)
	1, 2, 3, and 4	21(b)
	1, 2, 3, 4, and 5	21(c)
2, 3, and 4	1, 2, 3, and 4	22(a)
	1, 2, 3, 4, and 5	22(b)
3	1, 2, and 3	23(a)
	1, 2, 3, and 4	23(b)
	1, 2, 3, 4, and 5	23(c)
3 and 4	1, 2, 3, and 4	24(a)
	1, 2, 3, 4, and 5	24(b)
4	1, 2, 3, and 4	25(a)
	1, 2, 3, 4, and 5	25(b)

[a]The propeller was always on rotating section farthest from nose of model.

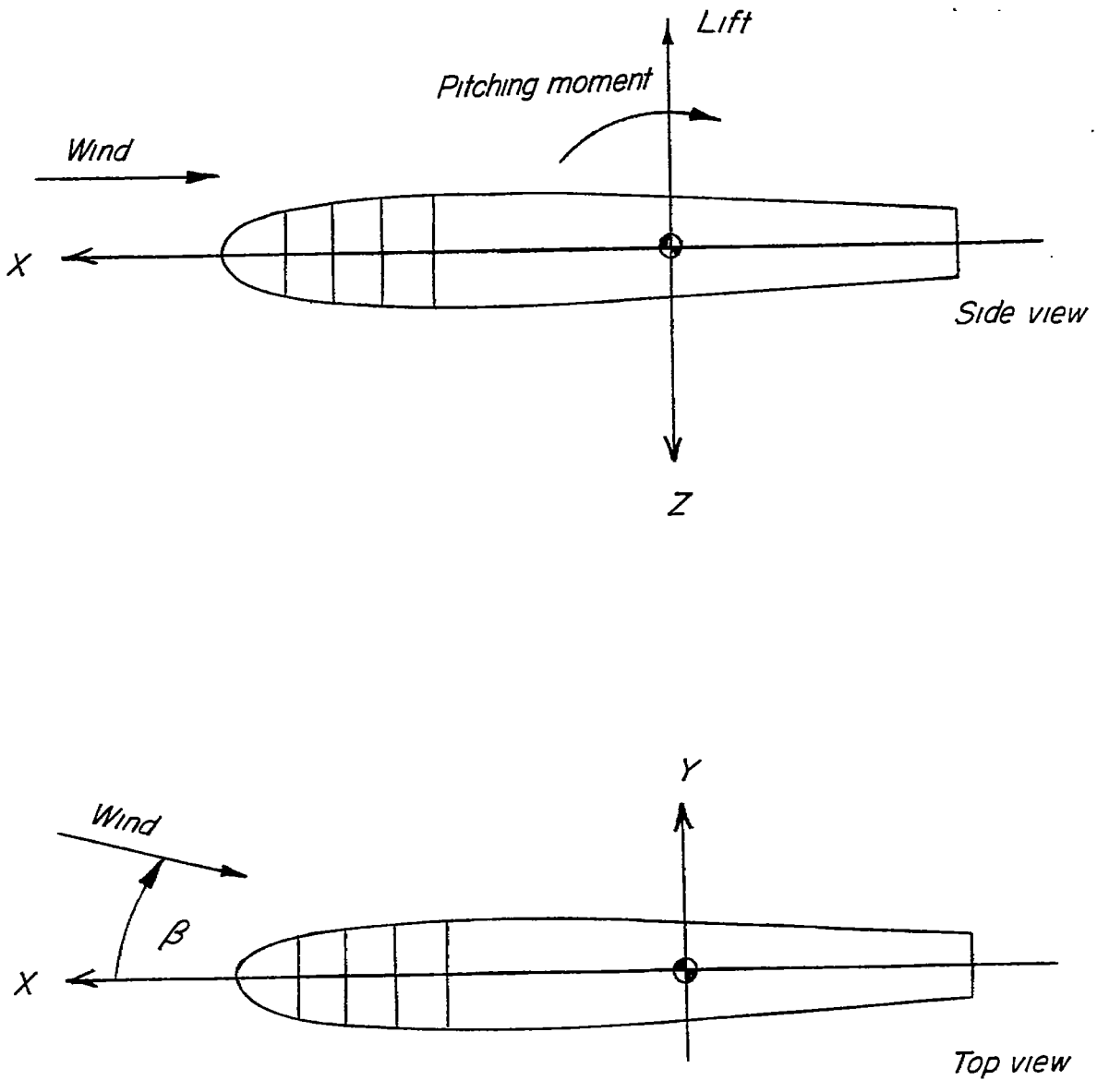

Figure 1.- System of body axes. Arrows indicate positive directions of force, moment, and angular displacement.

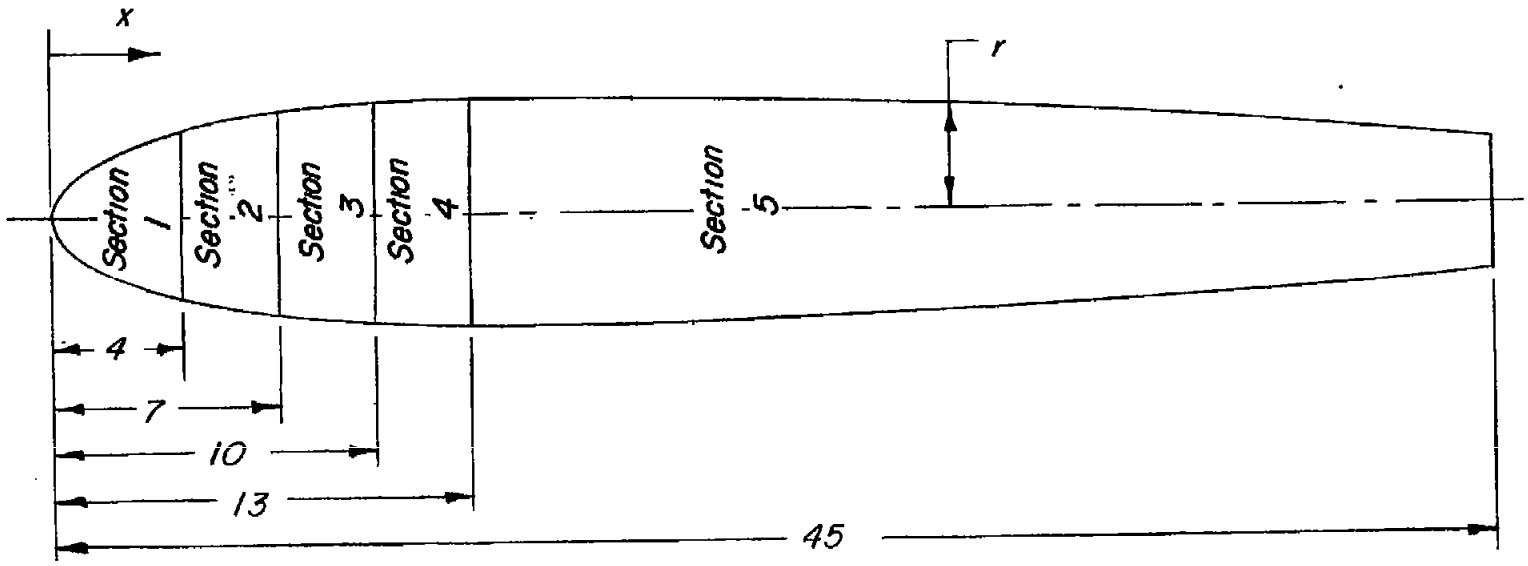

x	r	x	r	x	r
0	0	7.00	2.91	31.73	3.00
.25	.56	10.00	3.37	34.53	2.84
.50	.90	13.06	3.50	37.33	2.65
1.00	1.37	15.86	3.49	40.13	2.44
1.50	1.68	18.66	3.45	41.99	2.30
2.00	1.93	21.46	3.40	43.86	2.15
2.50	2.15	23.33	3.34	45.00	2.06
3.00	2.30	25.19	3.28		
4.00	2.56	27.06	3.21		
5.00	2.78	28.93	3.14		

Figure 2.- Body ordinates and geometric details of model. All dimensions are in inches.

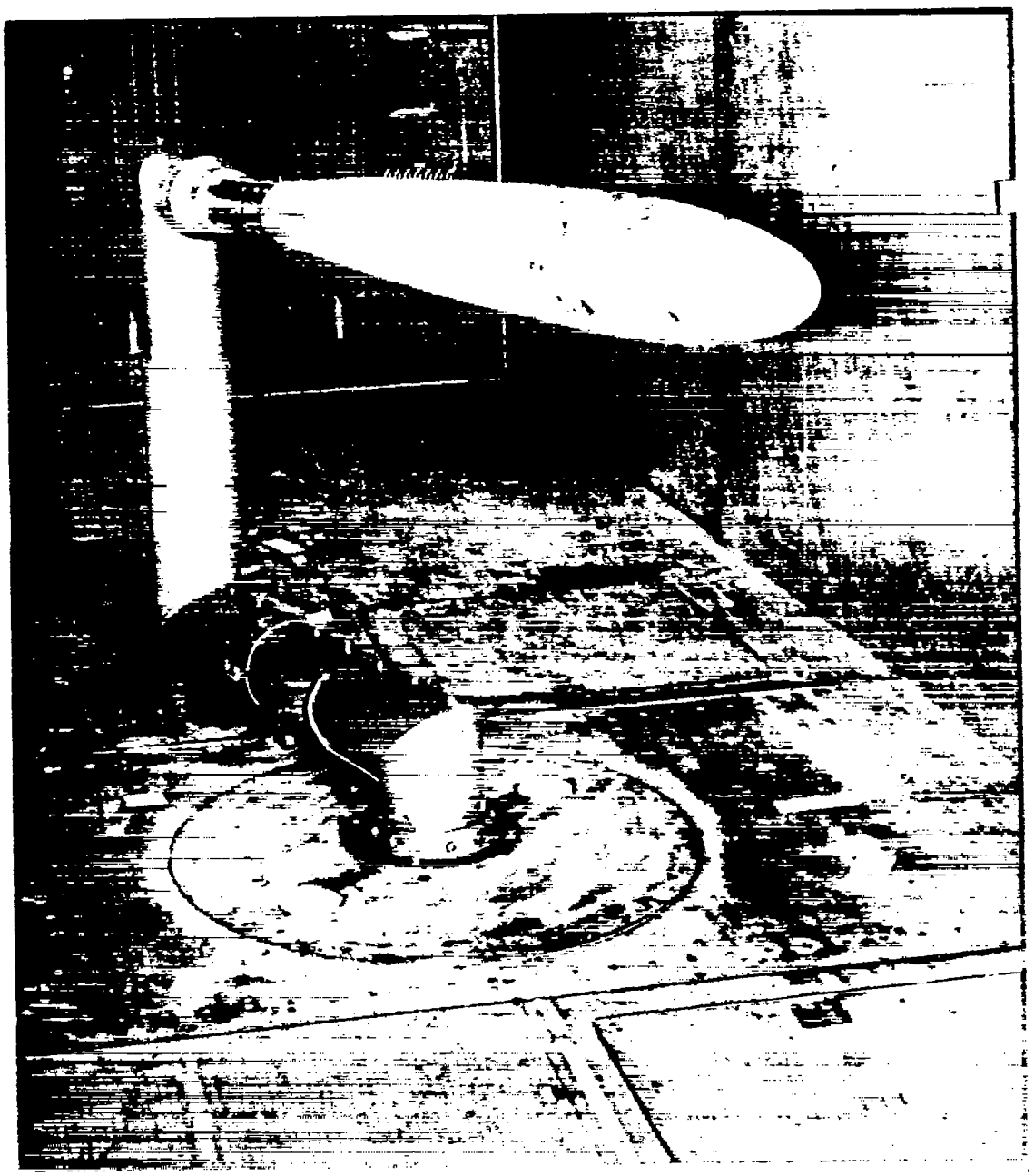

(a) Propeller off. L-92303

Figure 3.- Photographs of model used in investigation.

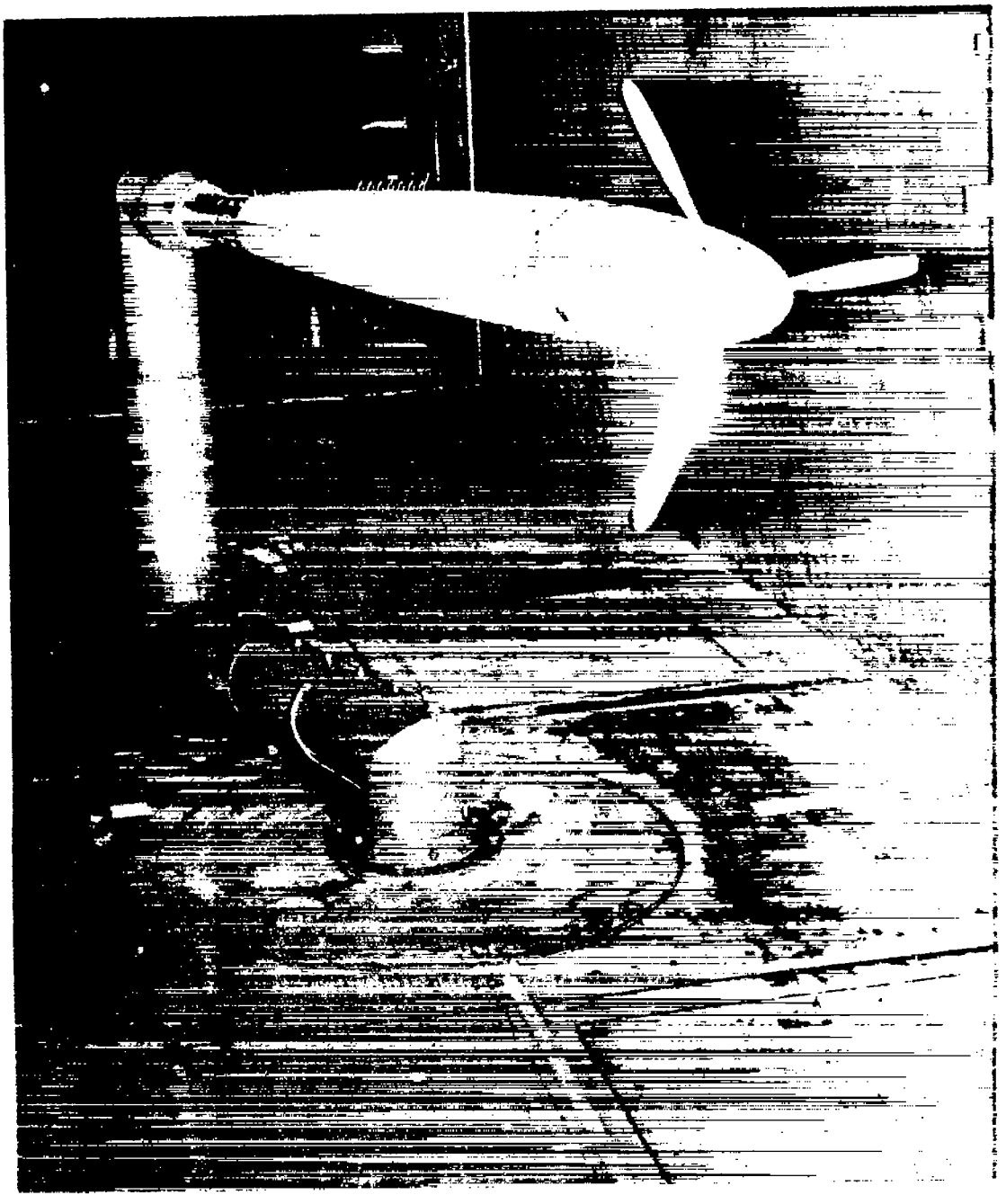

(b) Propeller on. L-92302

Figure 3.- Concluded.

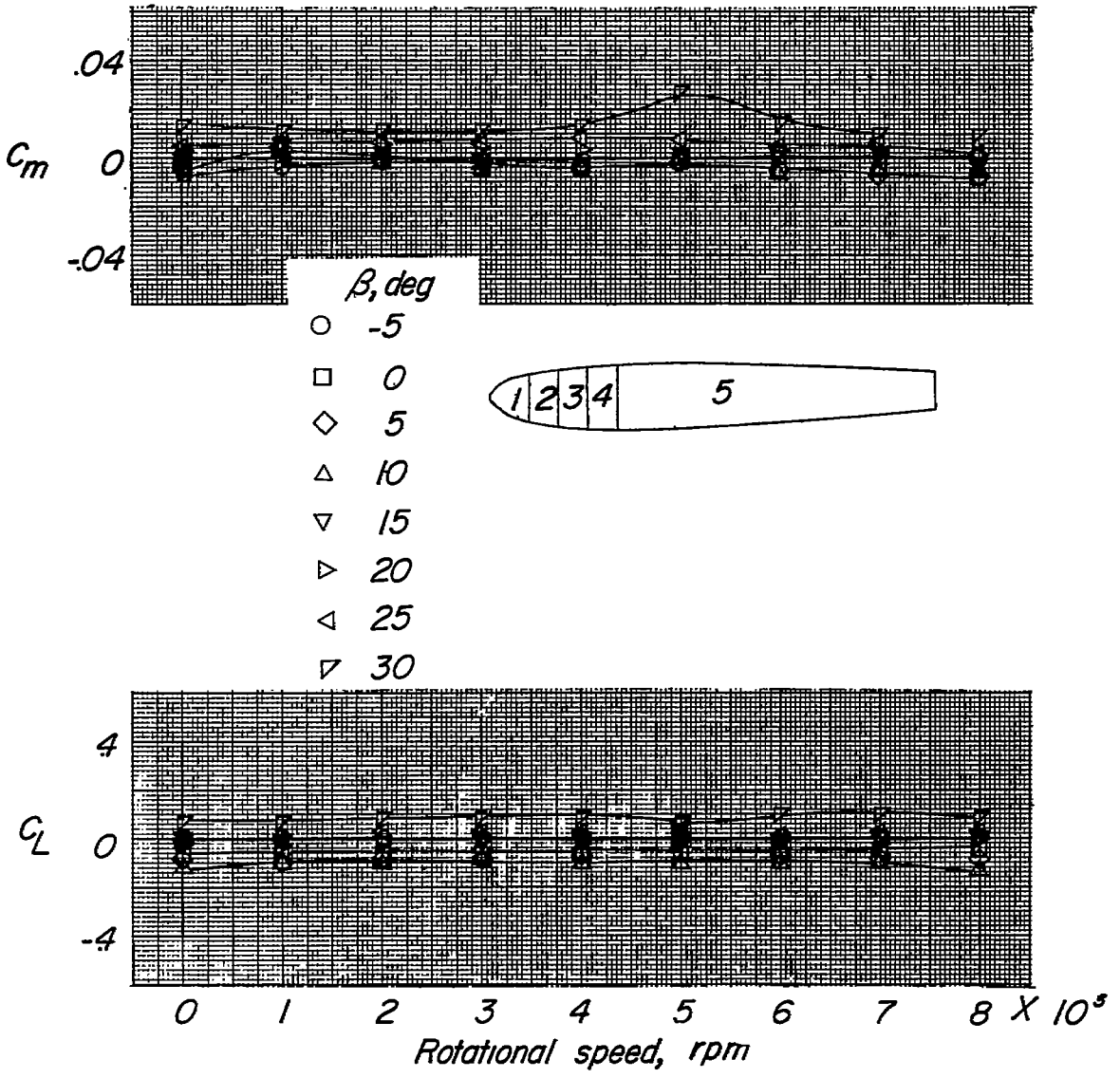

(a) C_m and C_L measured on section 1.

Figure 4.- Variation of C_m and C_L with rotational speed. Section 1 rotating; propeller off.

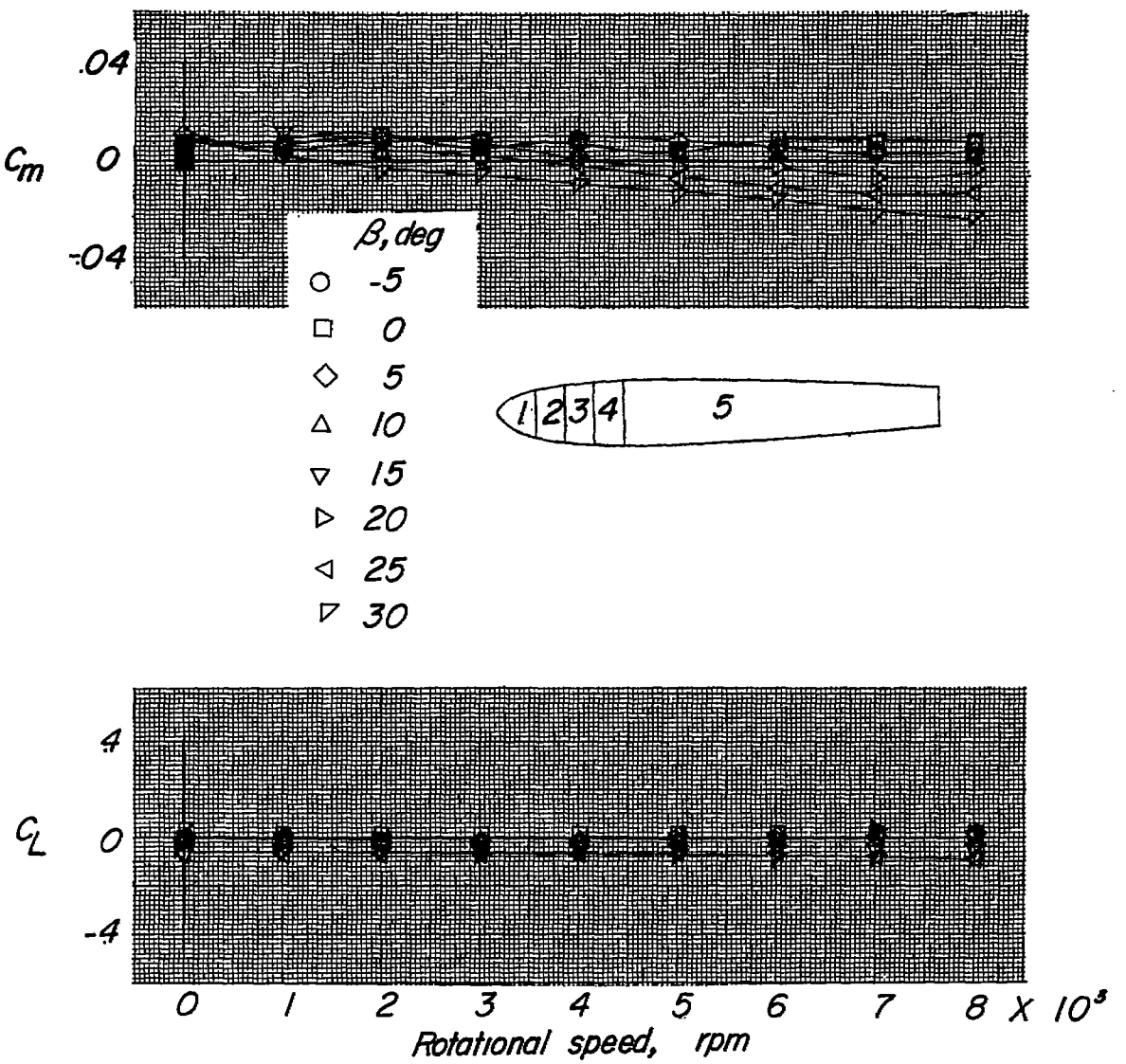

(b) C_m and C_L measured on sections 1, 2, 3, and 4.

Figure 4.- Continued.

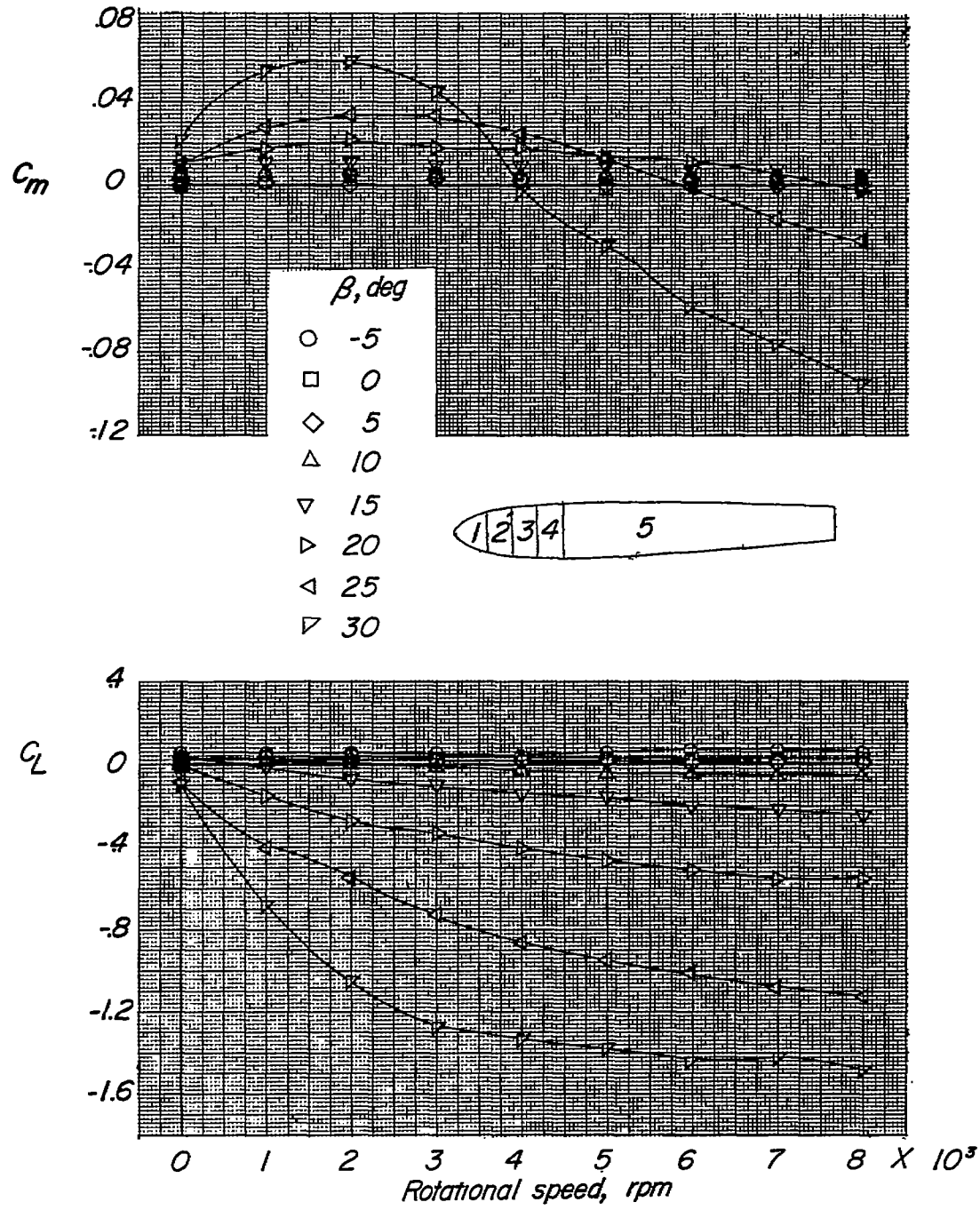

(c) C_m and C_L measured on sections 1, 2, 3, 4, and 5.

Figure 4.- Concluded.

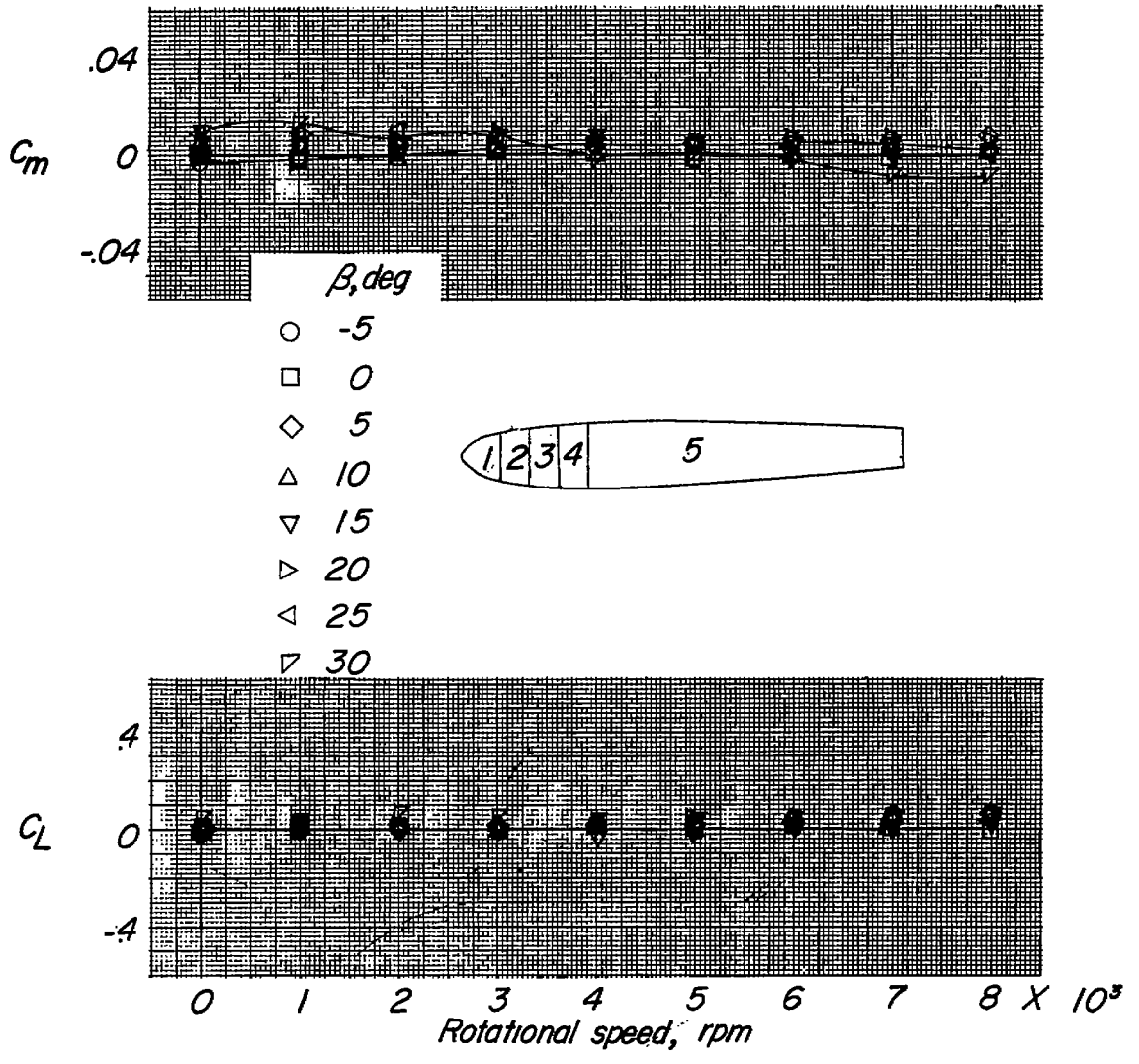

(a) C_m and C_L measured on sections 1 and 2.

Figure 5.- Variation of C_m and C_L with rotational speed. Sections 1 and 2 rotating; propeller off.

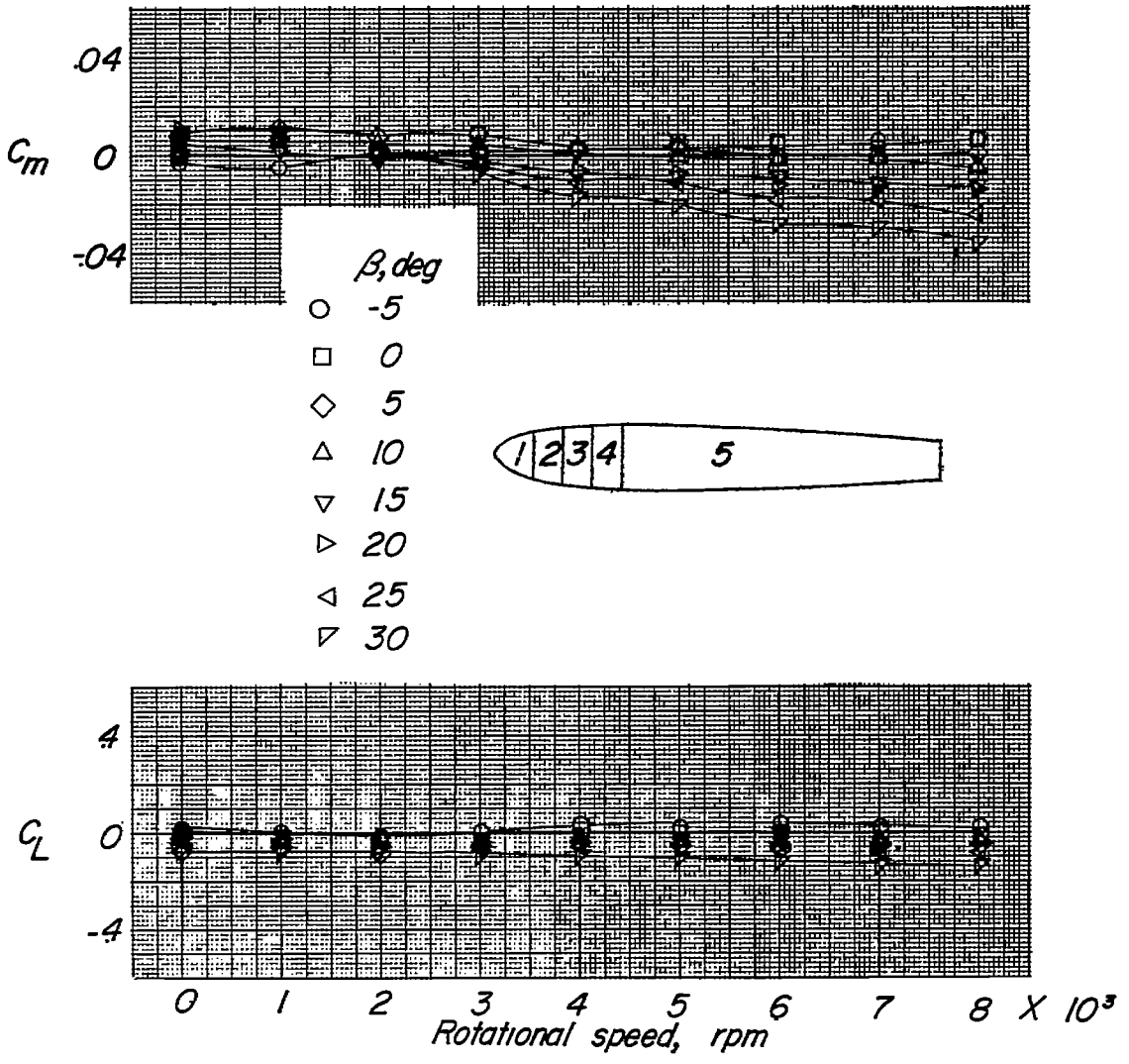

(b) C_m and C_L measured on sections 1, 2, 3, and 4.

Figure 5.- Continued.

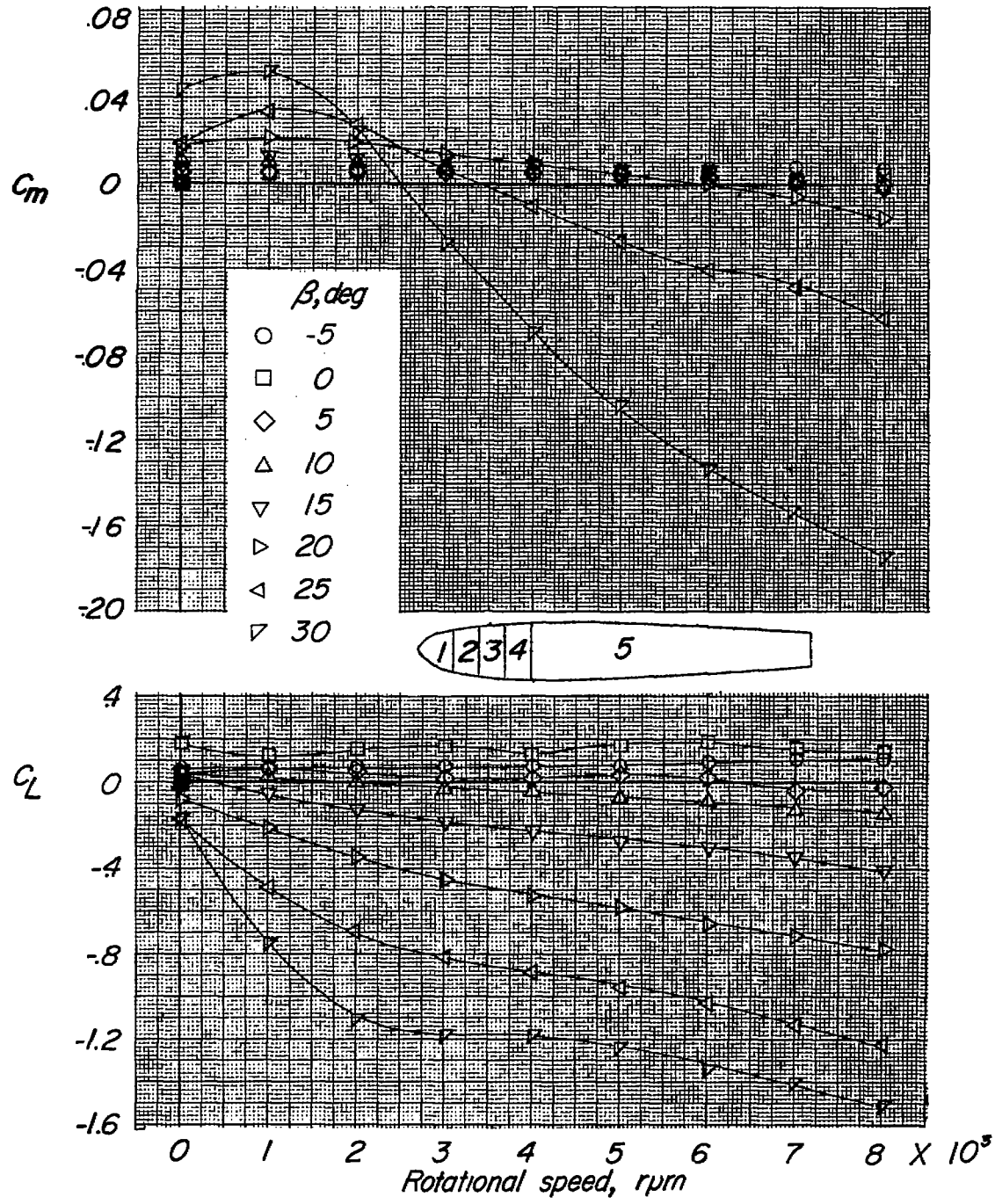

(c) C_m and C_L measured on sections 1, 2, 3, 4, and 5.

Figure 5.- Concluded.

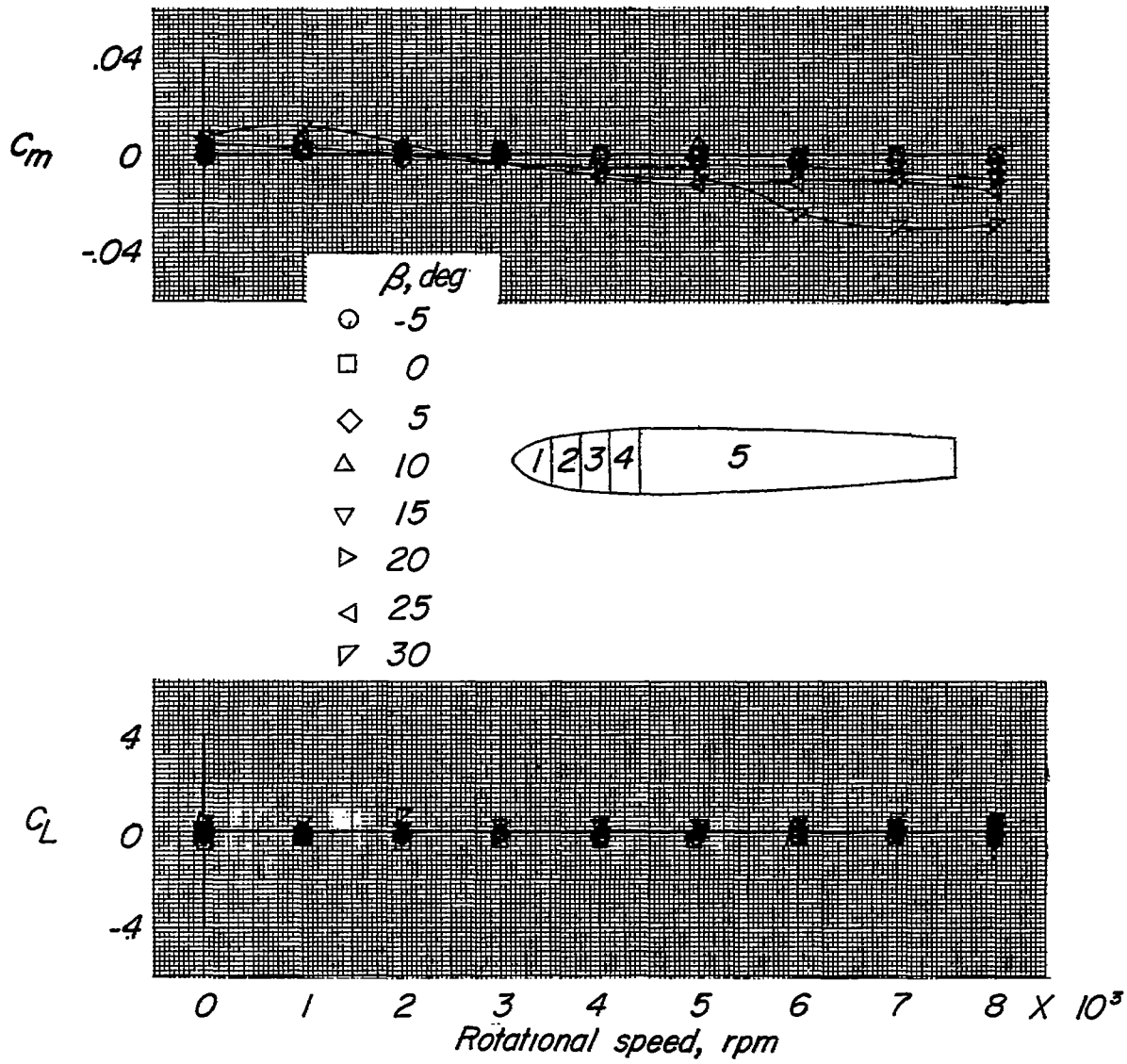

(a) C_m and C_L measured on sections 1, 2, and 3.

Figure 6.- Variation of C_m and C_L with rotational speed. Sections 1, 2, and 3 rotating; propeller off.

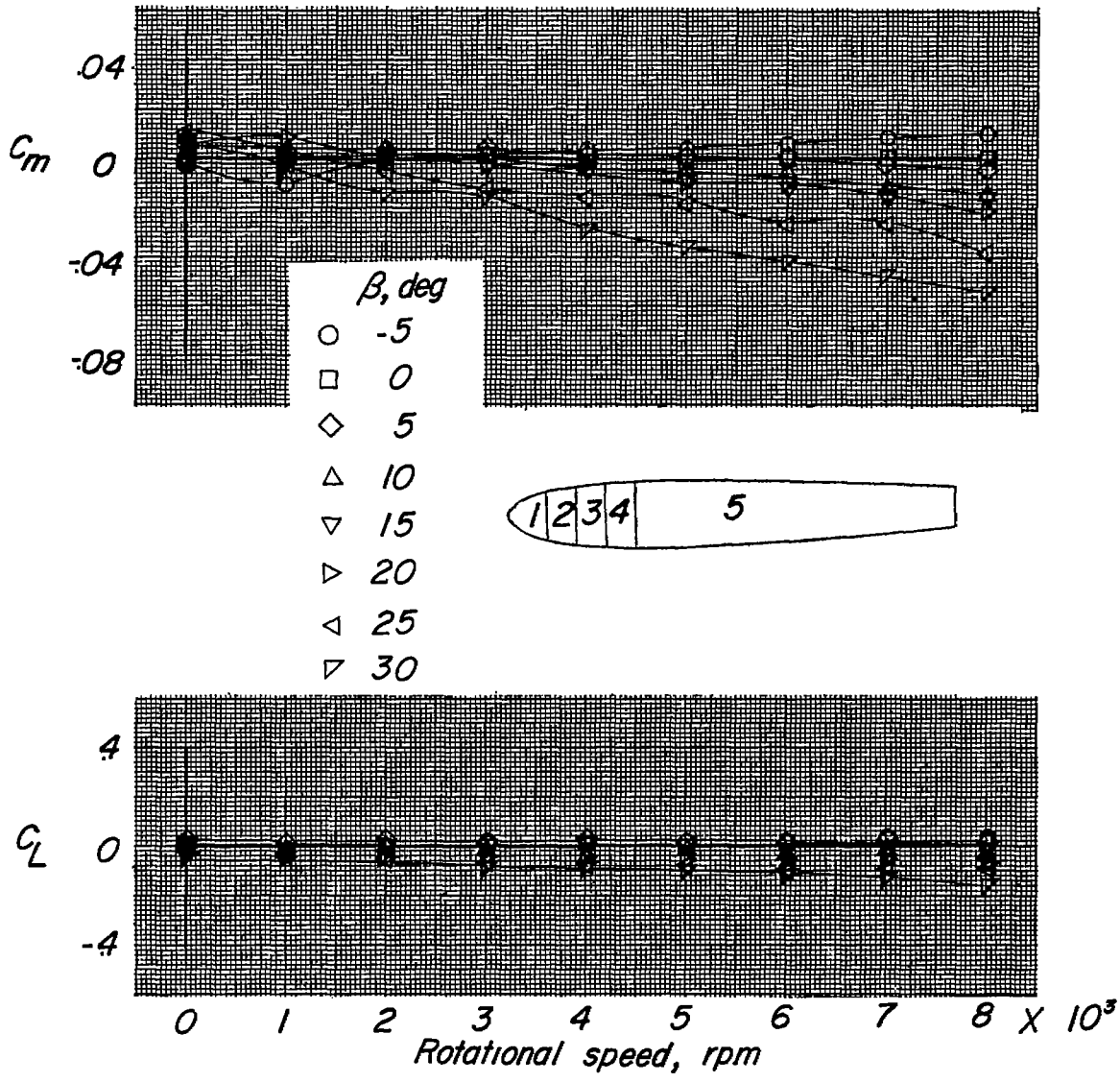

(b) C_m and C_L measured on sections 1, 2, 3, and 4.

Figure 6.- Continued.

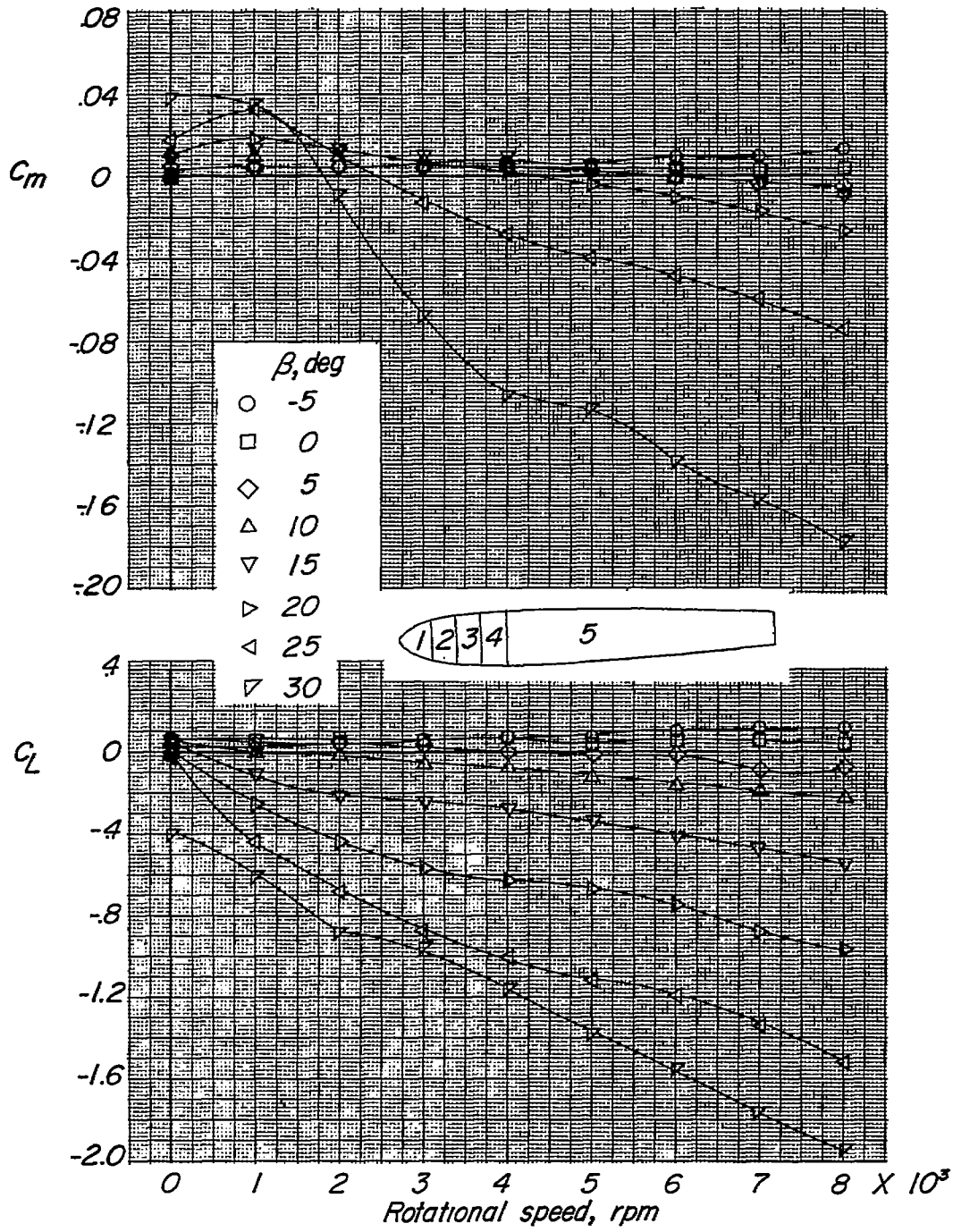

(c) C_m and C_L measured on sections 1, 2, 3, 4, and 5.

Figure 6.- Concluded.

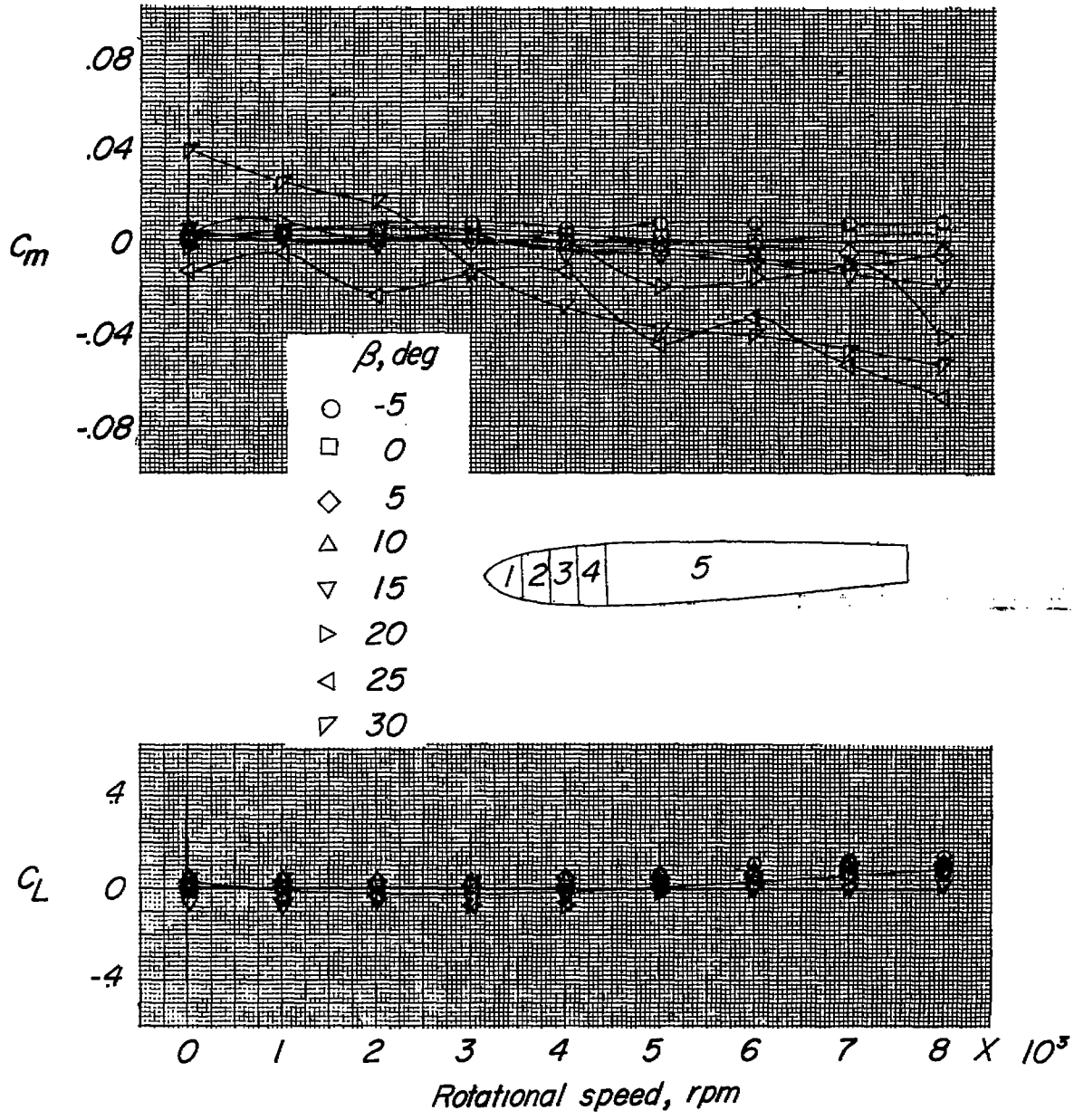

(a) C_m and C_L measured on sections 1, 2, 3, and 4.

Figure 7.- Variation of C_m and C_L with rotational speed. Sections 1, 2, 3, and 4 rotating; propeller off.

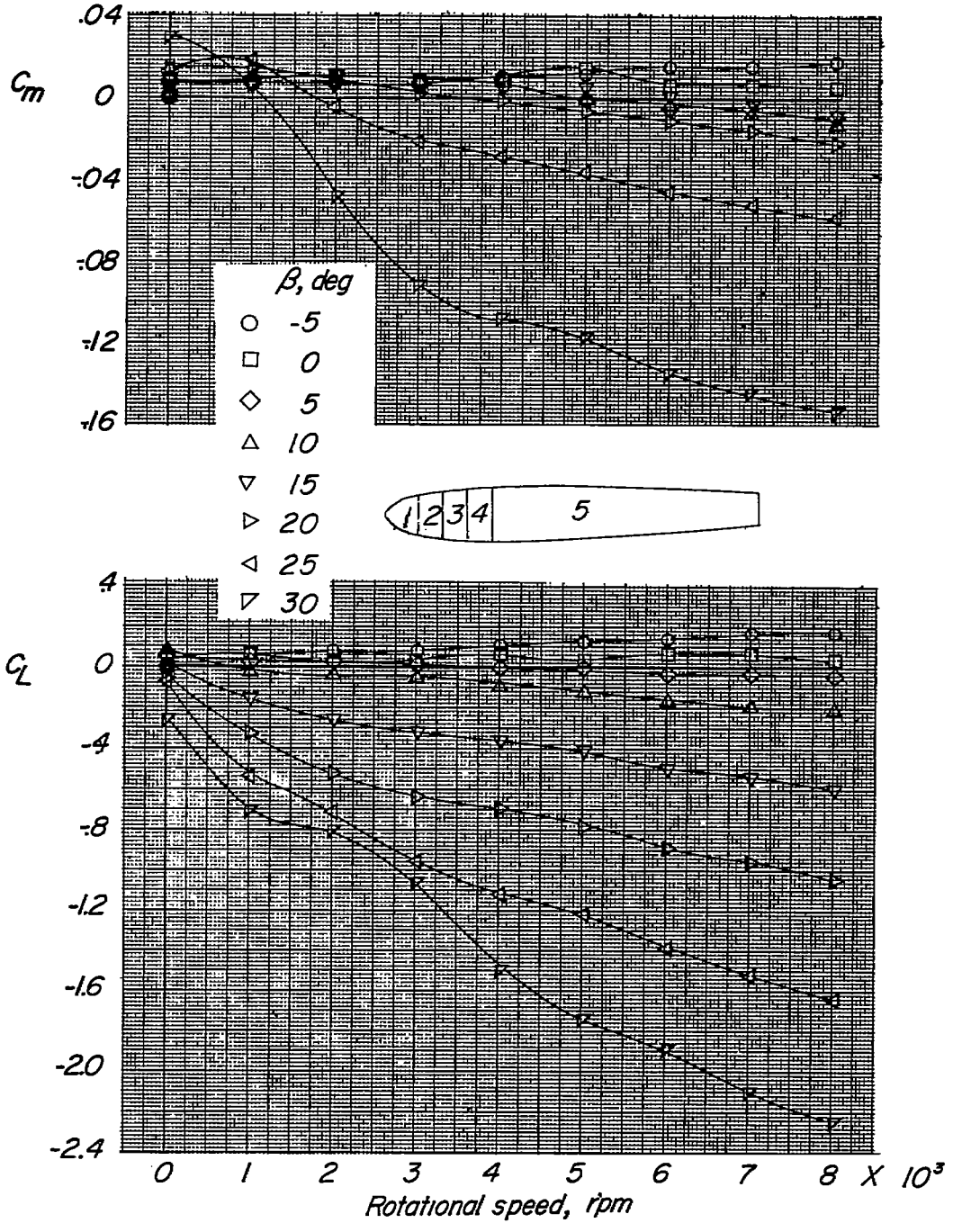

(b) C_m and C_L measured on sections 1, 2, 3, 4, and 5.

Figure 7.- Concluded.

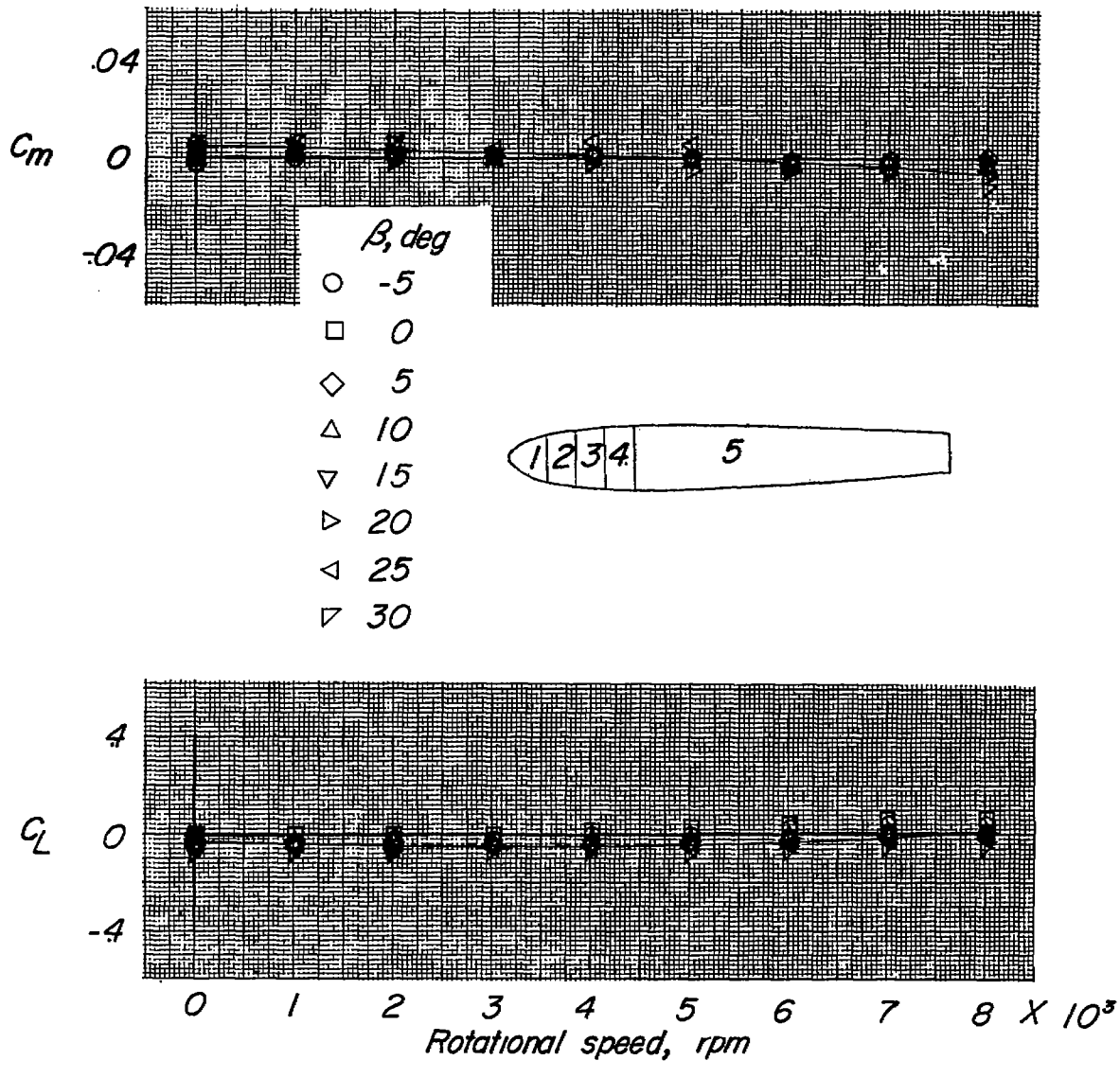

(a) C_m and C_L measured on sections 1 and 2.

Figure 8.- Variation of C_m and C_L with rotational speed. Section 2 rotating; propeller off.

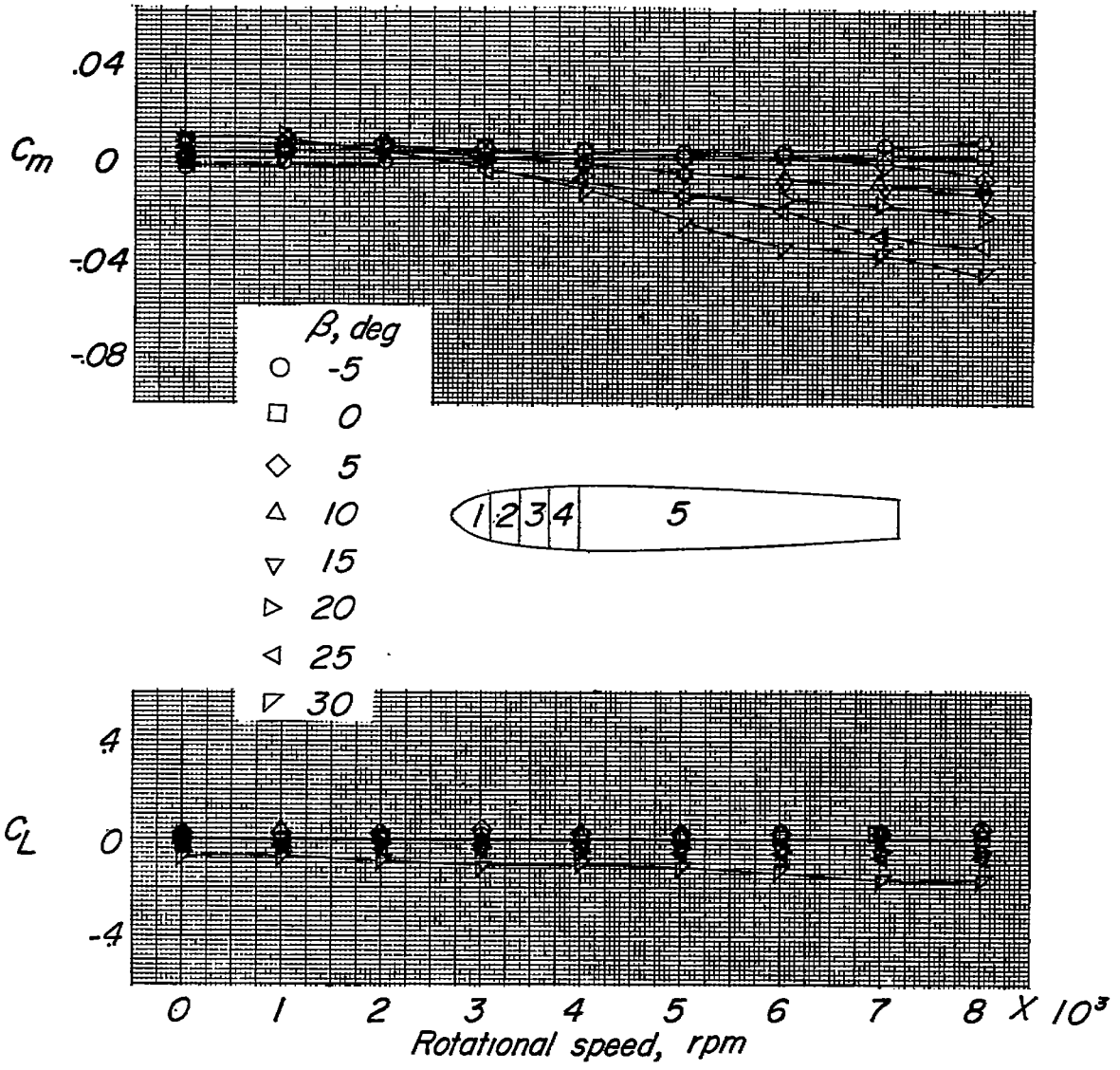

(b) C_m and C_L measured on sections 1, 2, 3, and 4.

Figure 8.- Continued.

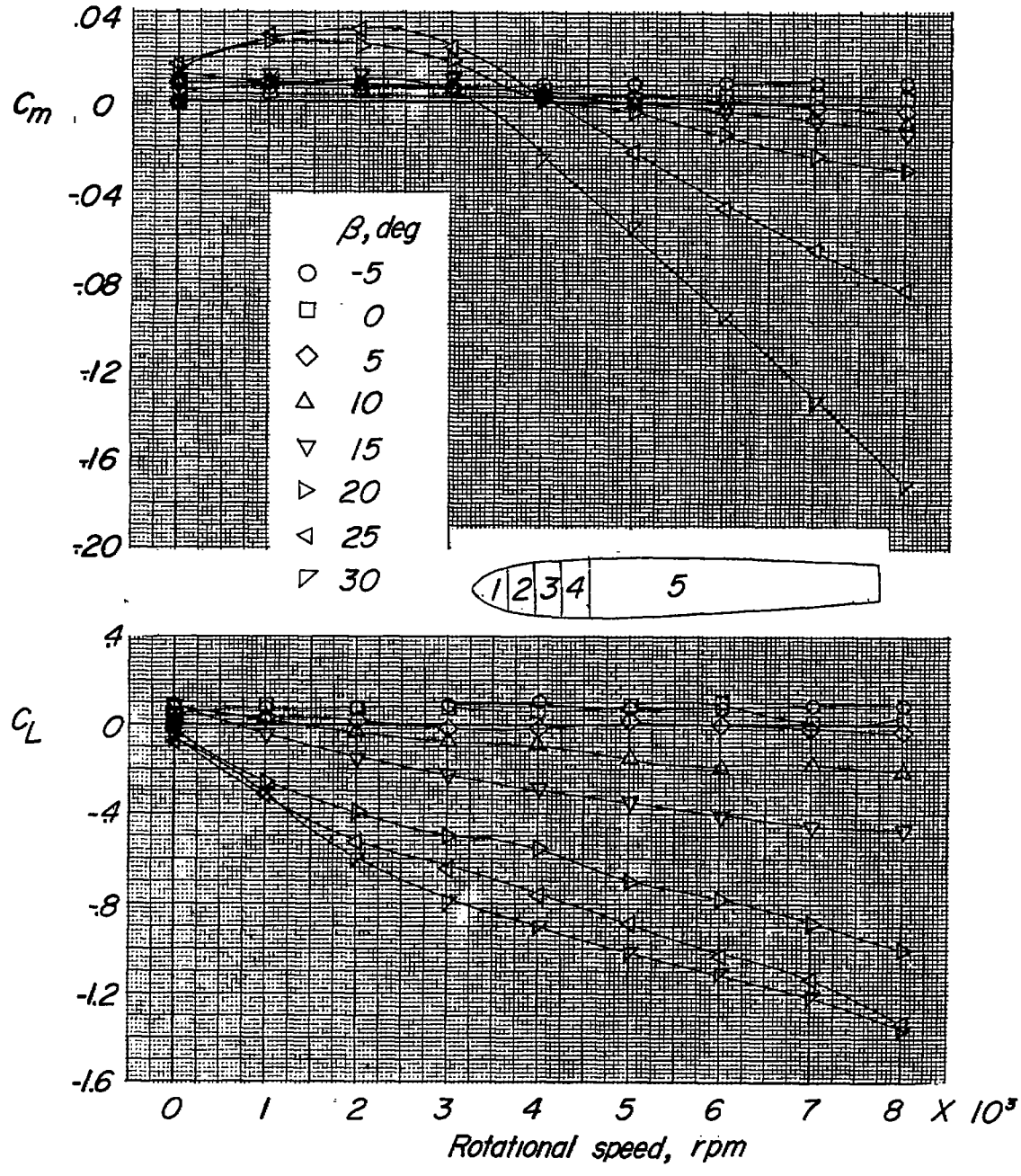

(c) C_m and C_L measured on sections 1, 2, 3, 4, and 5.

Figure 8.- Concluded.

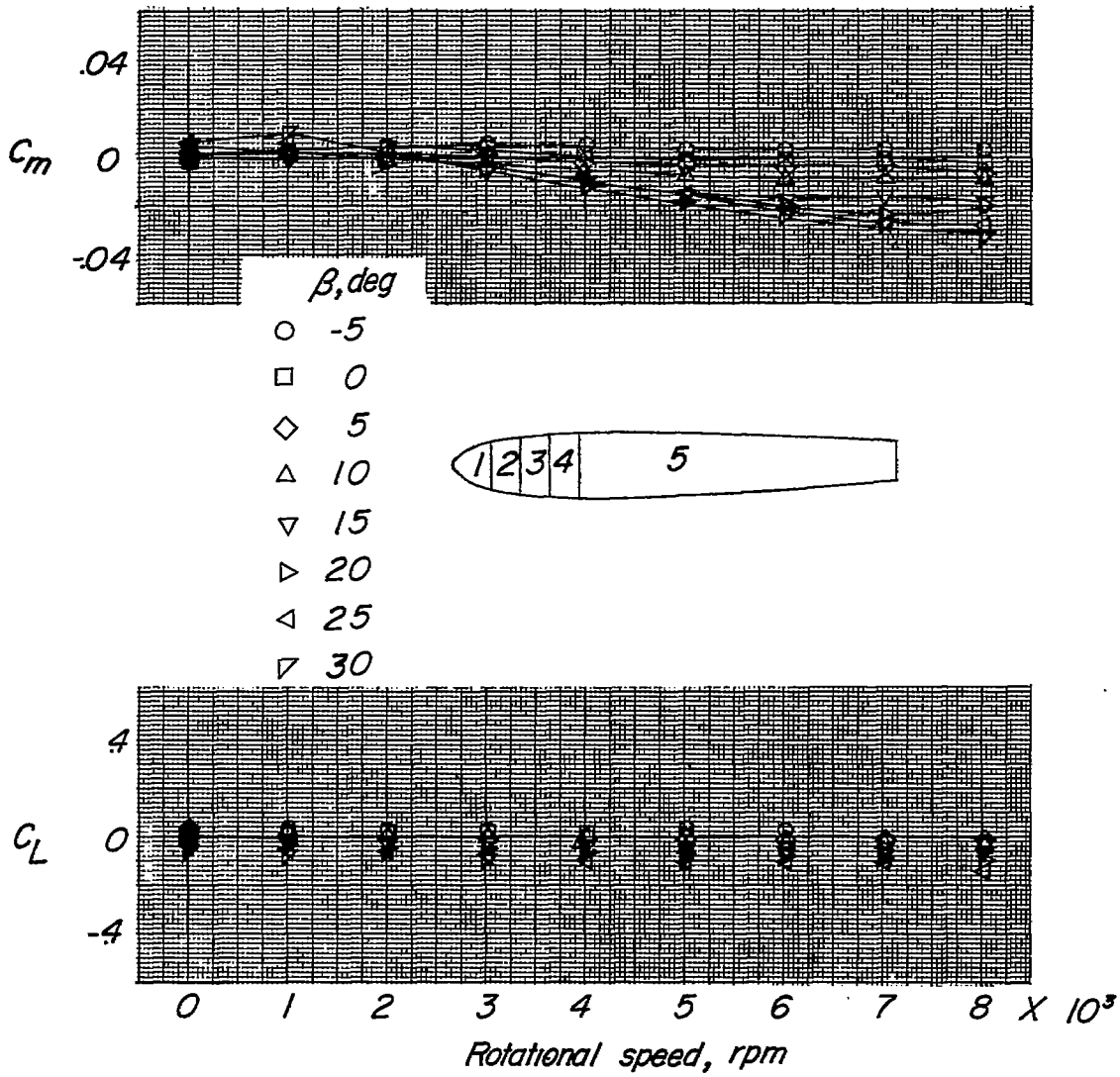

(a) C_m and C_L measured on sections 1, 2, and 3.

Figure 9.- Variation of C_m and C_L with rotational speed. Sections 2 and 3 rotating; propeller off.

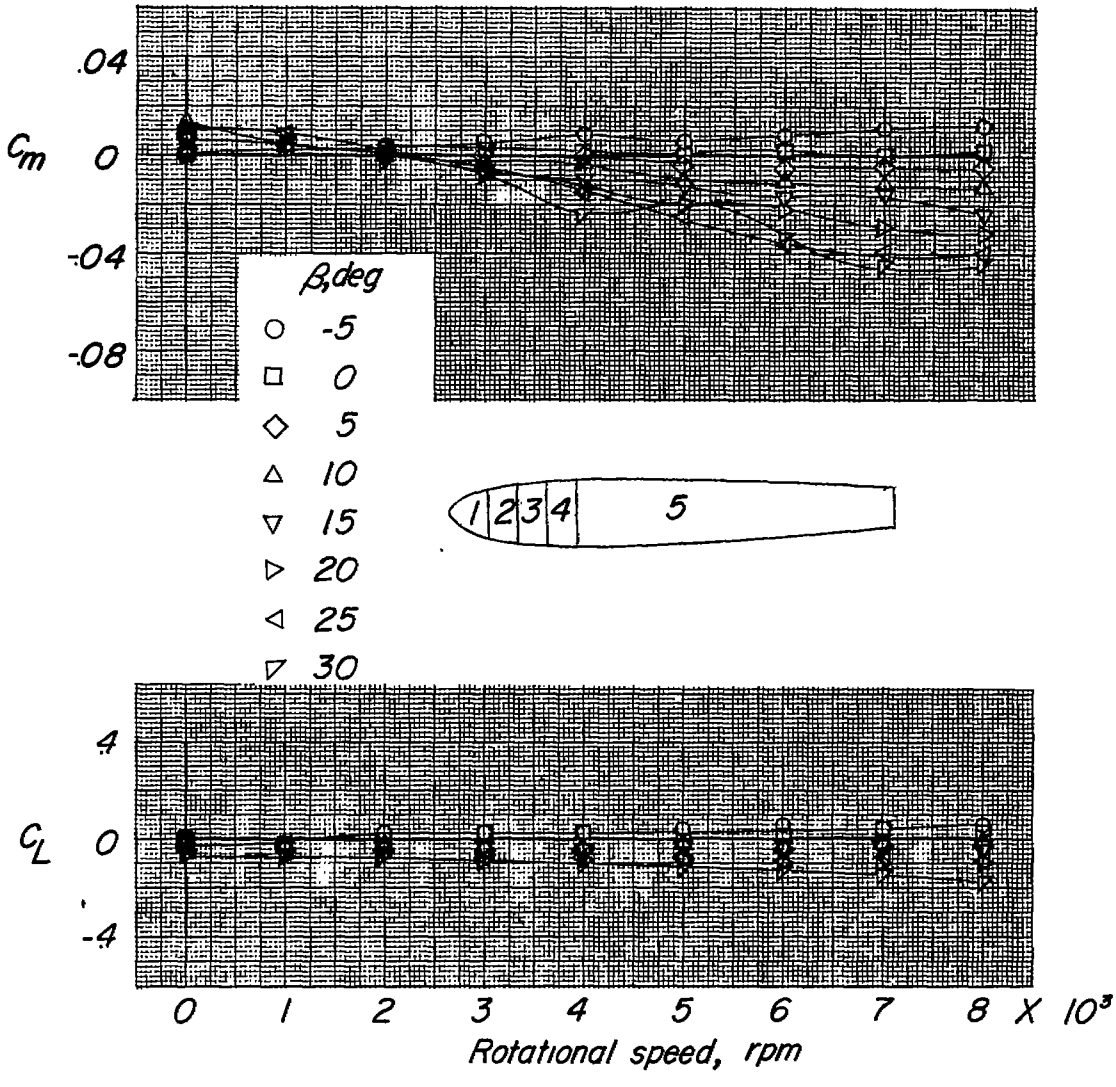

(b) C_m and C_L measured on sections 1, 2, 3, and 4.

Figure 9.- Continued.

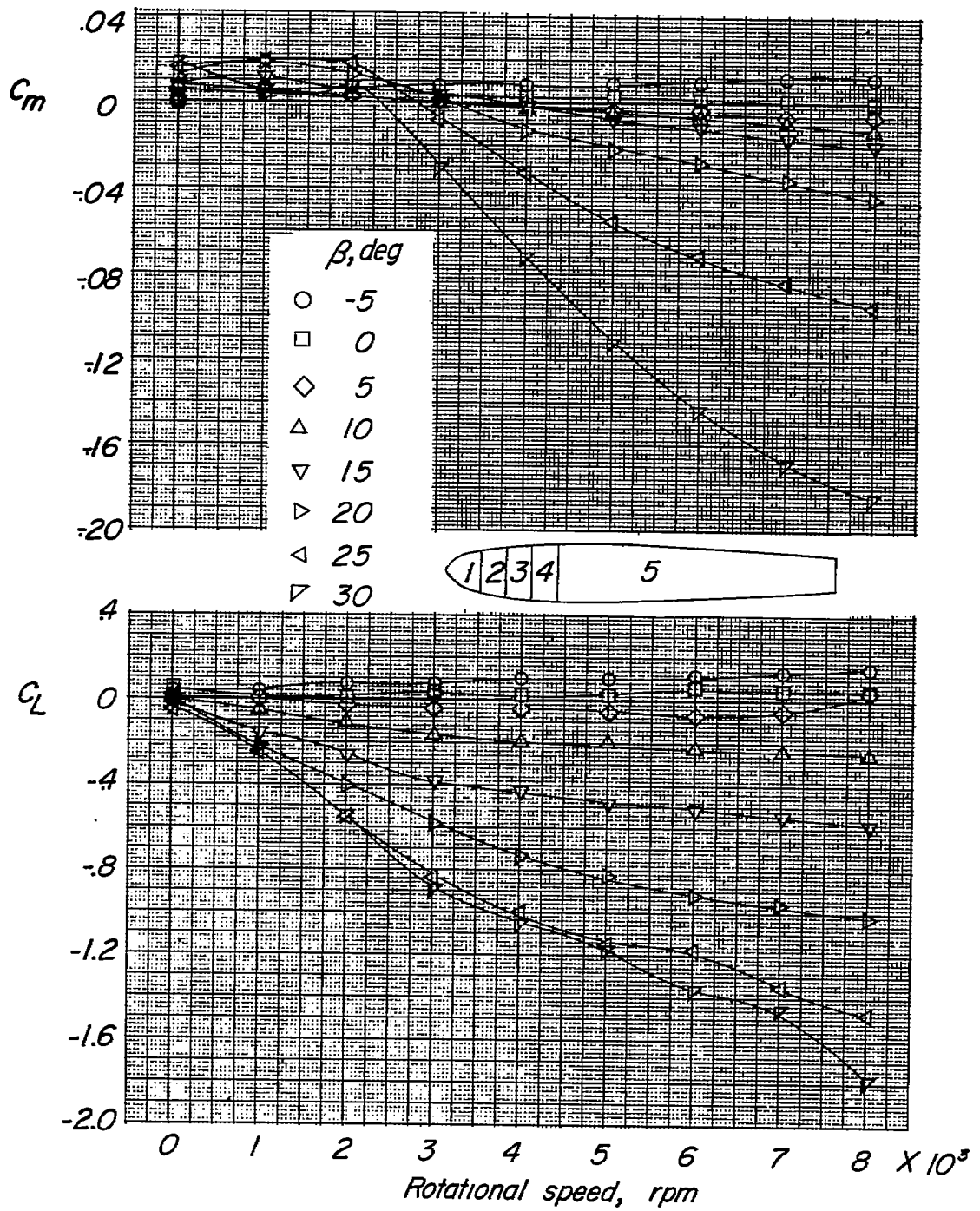

(c) C_m and C_L measured on sections 1, 2, 3, 4, and 5.

Figure 9.- Concluded.

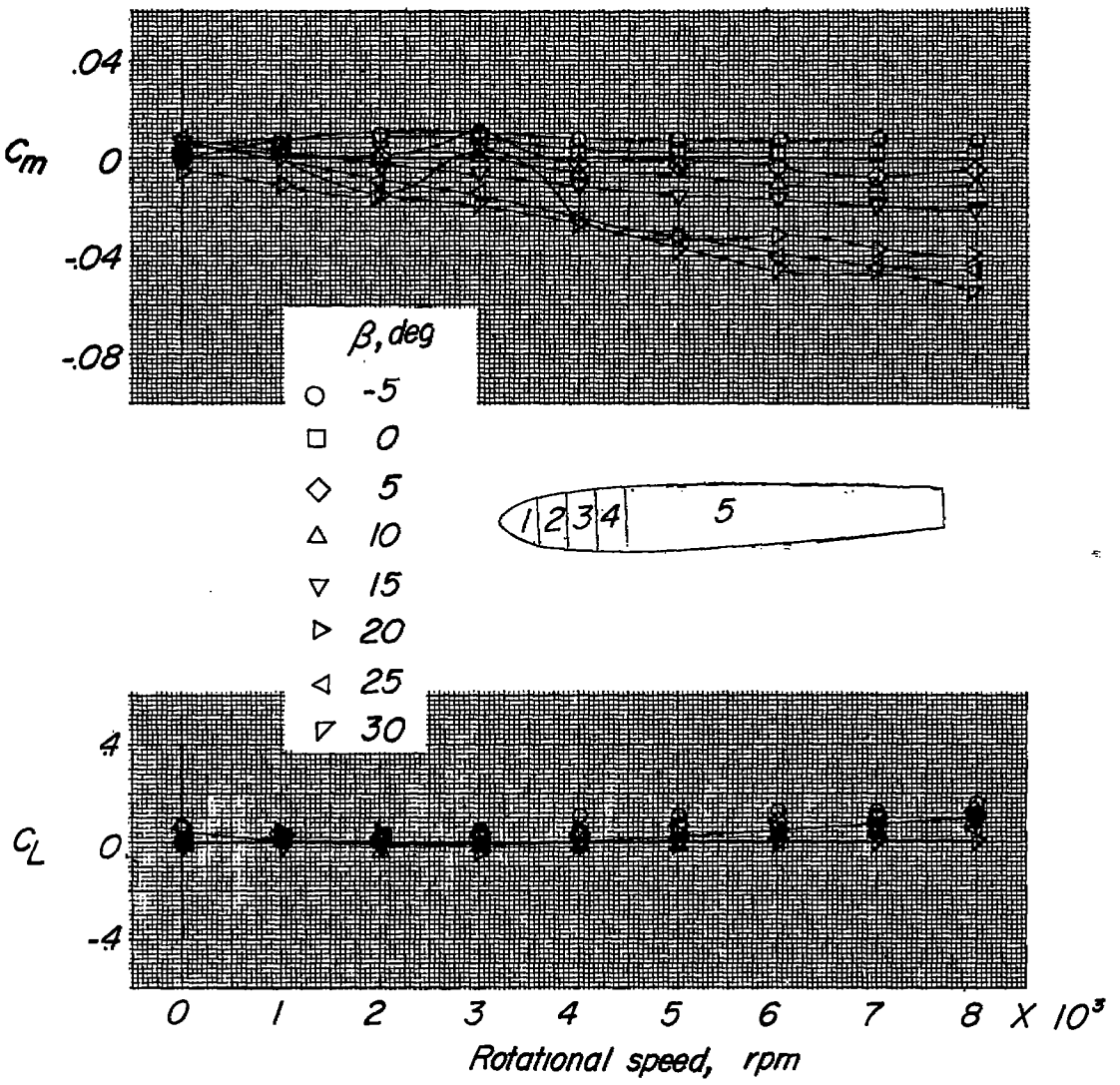

(a) C_m and C_L measured on sections 1, 2, 3, and 4.

Figure 10.- Variation of C_m and C_L with rotational speed. Sections 2, 3, and 4 rotating; propeller off.

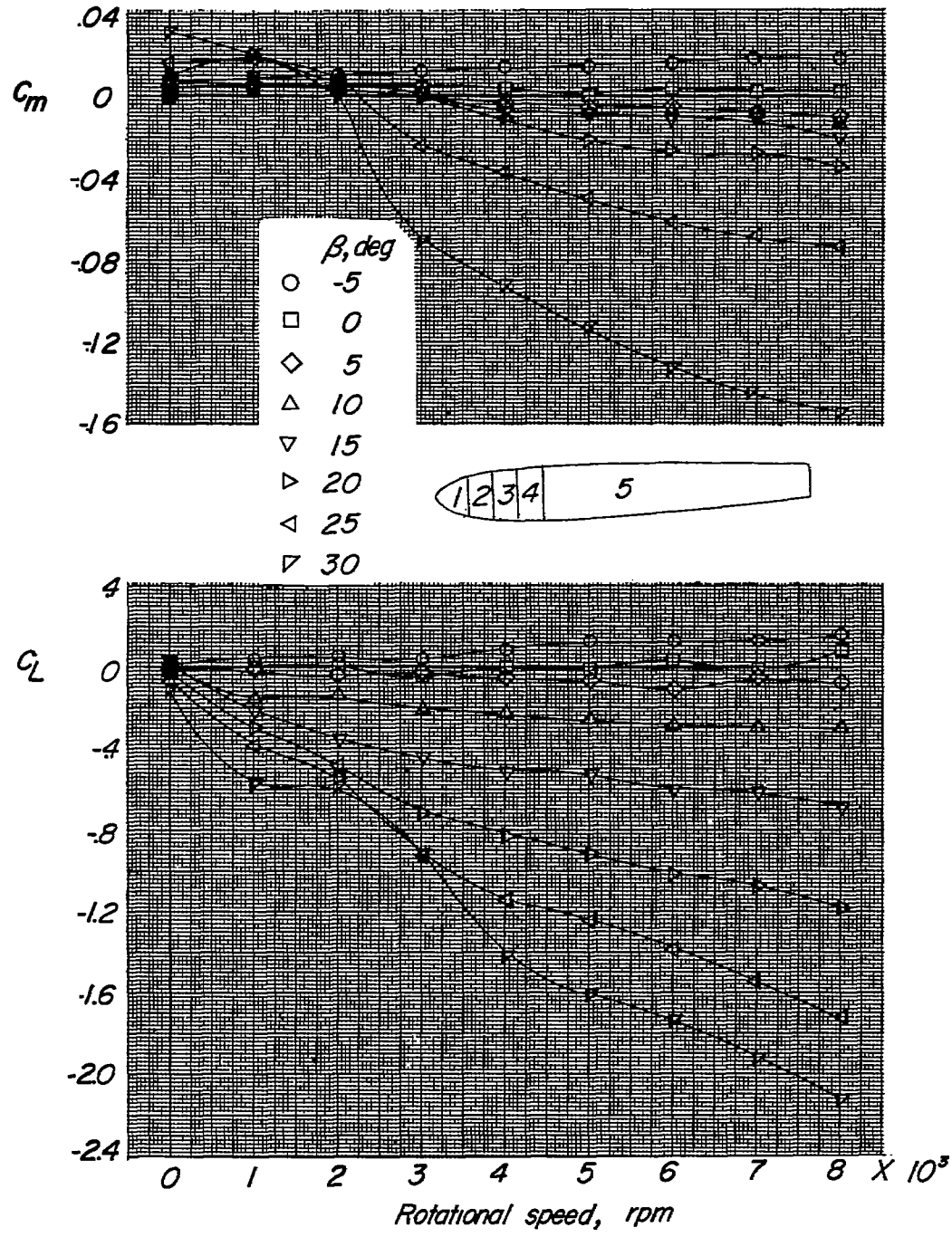

(b) C_m and C_L measured on sections 1, 2, 3, 4, and 5.

Figure 10.- Concluded.

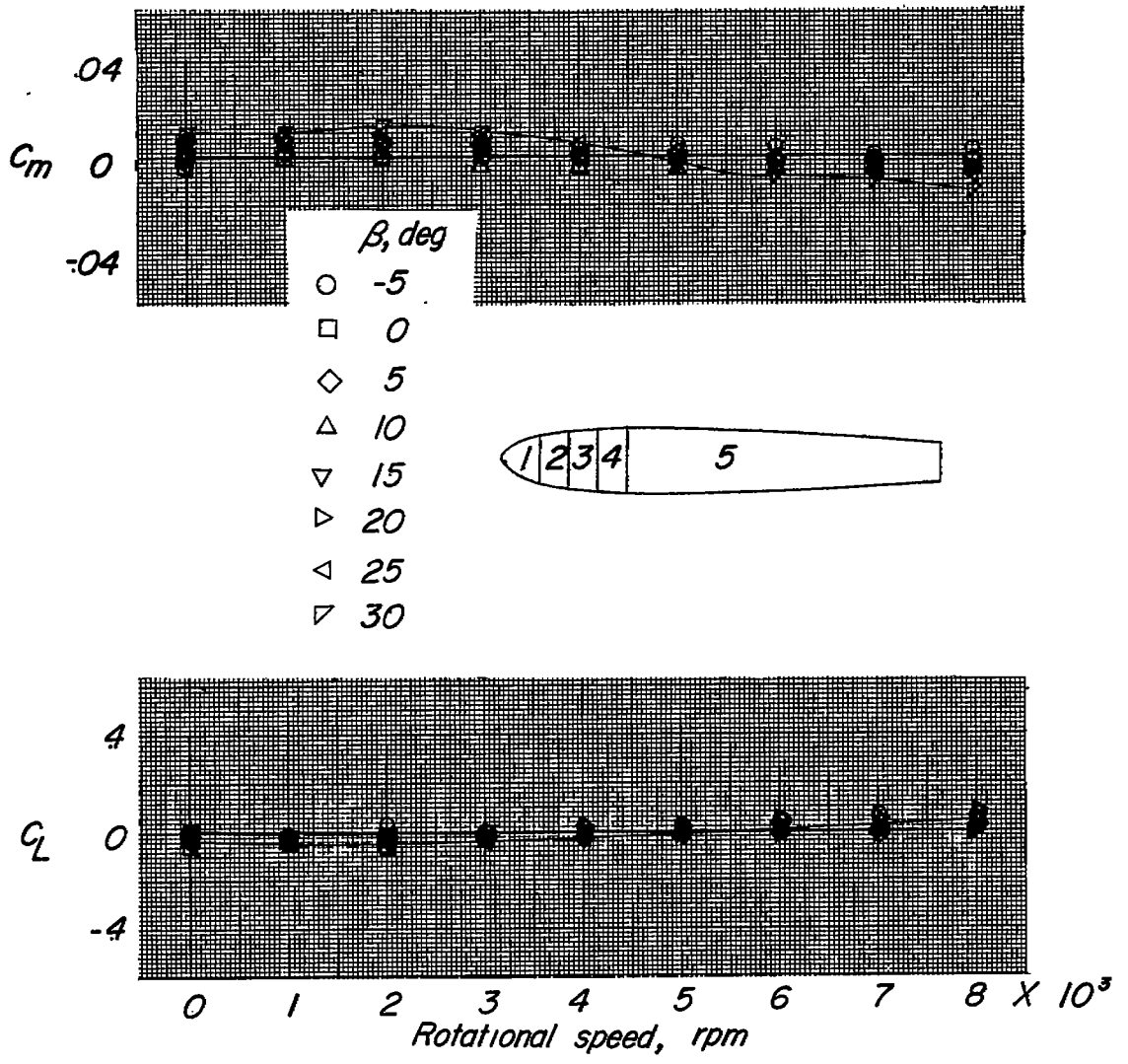

(a) C_m and C_L measured on sections 1, 2, and 3.

Figure 11.- Variation of C_m and C_L with rotational speed. Section 3 rotating; propeller off.

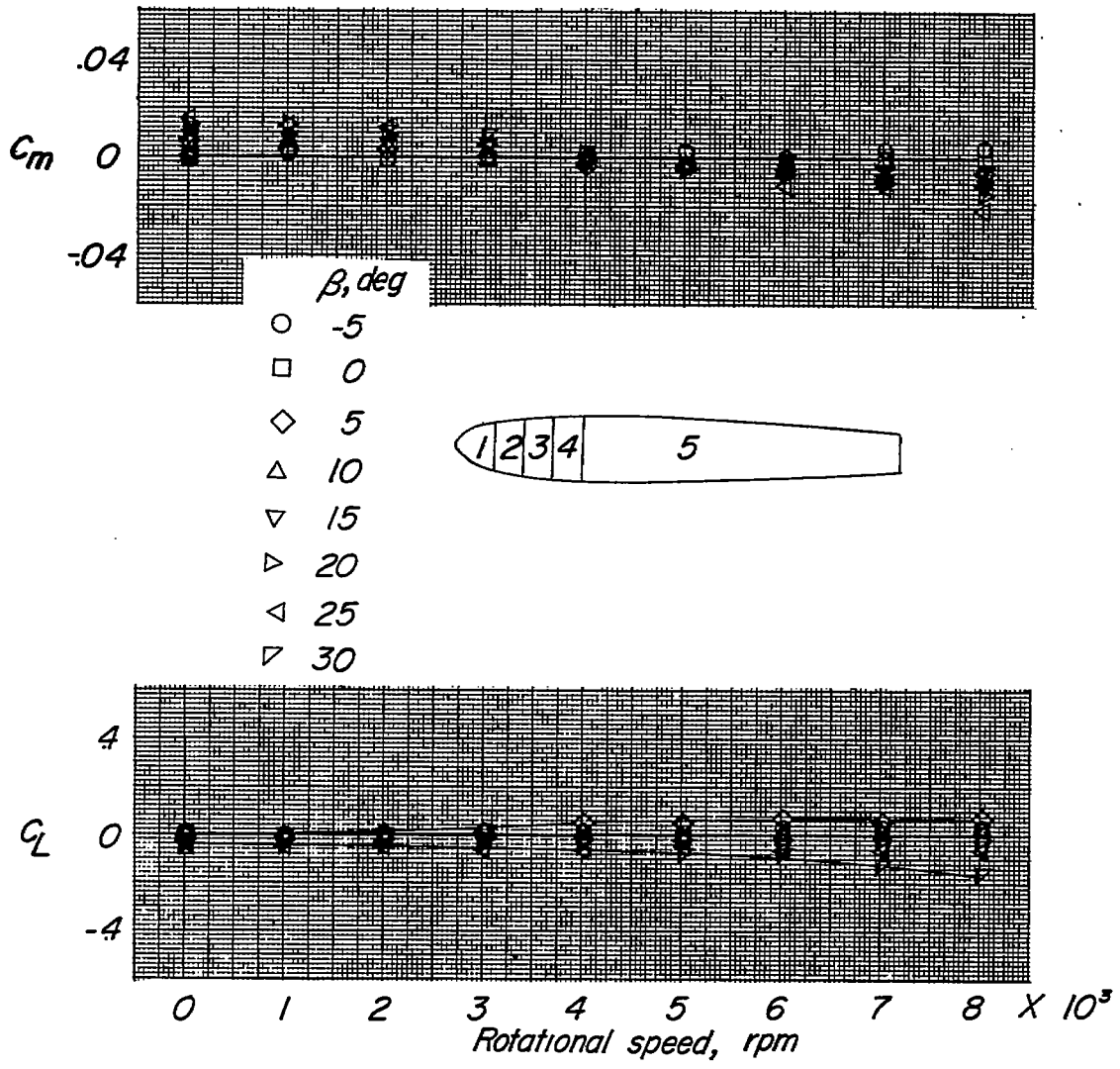

(b) C_m and C_L measured on sections 1, 2, 3, and 4.

Figure 11.- Continued.

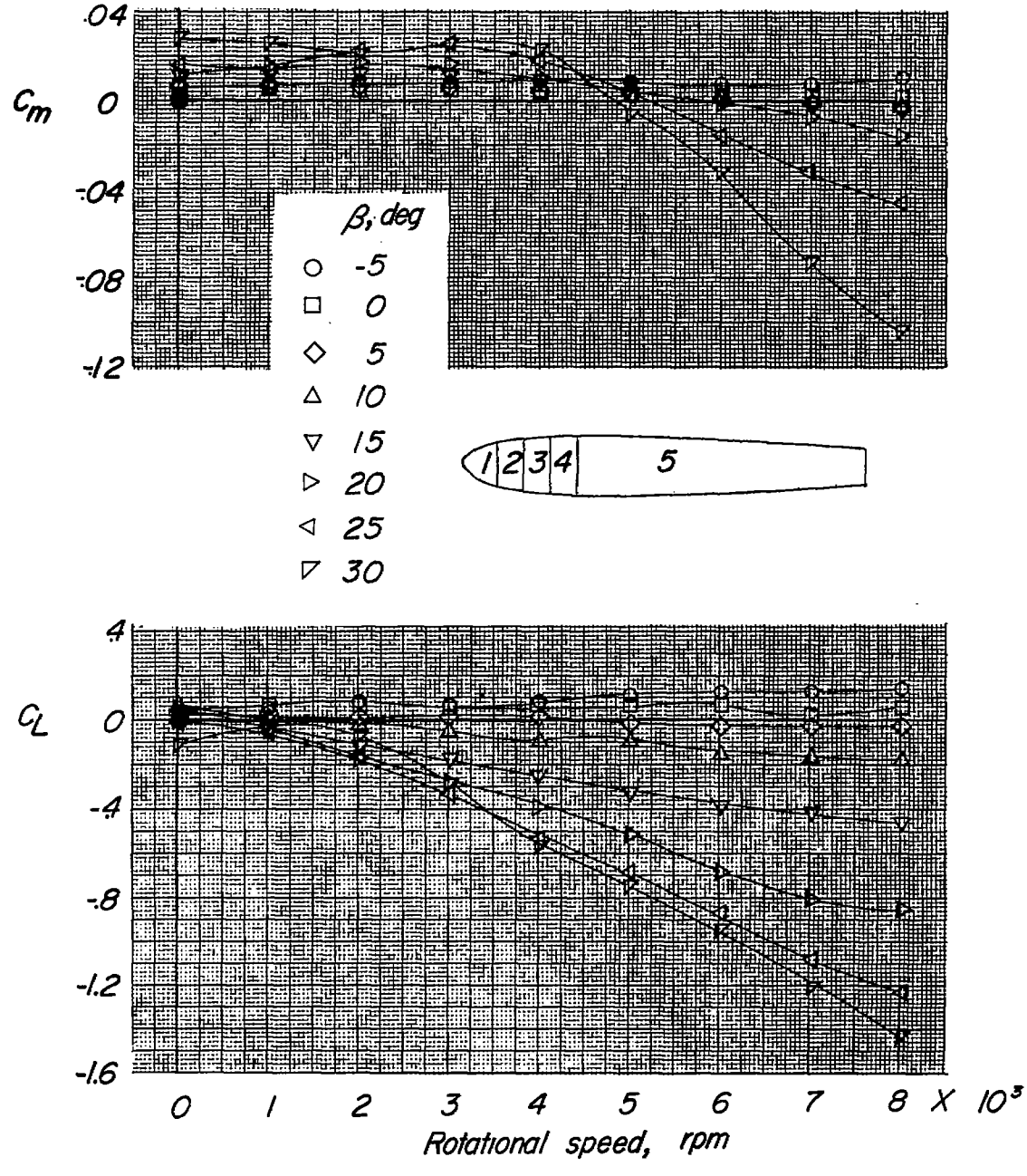

(c) C_m and C_L measured on sections 1, 2, 3, 4, and 5.

Figure 11.- Concluded.

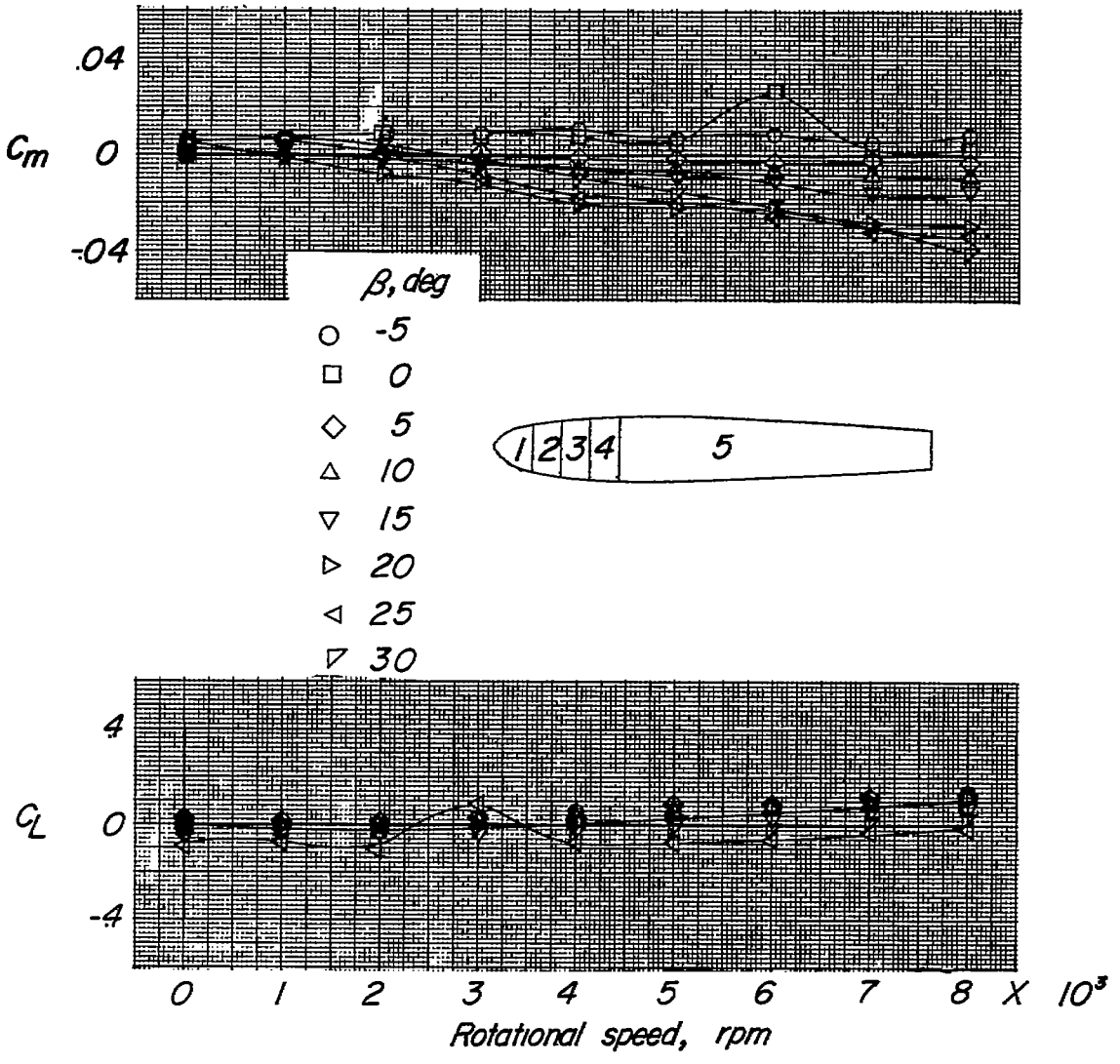

(a) C_m and C_L measured on sections 1, 2, 3, and 4.

Figure 12.- Variation of C_m and C_L with rotational speed. Sections 3 and 4 rotating; propeller off.

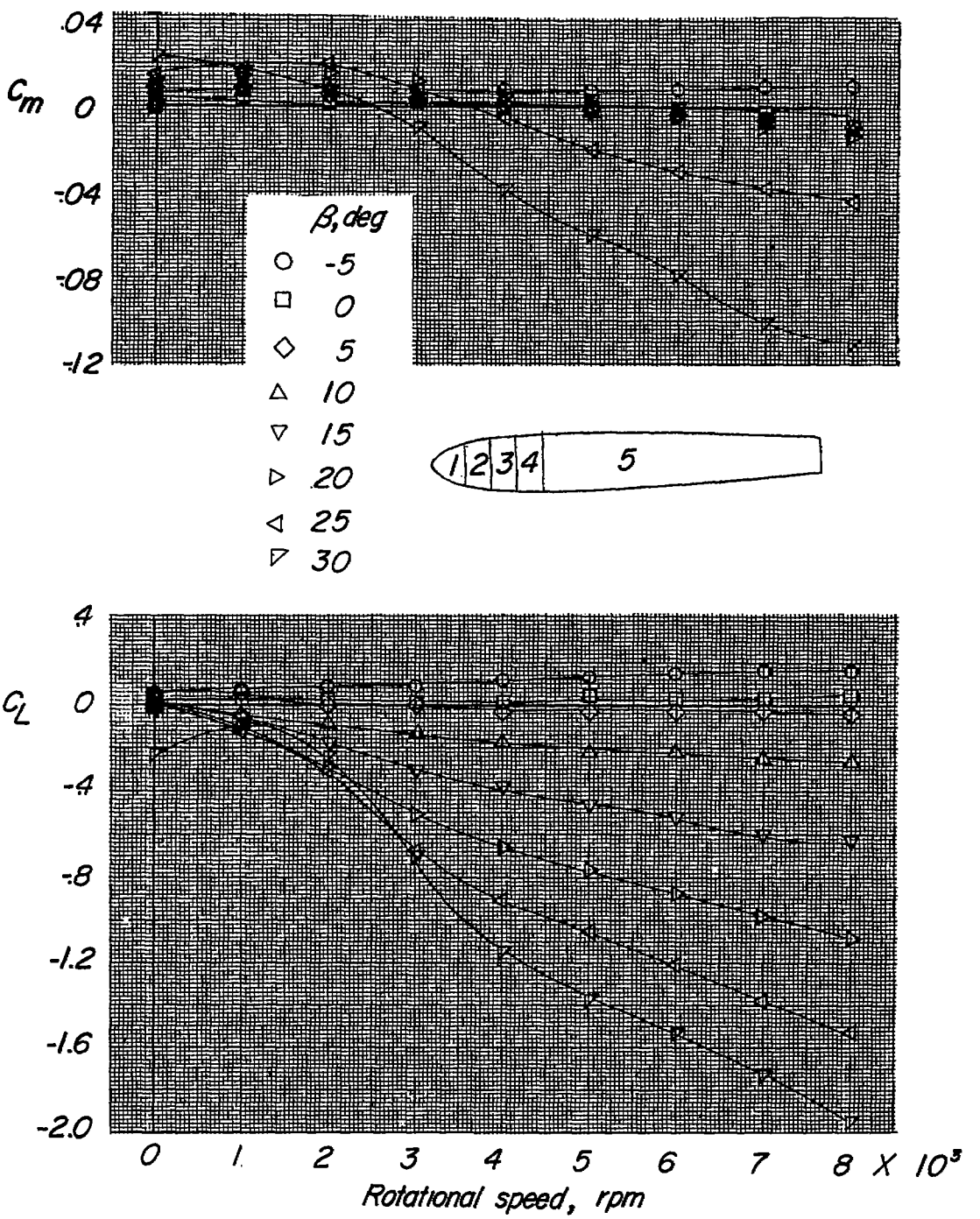

(b) C_m and C_L measured on sections 1, 2, 3, 4, and 5.

Figure 12.- Concluded.

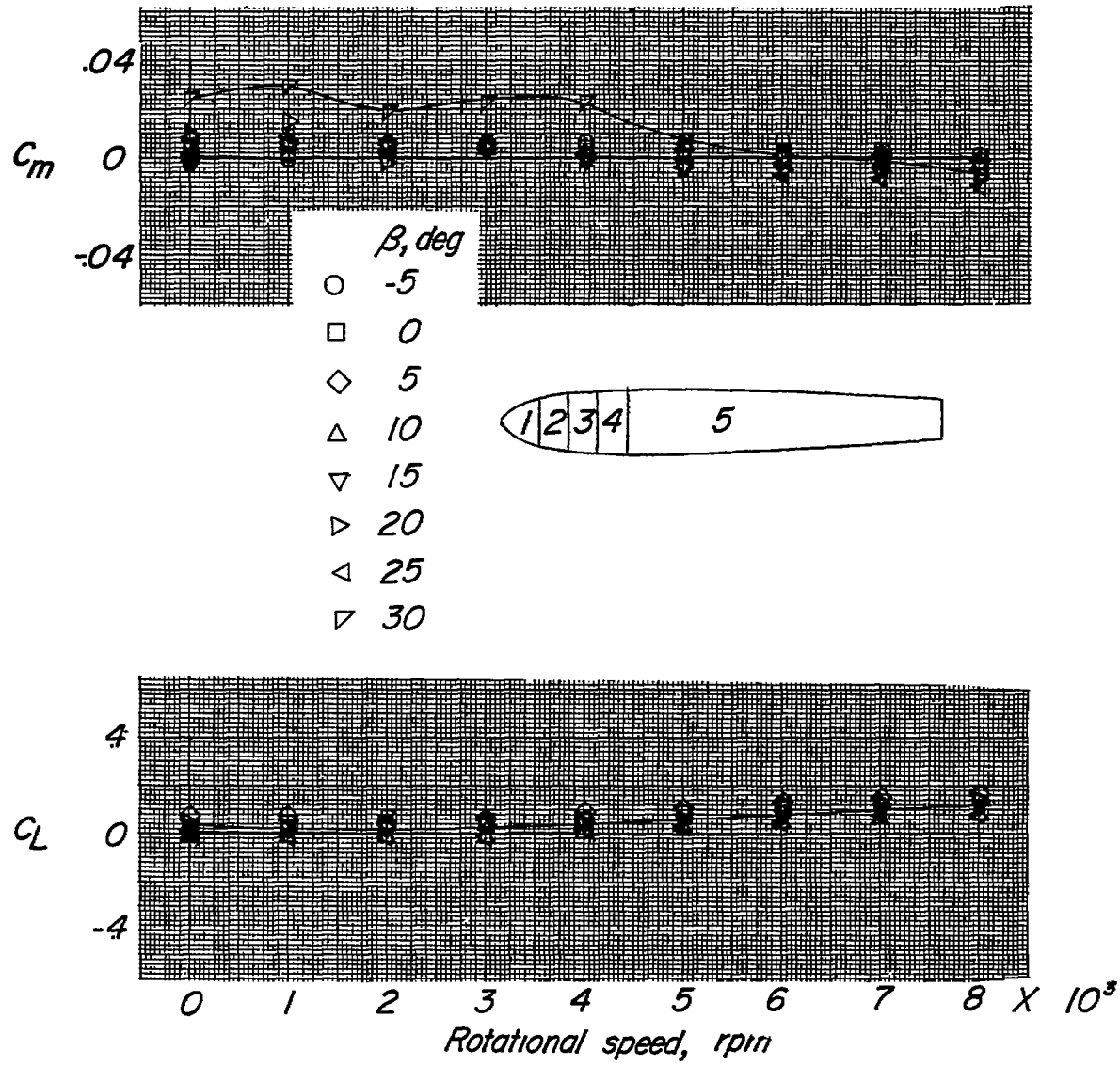

(a) C_m and C_L measured on sections 1, 2, 3, and 4.

Figure 13.- Variation of C_m and C_L with rotational speed. Section 4 rotating; propeller off.

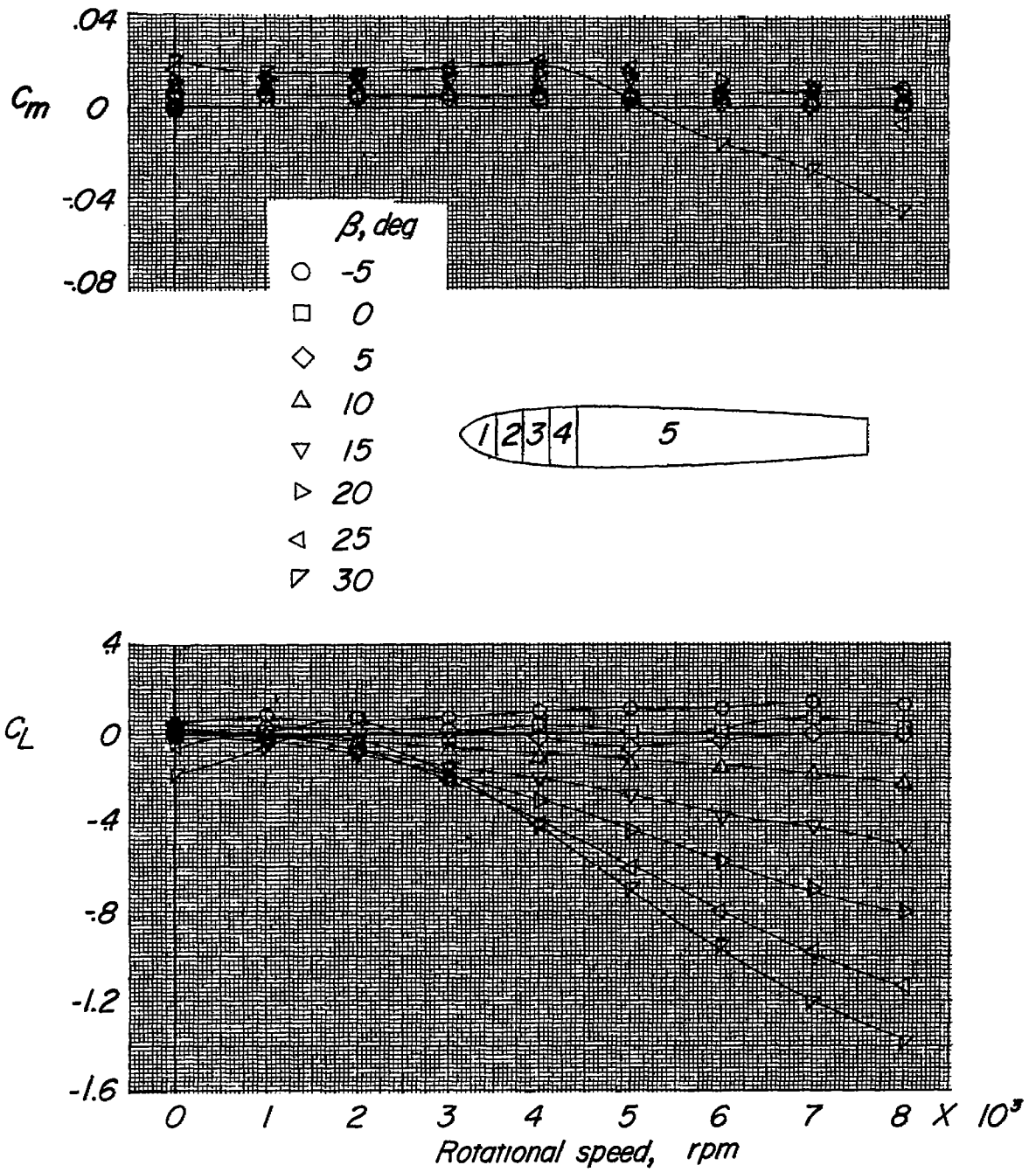

(b) C_m and C_L measured on sections 1, 2, 3, 4, and 5.

Figure 13.- Concluded.

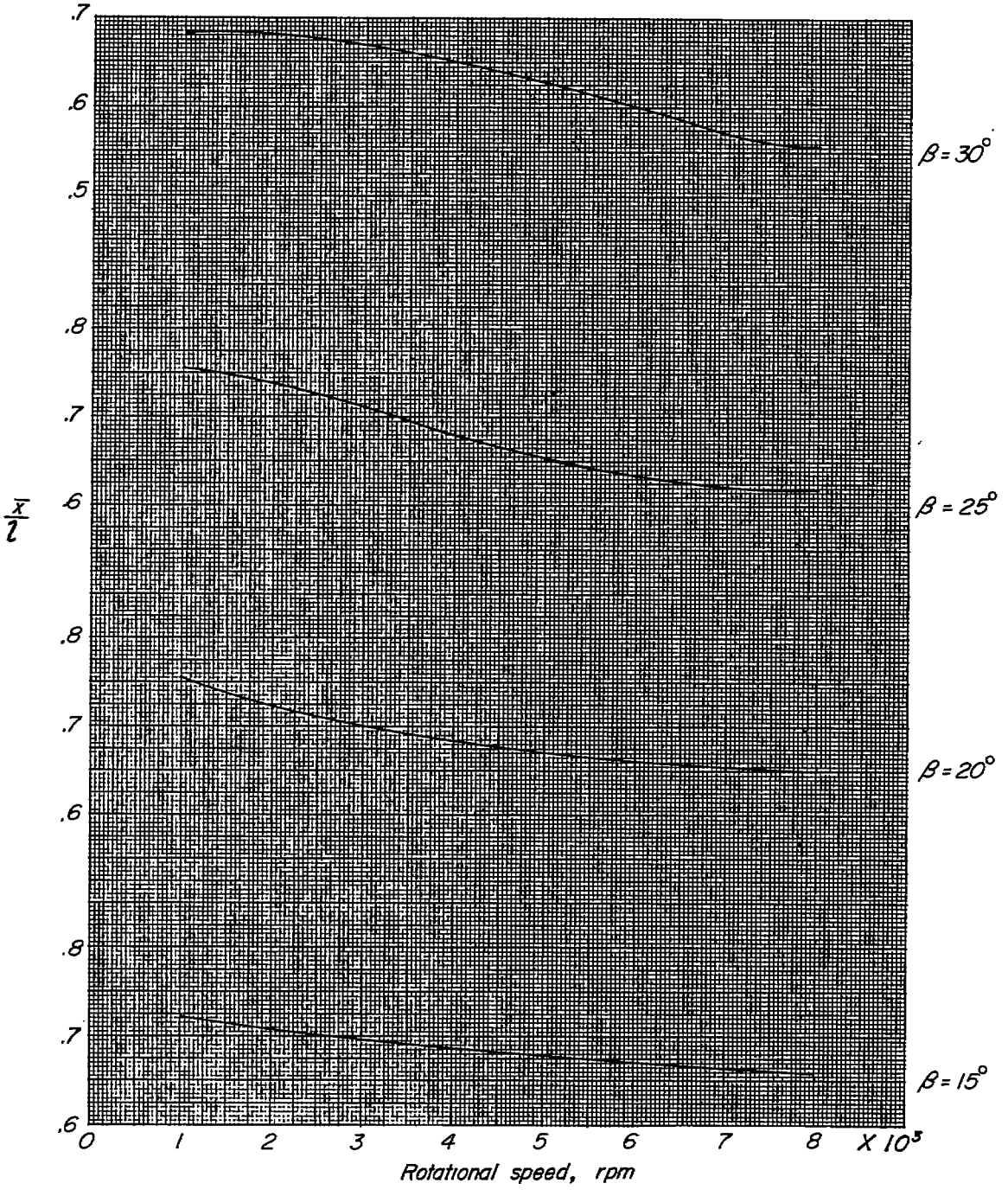

Figure 14.- Variation of center of pressure of Magnus force with rotational speed. Section 2 rotating; force measured on sections 1, 2, 3, 4, and 5; propeller off.

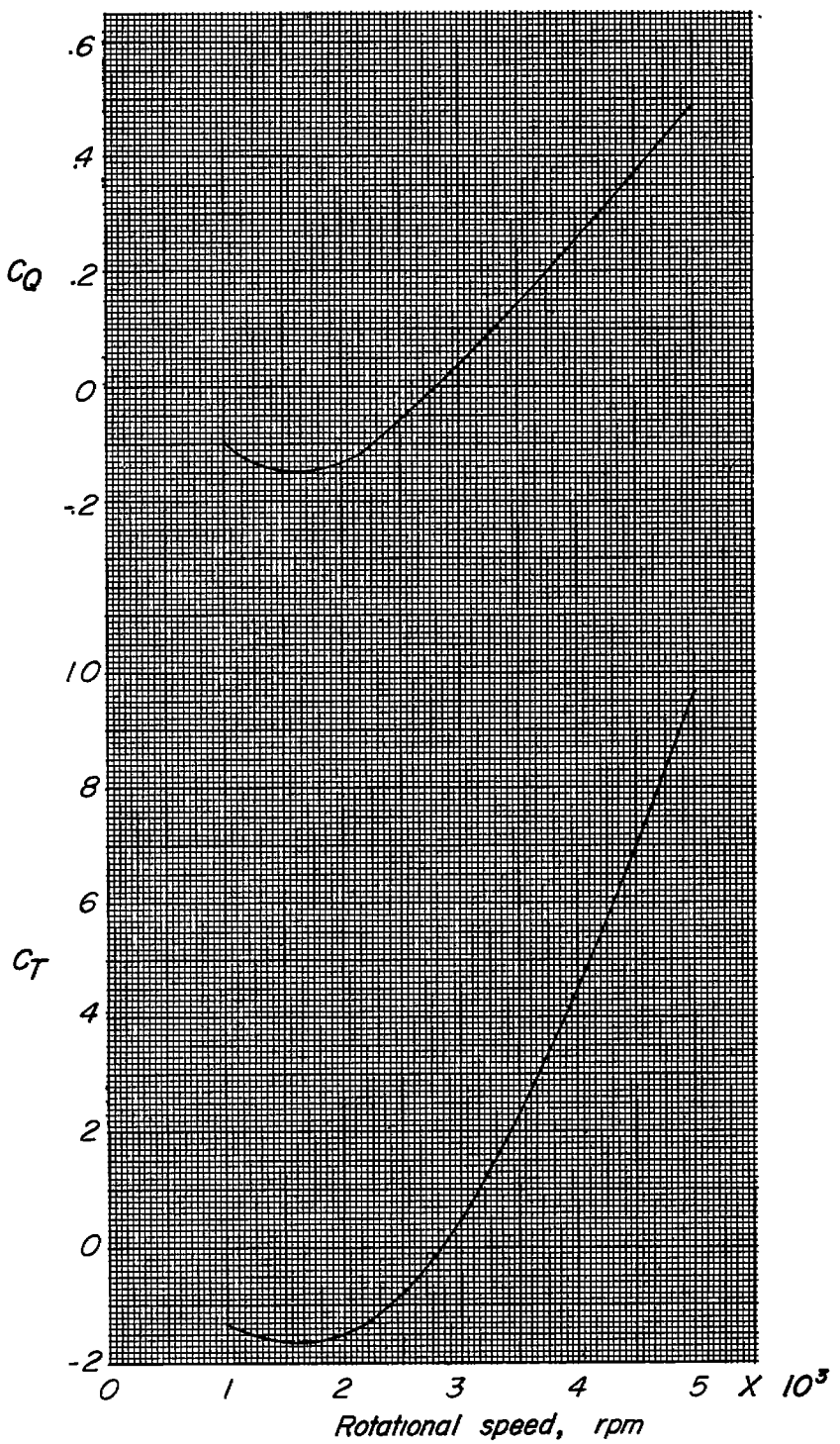

Figure 15.- Thrust and torque characteristics of the propeller mounted on section 1 of the body. $\beta = 0^\circ$.

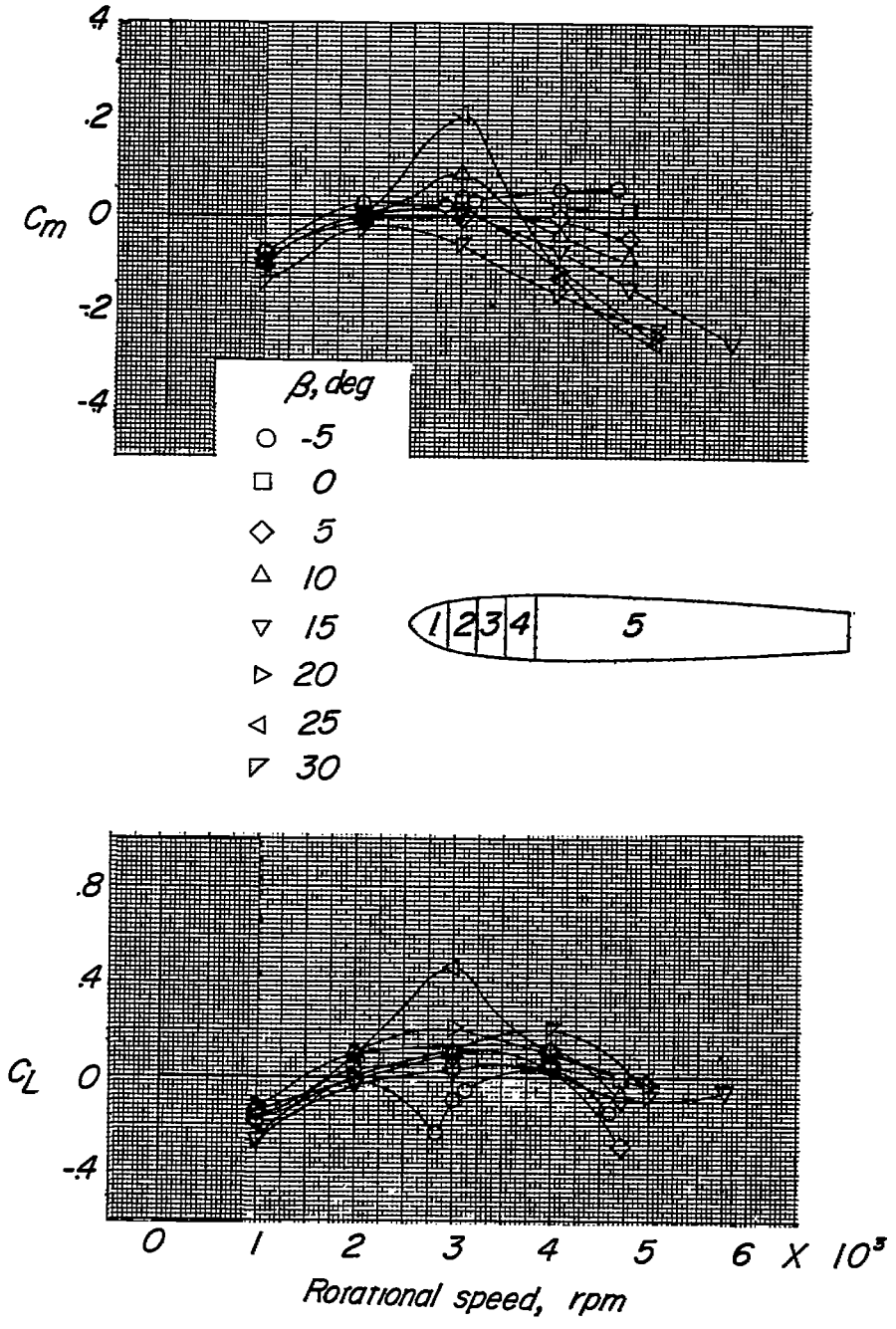

(a) C_m and C_L measured on section 1.

Figure 16.- Variation of C_m and C_L with rotational speed. Section 1 rotating; propeller on.

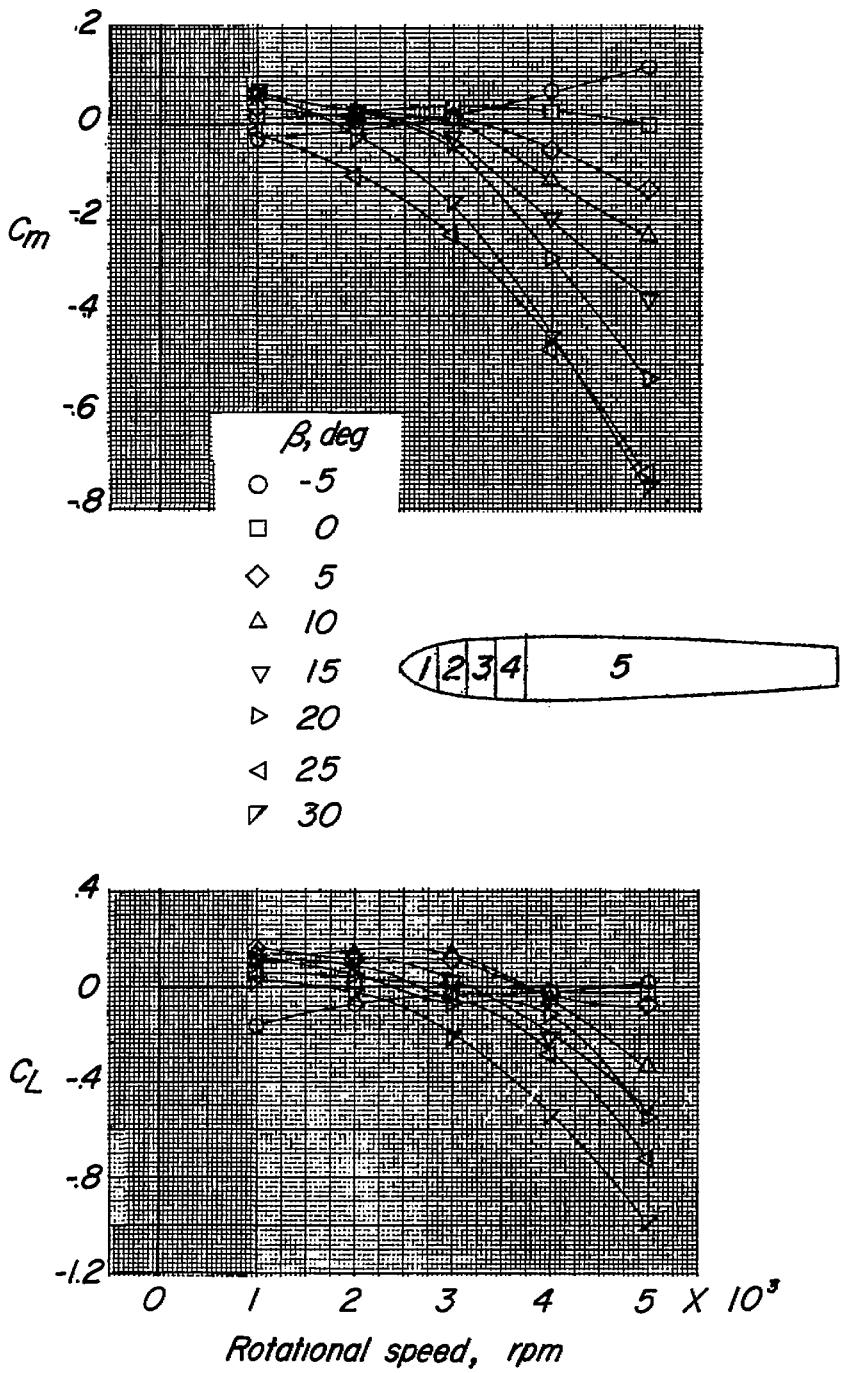

(b) C_m and C_L measured on sections 1, 2, 3, and 4.

Figure 16.- Continued.

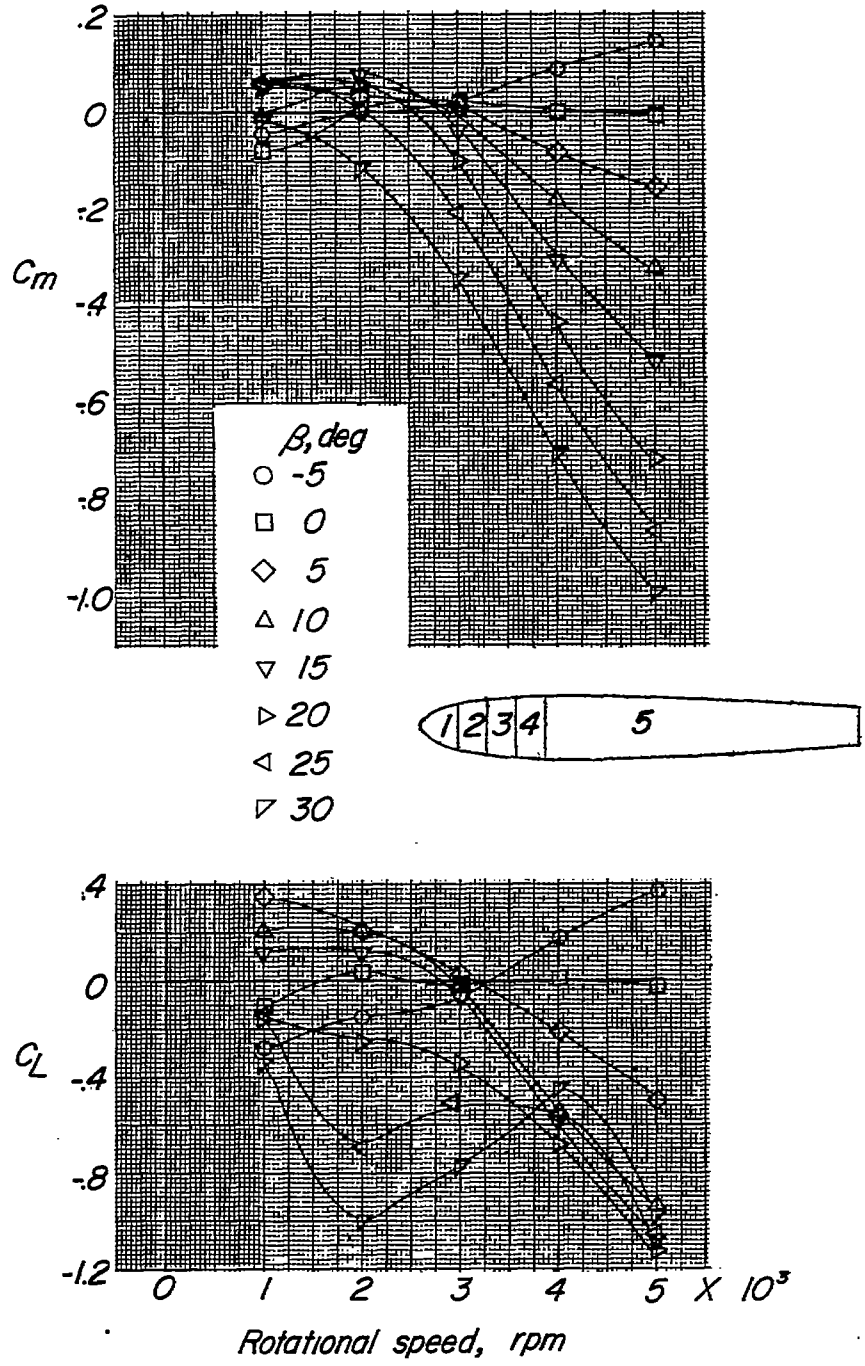

(c) C_m and C_L measured on sections 1, 2, 3, 4, and 5.

Figure 16.- Concluded.

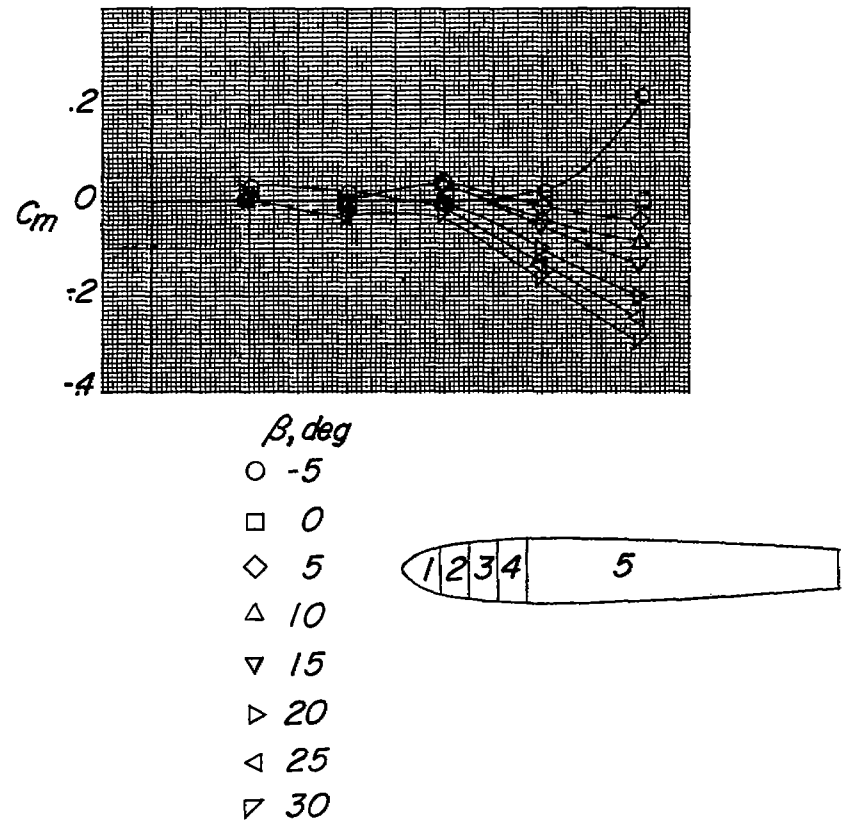

(a) C_m and C_L measured on sections 1 and 2.

Figure 17.- Variation of C_m and C_L with rotational speed. Sections 1 and 2 rotating; propeller on section 2.

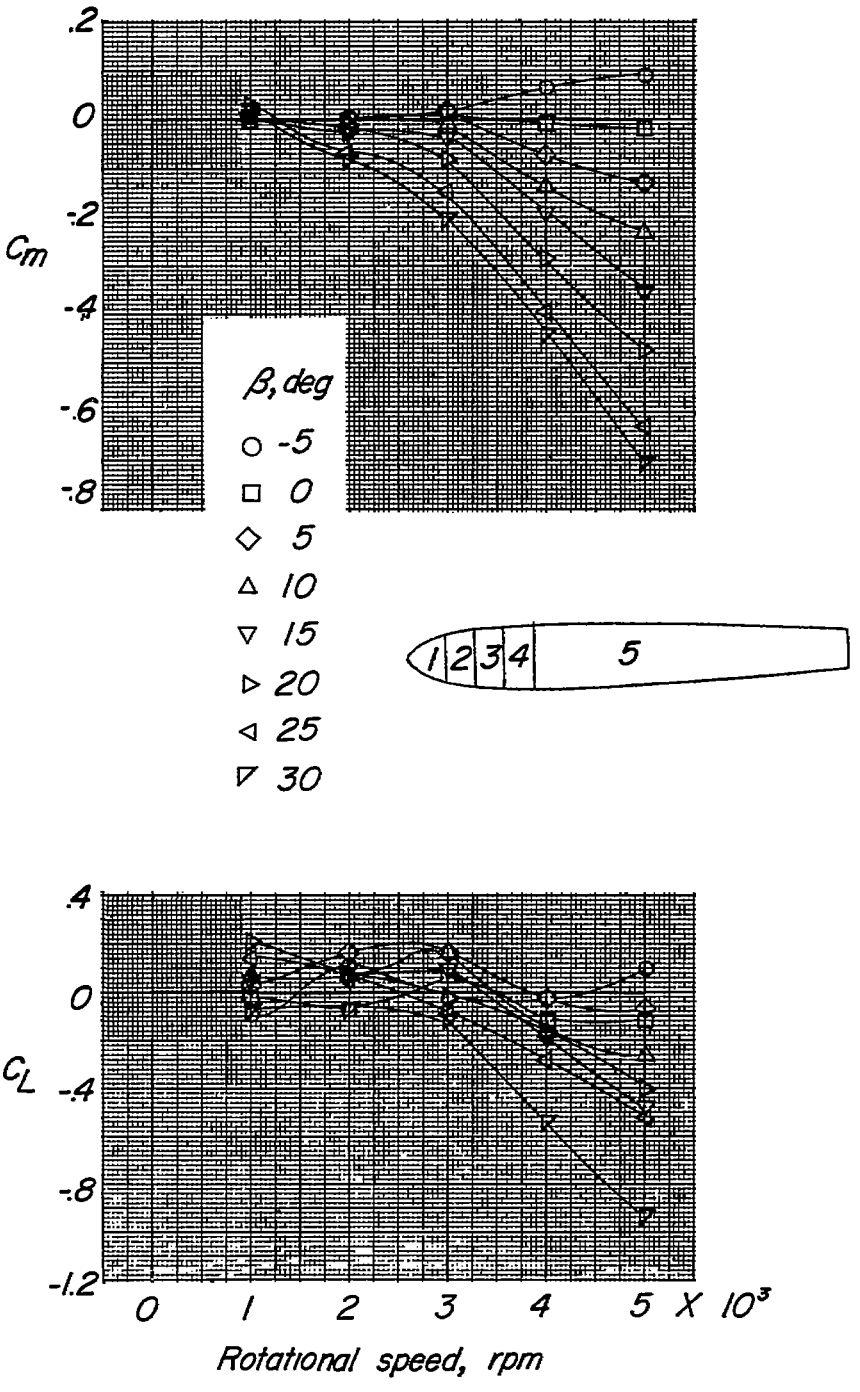

(b) C_m and C_L measured on sections 1, 2, 3, and 4.

Figure 17.- Continued.

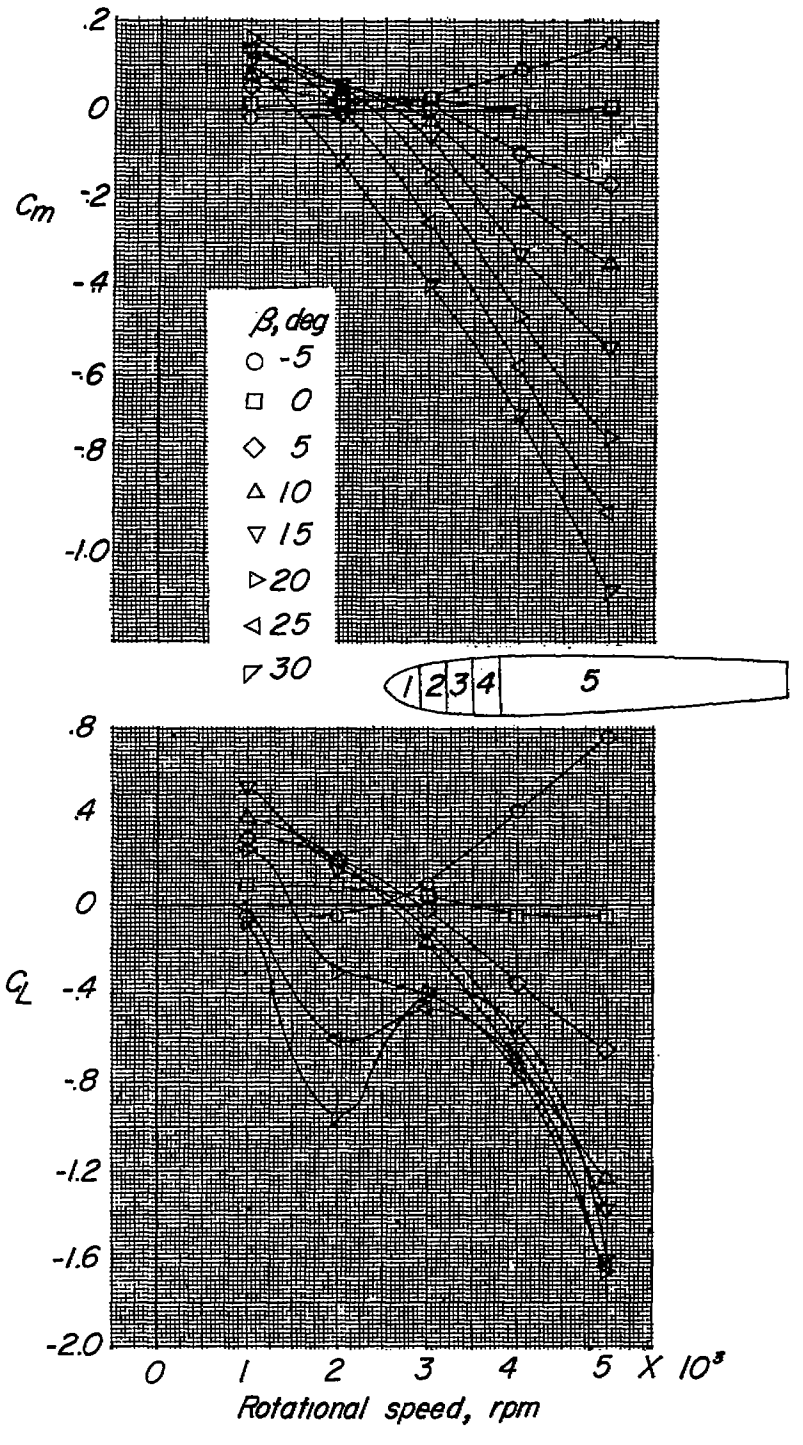

(c) C_m and C_L measured on sections 1, 2, 3, 4, and 5.

Figure 17.- Concluded.

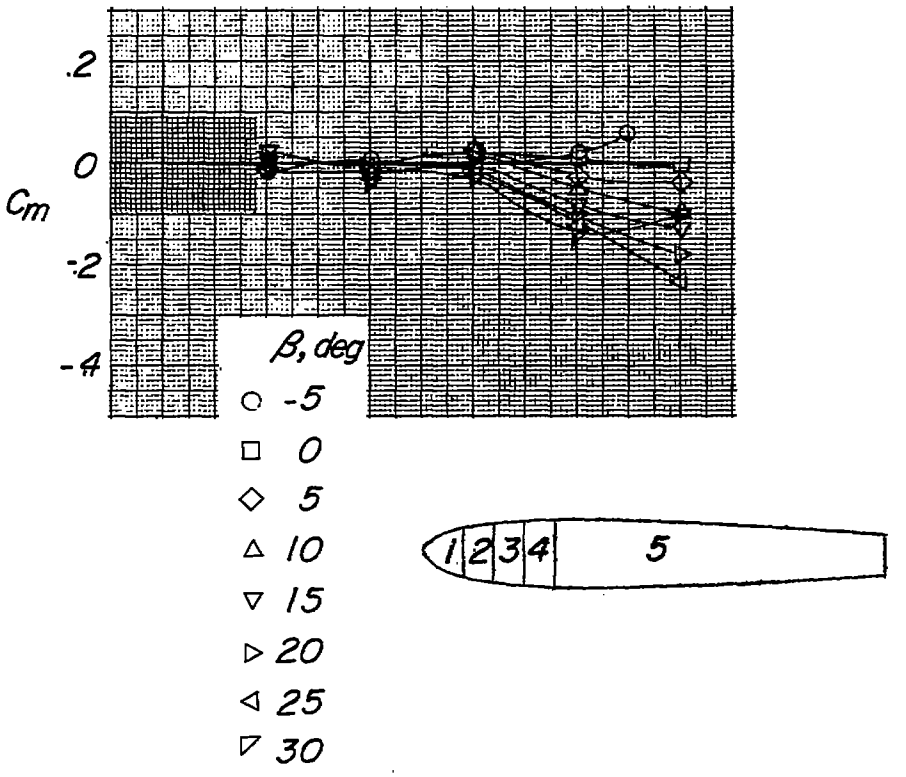

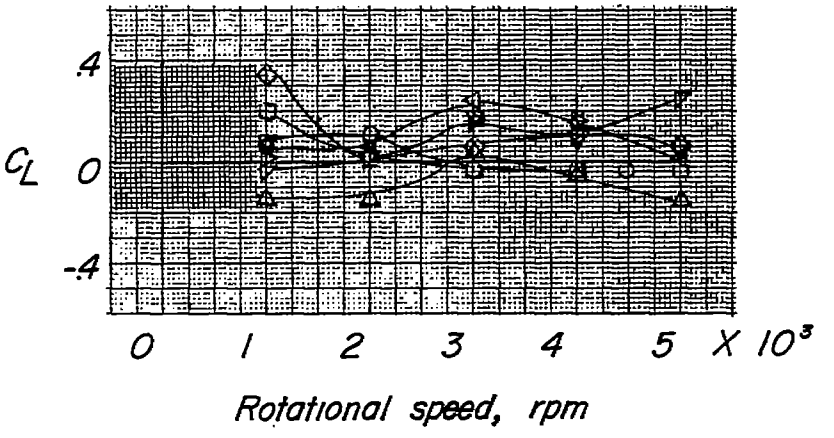

(a) C_m and C_L measured on sections 1, 2, and 3.

Figure 18.- Variation of C_m and C_L with rotational speed. Sections 1, 2, and 3 rotating; propeller on section 3.

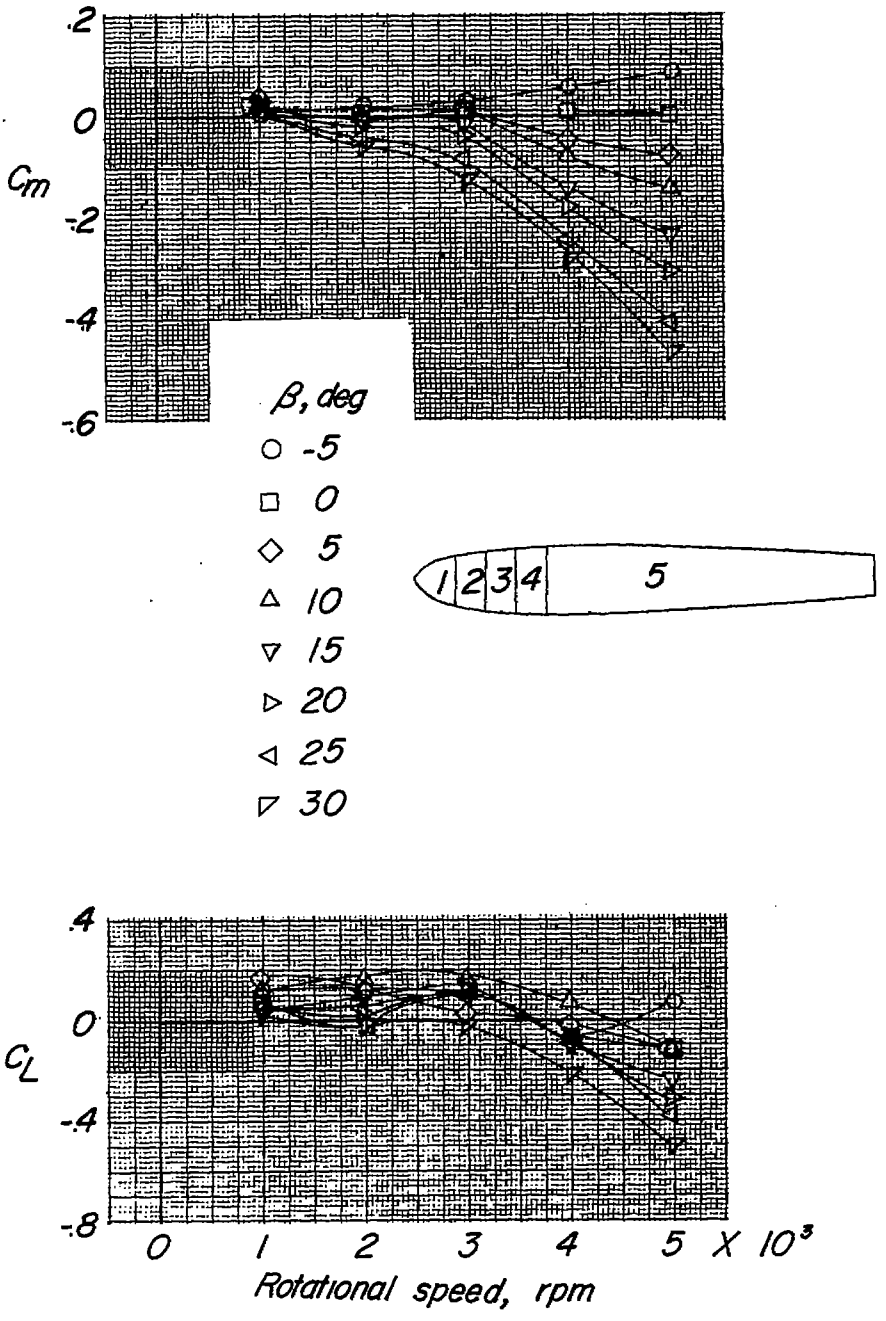

(b) C_m and C_L measured on sections 1, 2, 3, and 4.

Figure 18.- Continued.

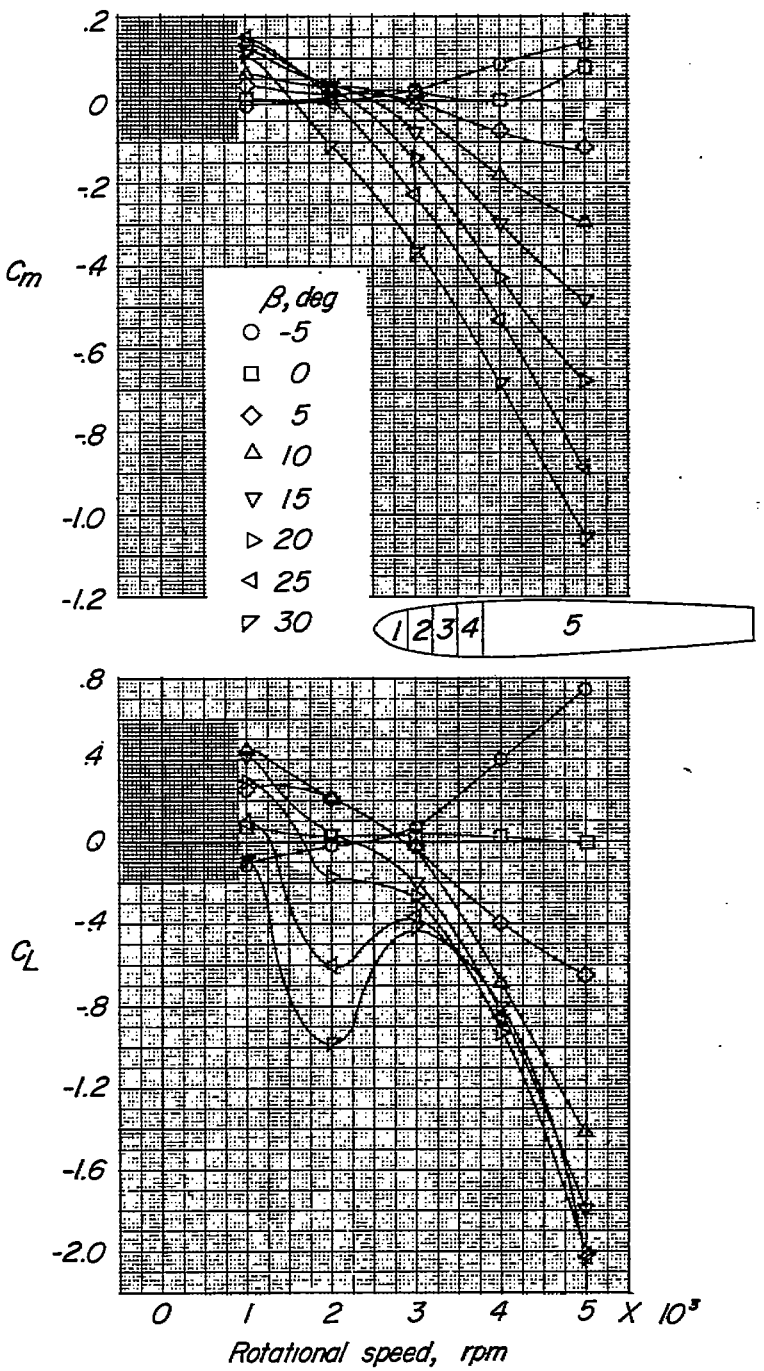

(c) C_m and C_L measured on sections 1, 2, 3, 4, and 5.

Figure 18.- Concluded.

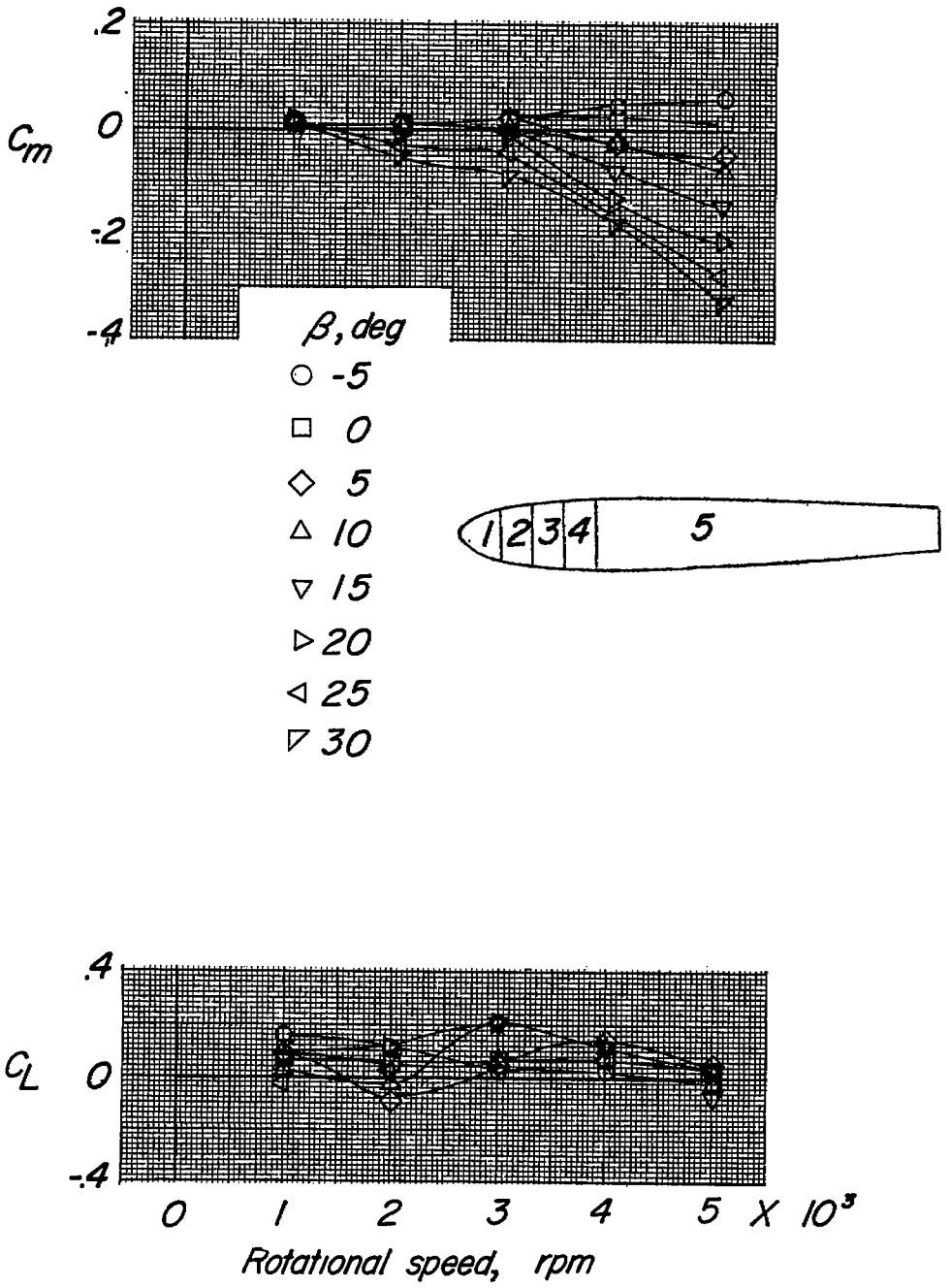

(a) C_m and C_L measured on sections 1, 2, 3, and 4.

Figure 19.- Variation of C_m and C_L with rotational speed. Sections 1, 2, 3, and 4 rotating; propeller on section 4.

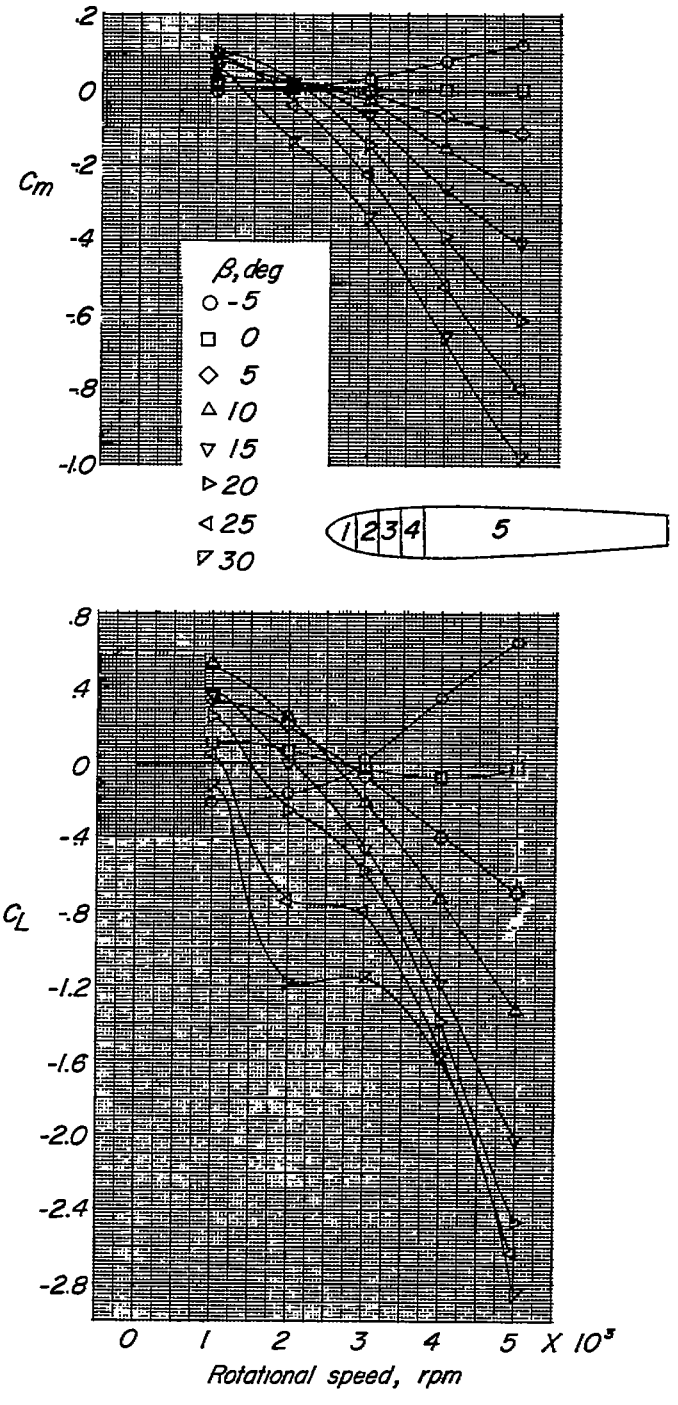

(b) C_m and C_L measured on sections 1, 2, 3, 4, and 5.

Figure 19.- Concluded.

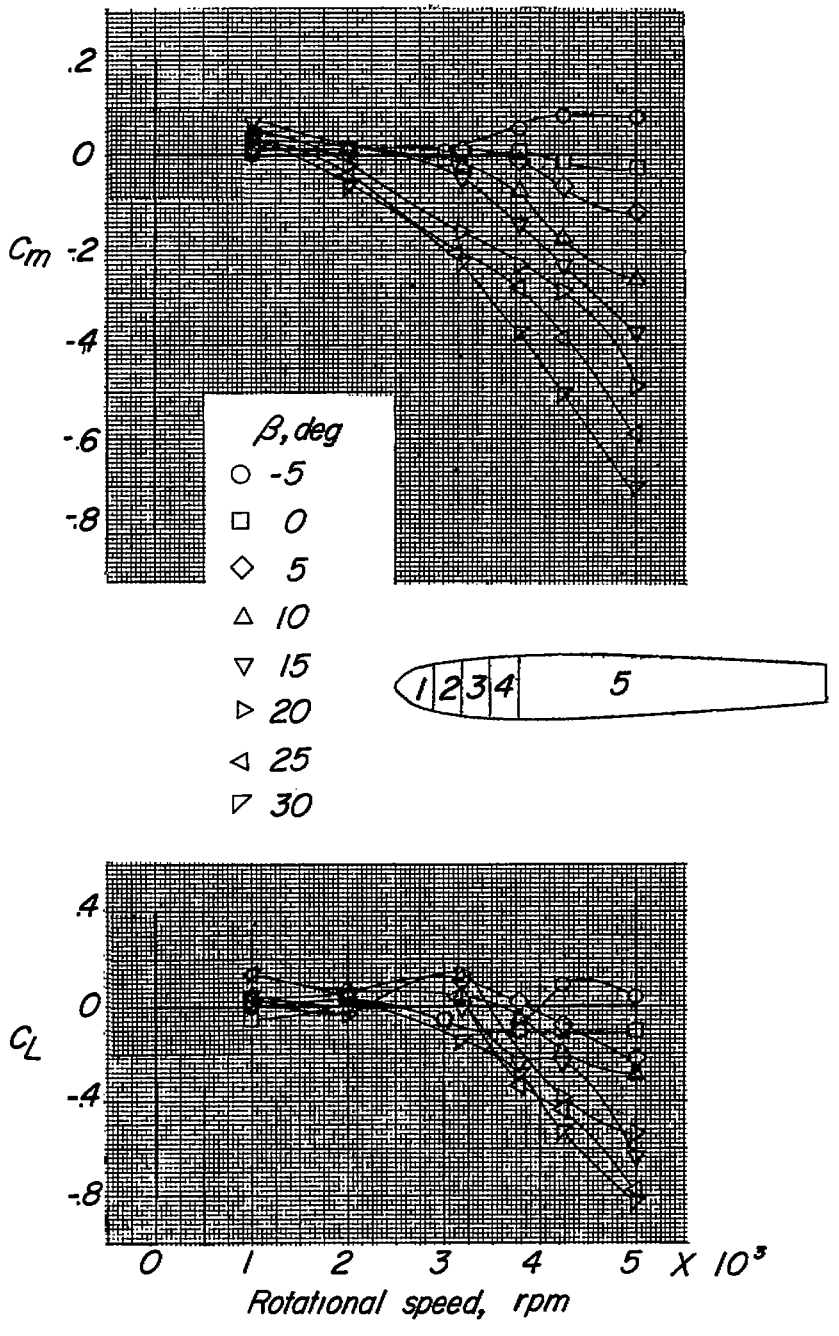

(a) C_m and C_L measured on sections 1, 2, 3, and 4.

Figure 20.- Variation of C_m and C_L with rotational speed. Section 2 rotating; propeller on.

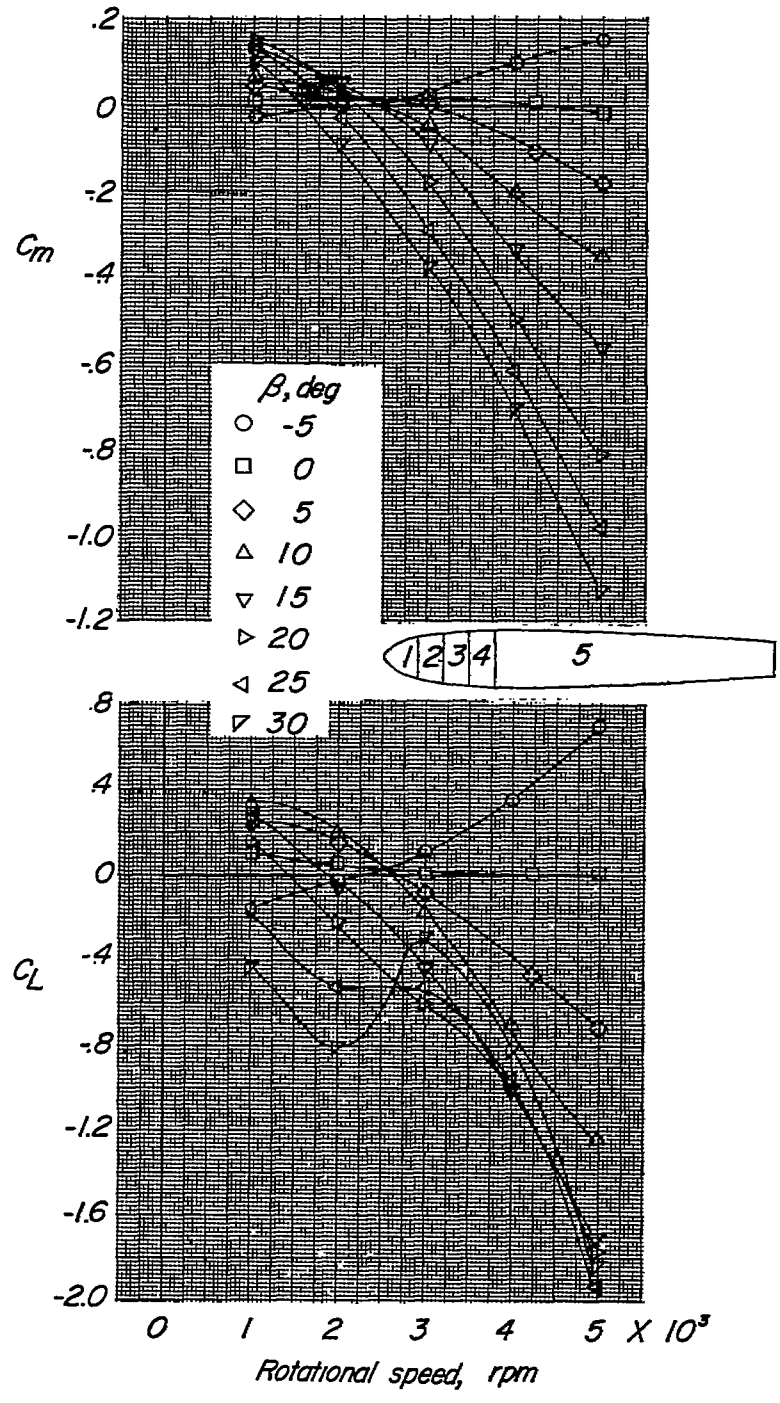

(b) C_m and C_L measured on sections 1, 2, 3, 4, and 5.

Figure 20.- Concluded.

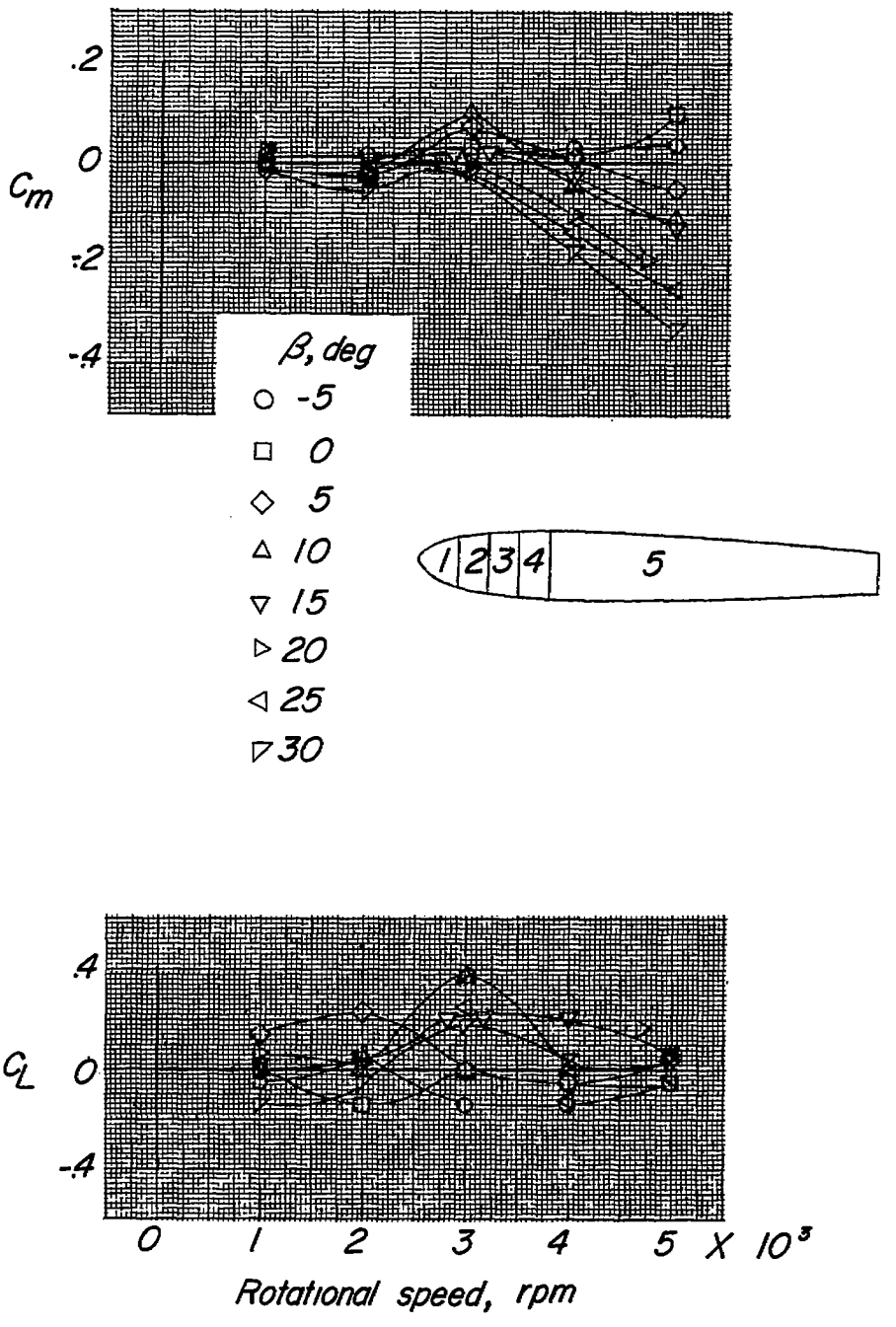

(a) C_m and C_L measured on sections 1, 2, and 3.

Figure 21.- Variation of C_m and C_L with rotational speed. Sections 2 and 3 rotating; propeller on section 3.

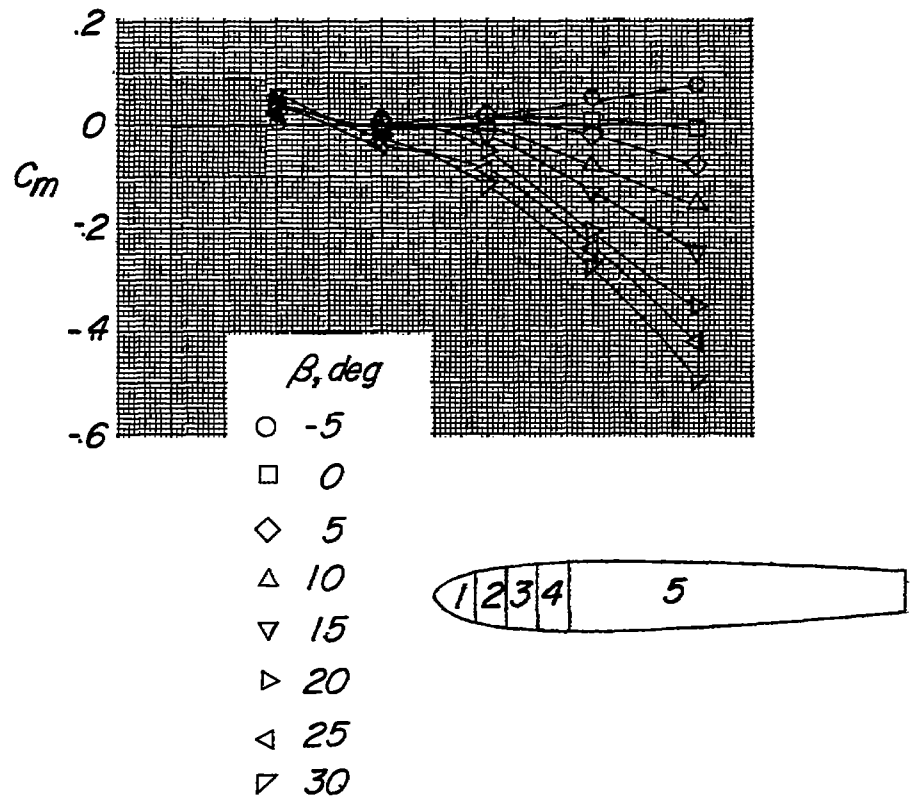

(b) C_m and C_L measured on sections 1, 2, 3, and 4.

Figure 21.- Continued.

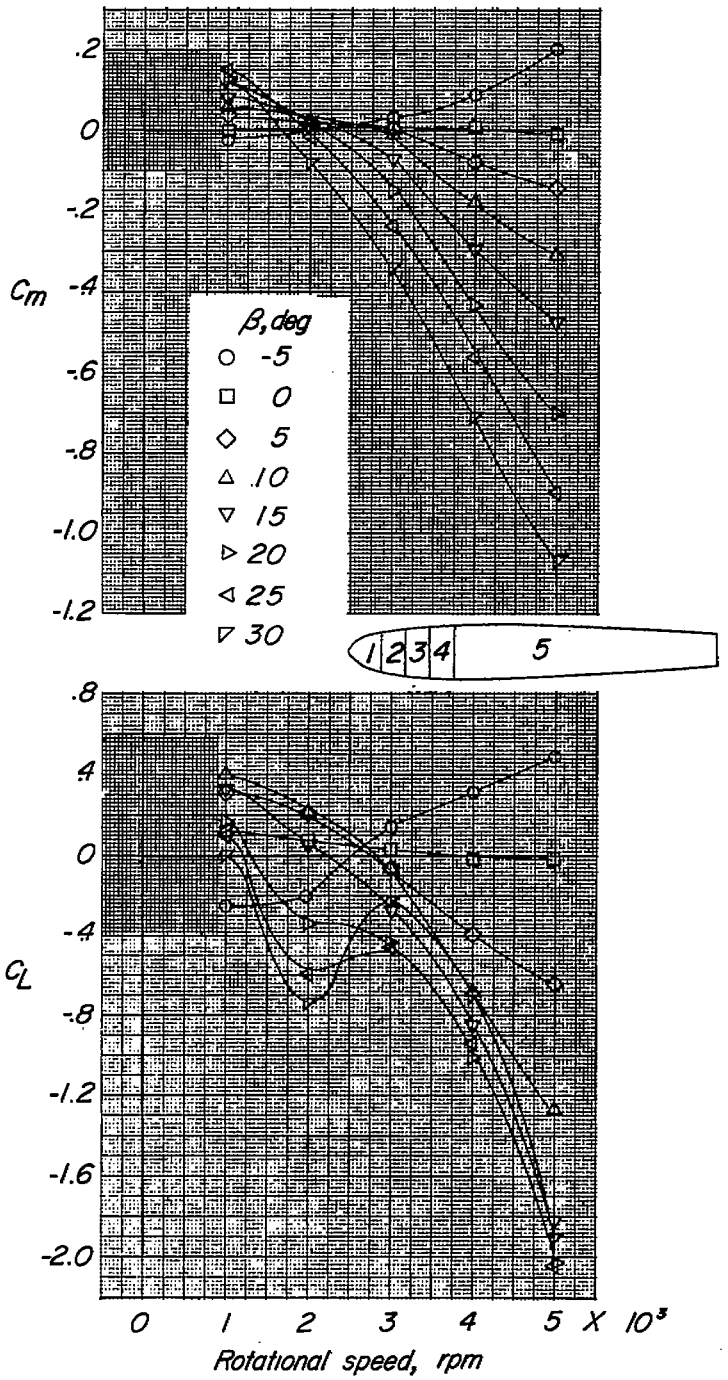

(c) C_m and C_L measured on sections 1, 2, 3, 4, and 5.

Figure 21.- Concluded.

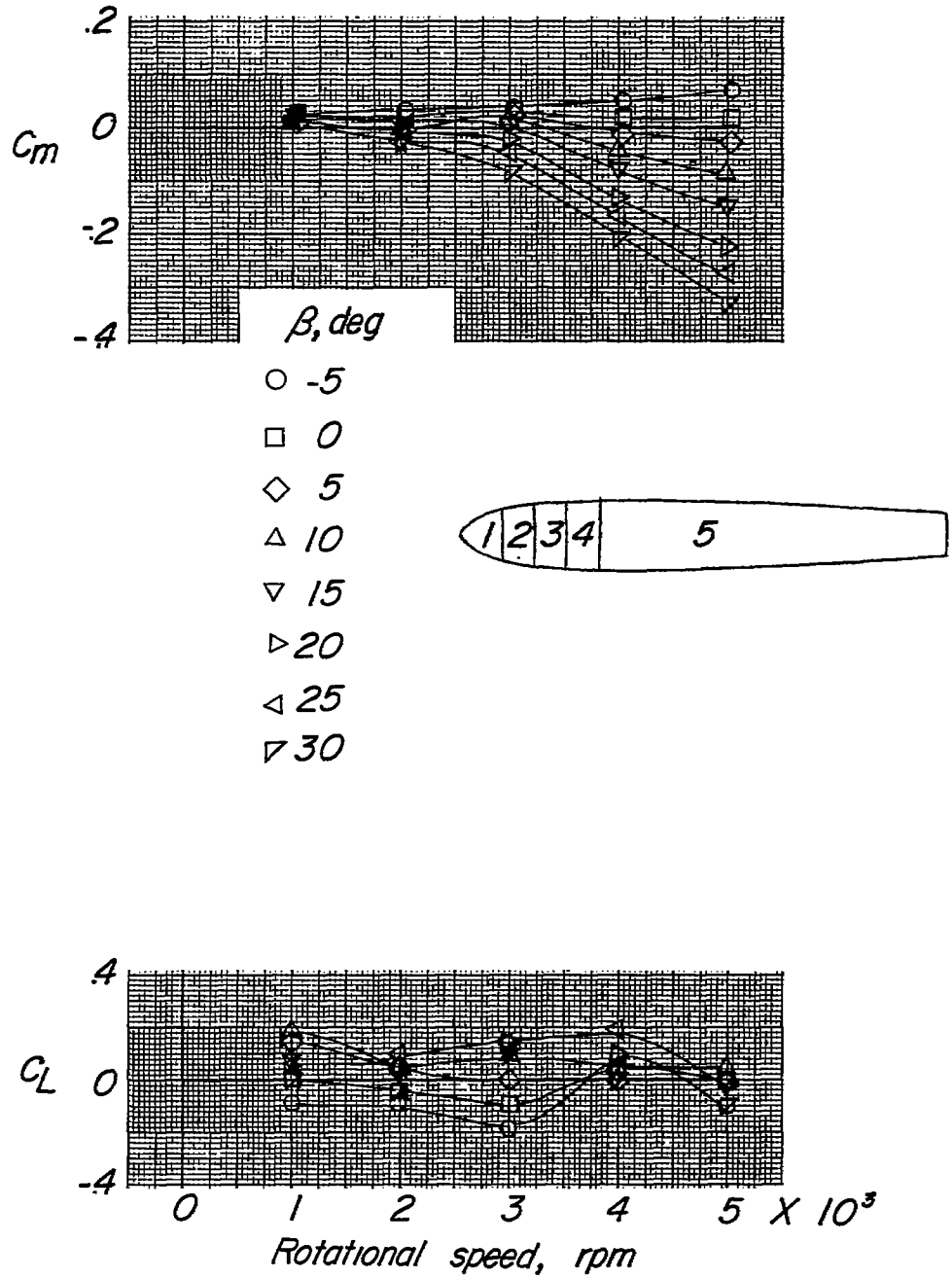

(a) C_m and C_L measured on sections 1, 2, 3, and 4.

Figure 22.- Variation of C_m and C_L with rotational speed. Sections 2, 3, and 4 rotating; propeller on section 4.

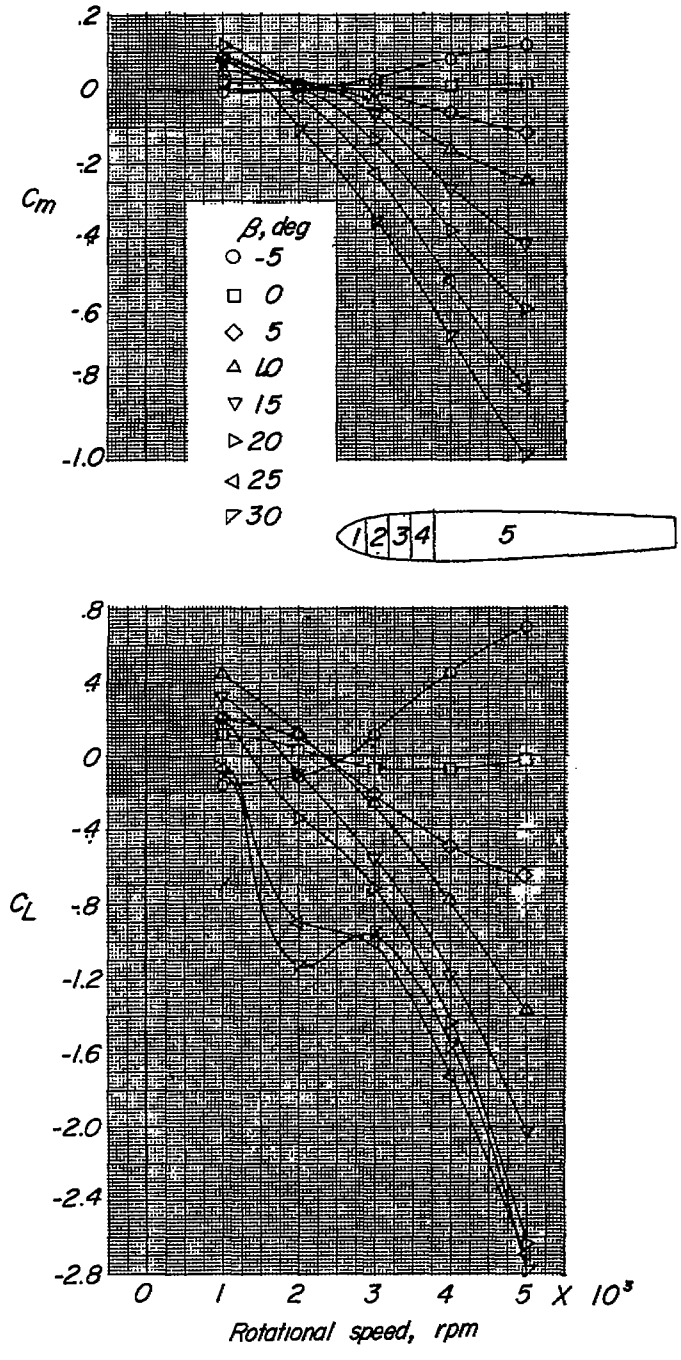

(b) C_m and C_L measured on sections 1, 2, 3, 4, and 5.

Figure 22.- Concluded.

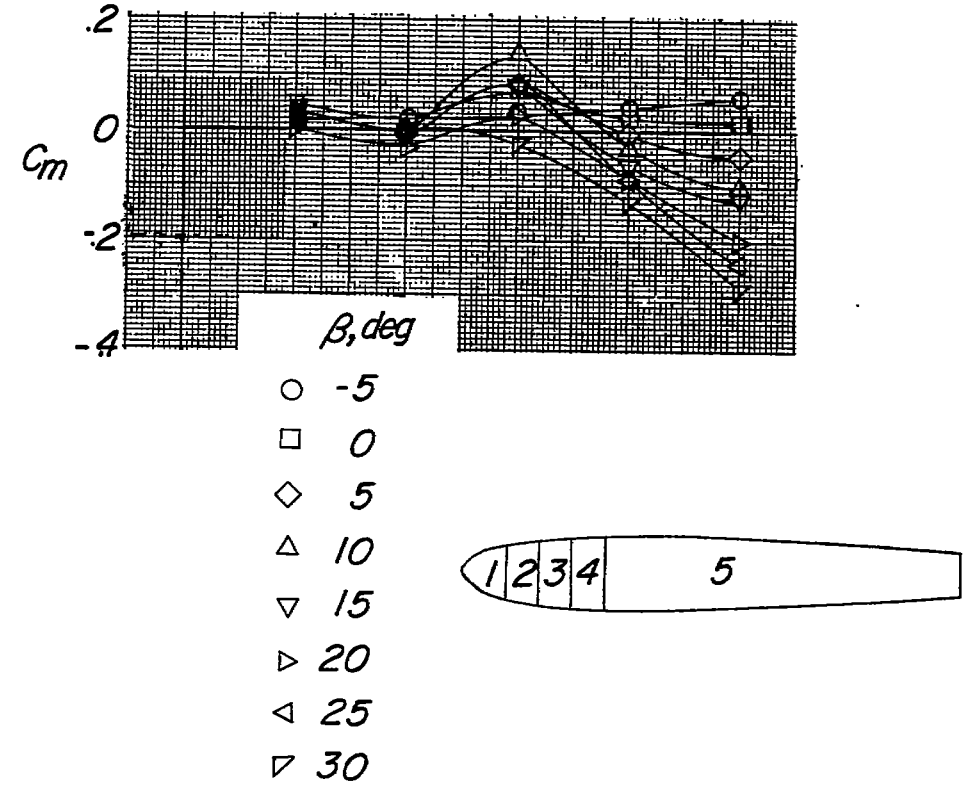

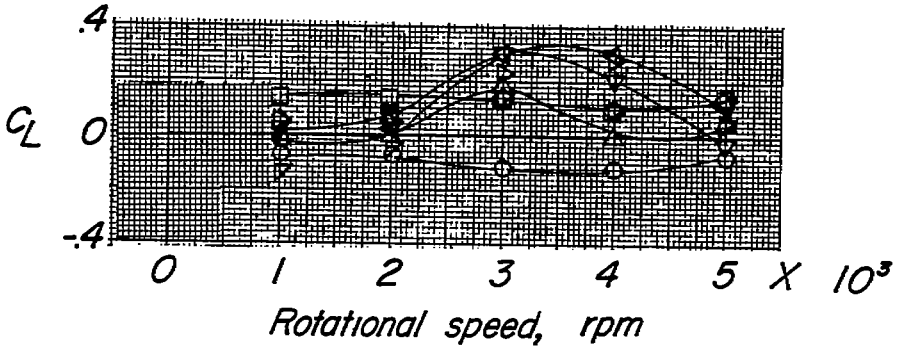

(a) C_m and C_L measured on sections 1, 2, and 3.

Figure 23.- Variation of C_m and C_L with rotational speed. Section 3 rotating; propeller on.

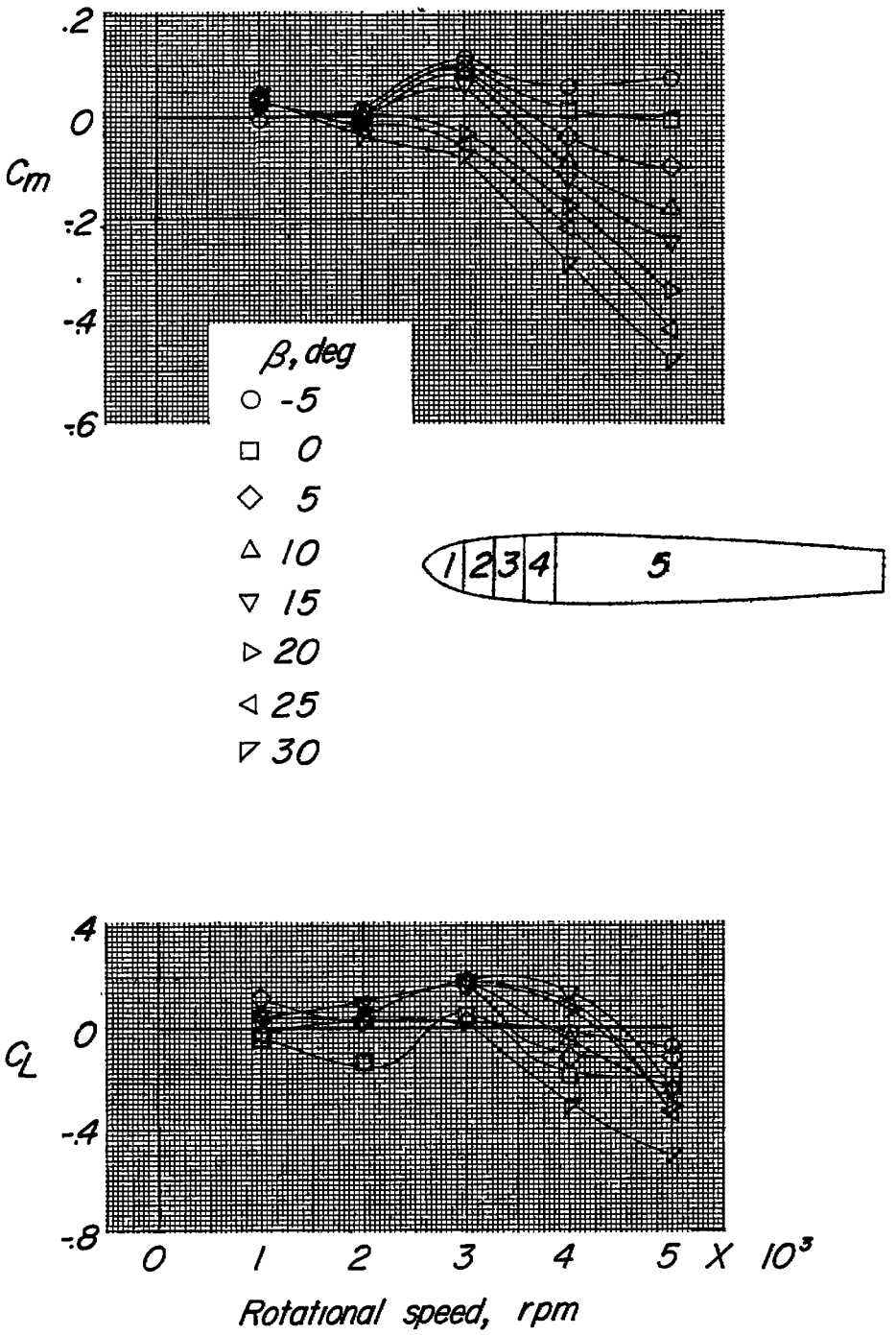

(b) C_m and C_L measured on sections 1, 2, 3, and 4.

Figure 23.- Continued.

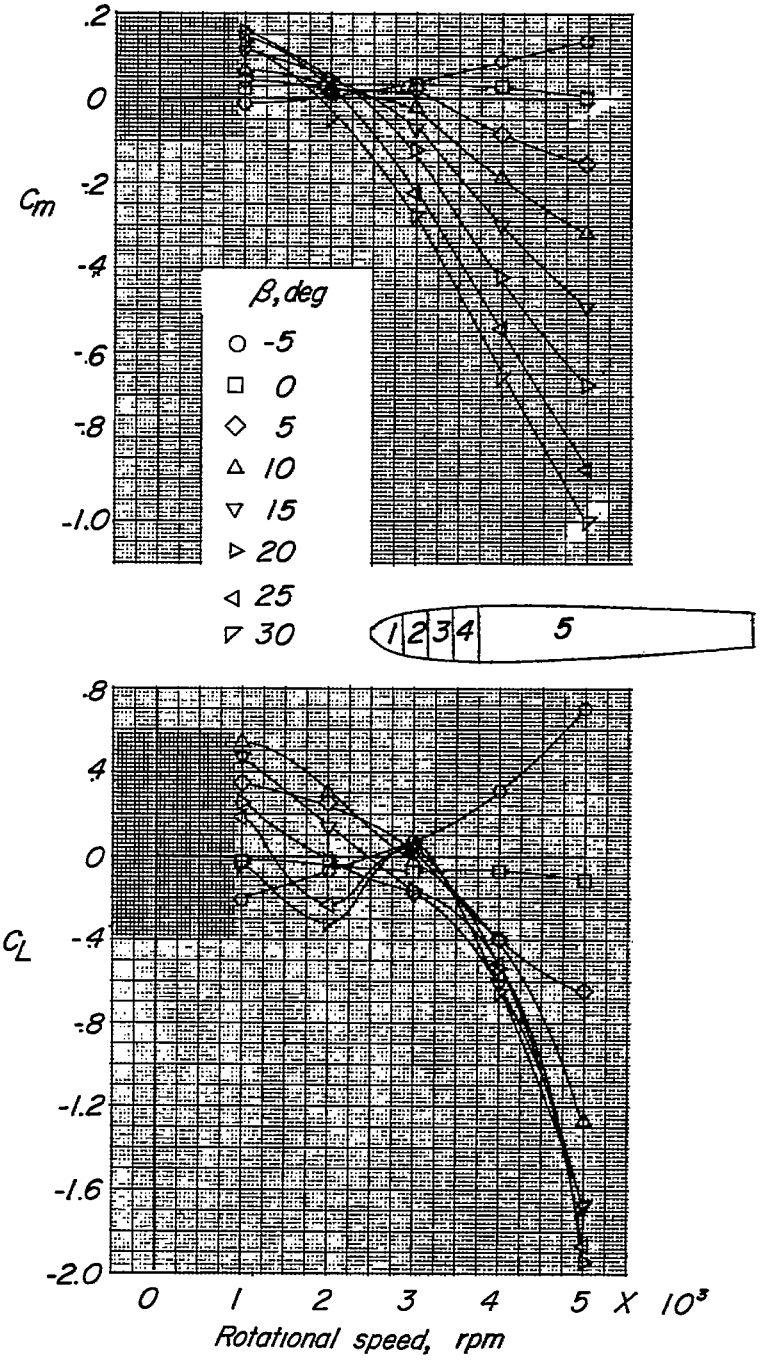

(c) C_m and C_L measured on sections 1, 2, 3, 4, and 5.

Figure 23.- Concluded.

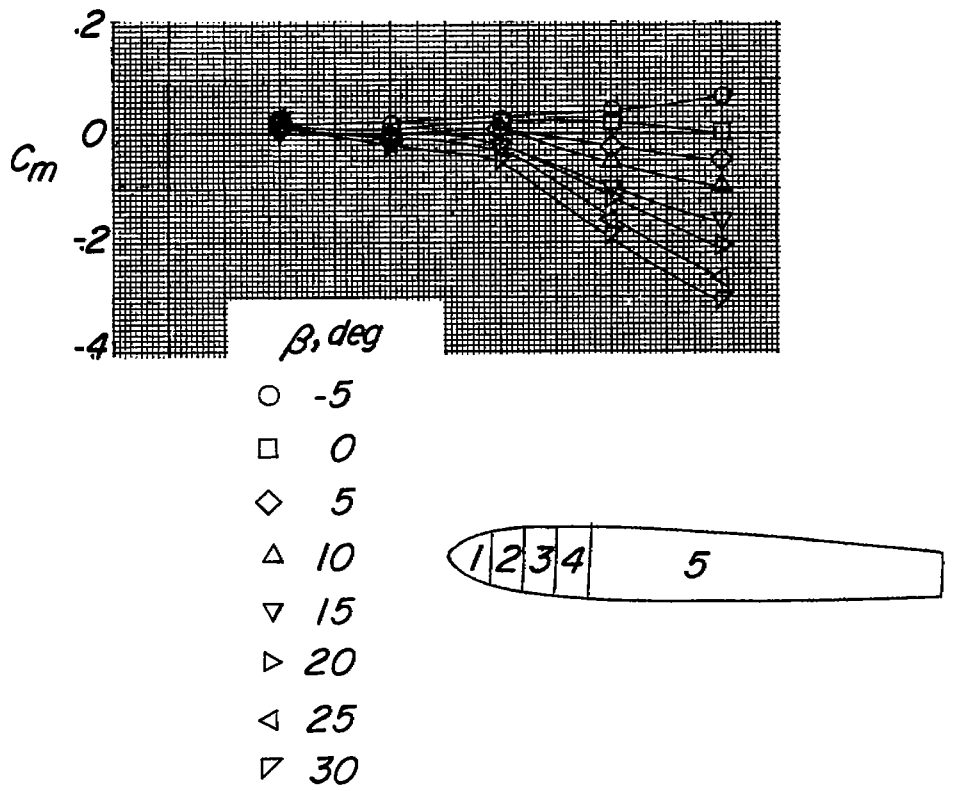

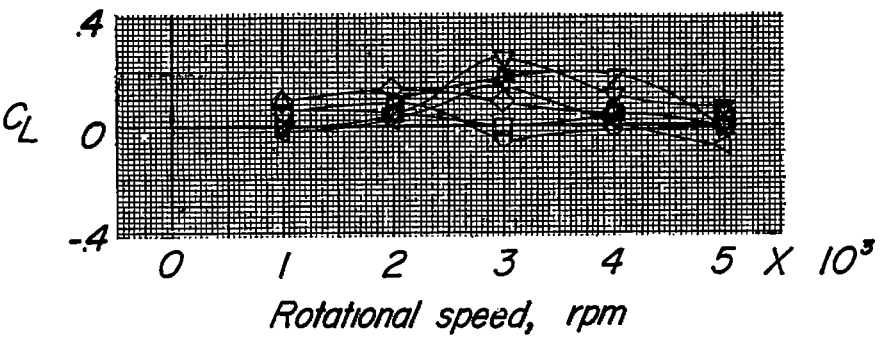

(a) C_m and C_L measured on sections 1, 2, 3, and 4.

Figure 24.- Variation of C_m and C_L with rotational speed. Sections 3 and 4 rotating; propeller on section 4.

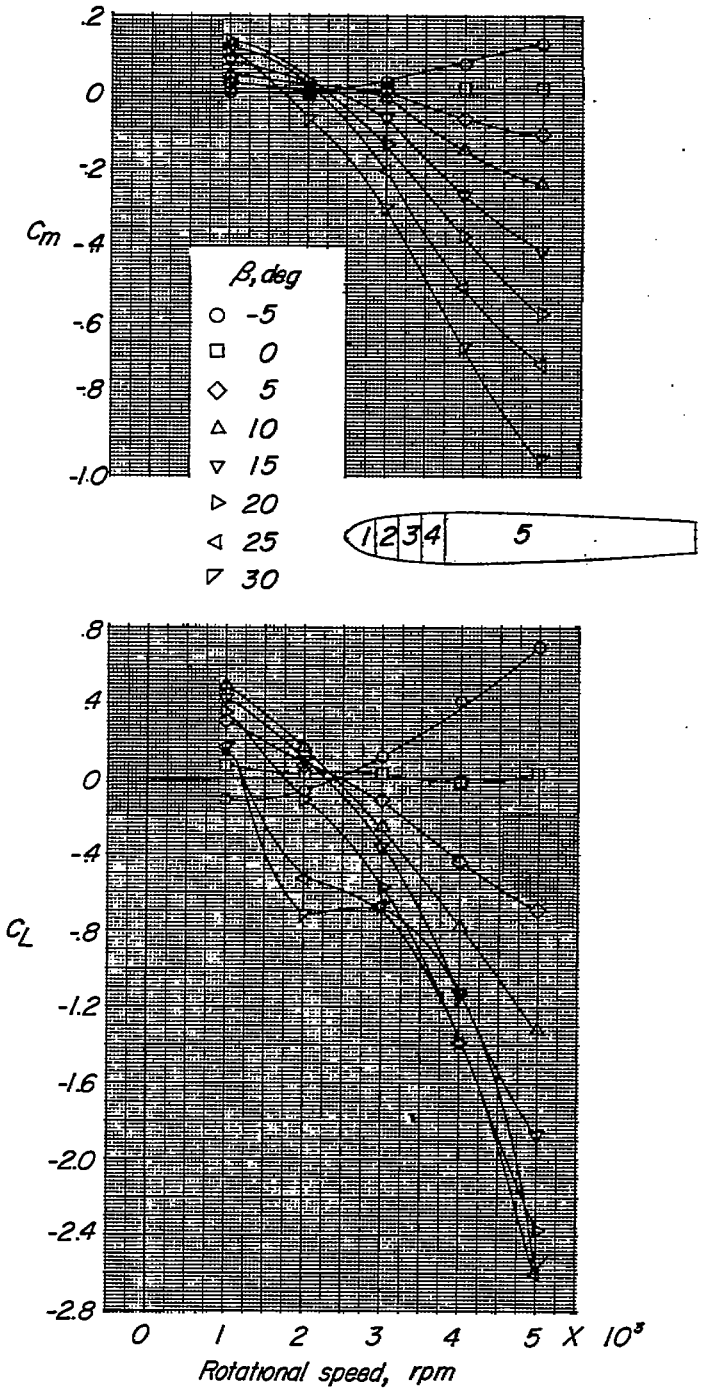

(b) C_m and C_L measured on sections 1, 2, 3, 4, and 5.

Figure 24.- Concluded.

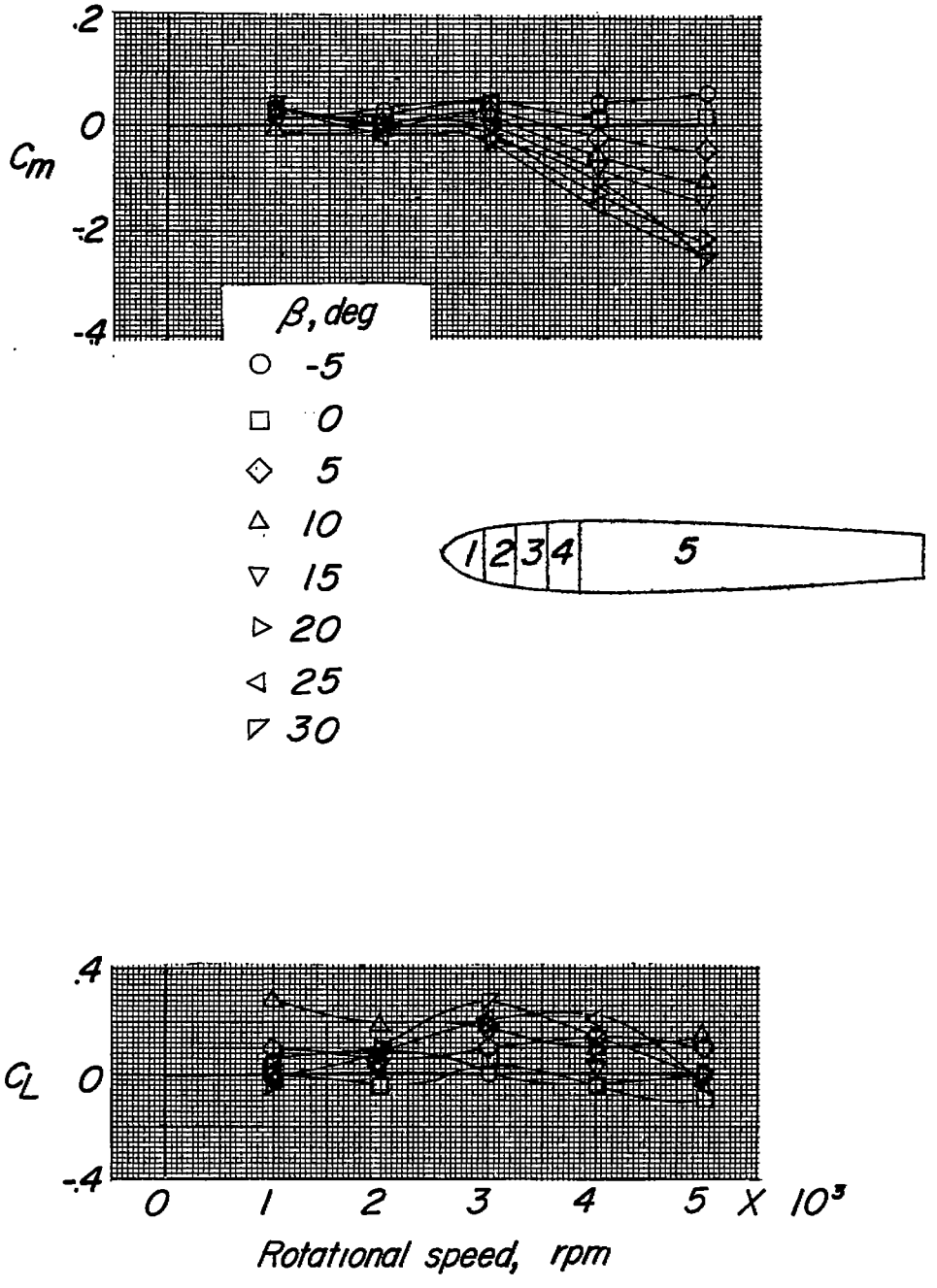

(a) C_m and C_L measured on sections 1, 2, 3, and 4.

Figure 25.- Variation of C_m and C_L with rotational speed. Section 4 rotating; propeller on.

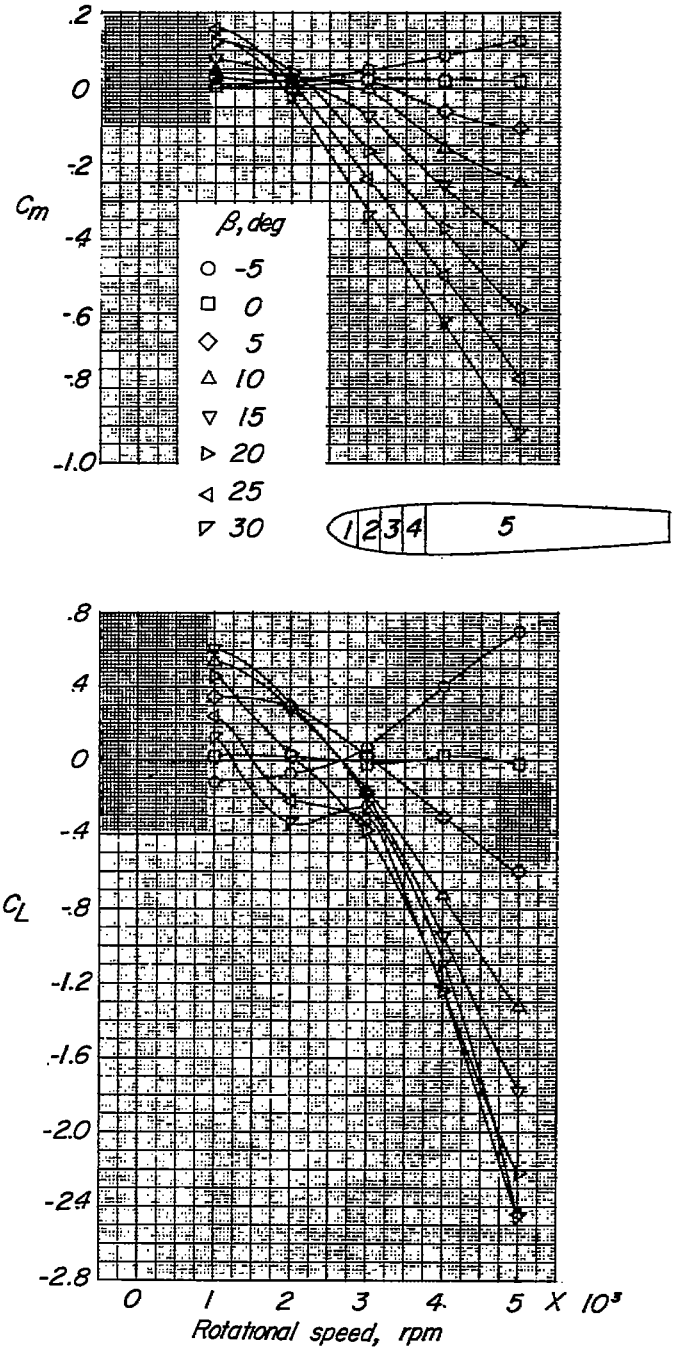

(b) C_m and C_L measured on sections 1, 2, 3, 4, and 5.

Figure 25.- Concluded.

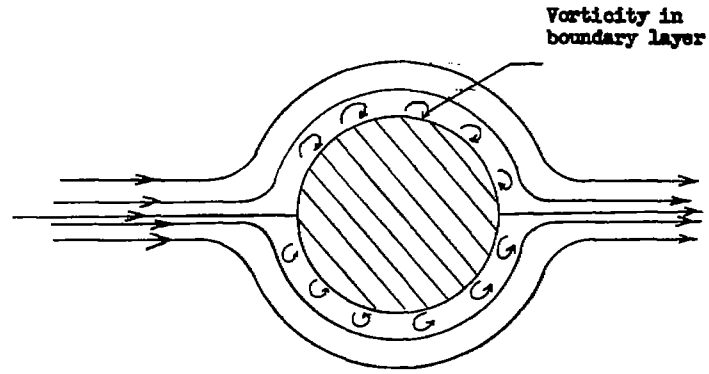

(a) No separation and no rotation.

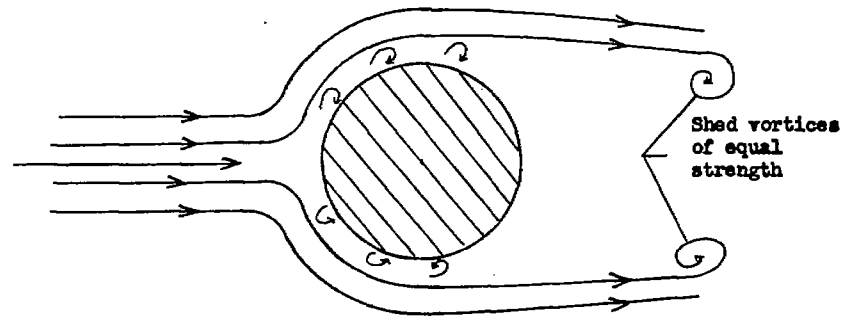

(b) Separation without rotation.

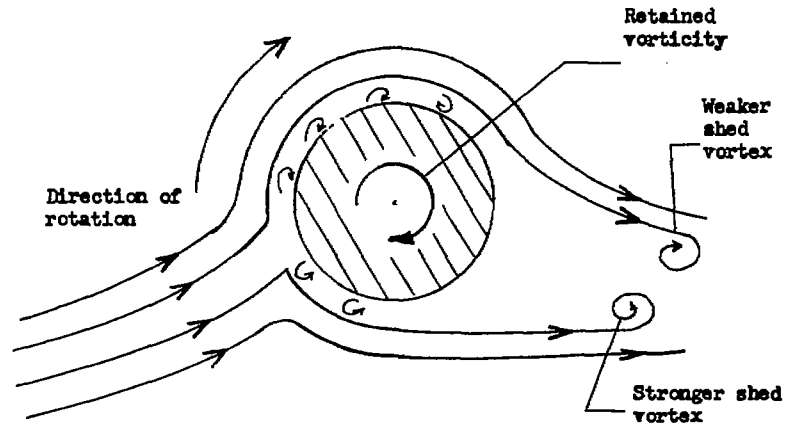

(c) Separation with rotation.

Figure 26.- Crossflow over a circular cylinder with and without rotation of the cylinder.